Optimal and On-Board Near-Optimal Midcourse Guidance

by

Shevach Katzir

Dissertation submitted to the Faculty of the

Virginia Polytechnic Institute and State University

in partial fulfillment of the requirements for the degree of

Doctor of Philosophy

in

Aerospace Engineering

APPROVED:

Eugene M. Cliff, Chairman

Frederick H. Lutze

Harold L. Stalford

John A. Burns

Stanoje Bingulac

November 1988

Blacksburg, Virginia

Optimal and On-Board Near-Optimal Midcourse Guidance

by

Shevach Katzir

Eugene M. Cliff, Chairman

Aerospace Engineering

(ABSTRACT)

Optimal midcourse guidance is examined for an air-to-air missile featuring boost-coast-sustain propulsion. A vertical plane, point-mass model is studied with load factor as a control variable. Time-range-energy optimal trajectories are computed, open-loop, via the usual necessary conditions and a multiple-shooting algorithm. A requirement on terminal velocity magnitude is examined for its effect on firing range.

Next, a study of the optimal midcourse guidance problem with reduced-order models is presented. The models under study, in addition to the point-mass model, are:

- Singularly perturbed model with γ as fast variable;
- Point mass model with approximation of the induced-drag;
- Energy model.

One of the major results in this study is that the reduced-order models are not accurate enough to approximate the optimal trajectories and so are of limited use as reference trajectories in an on-board scheme. Thus, optimal trajectories, computed by using the point-mass model, are selected as the reference trajectories for a closed-loop guidance scheme.

Finally, an approach to on-board real-time calculations for an optimal guidance approximation is derived. Extremal fields and neighboring extremal theory ideas are used together with pre-calculated Euler solutions to construct a closed-loop guidance algorithm. The method is applied to the midcourse guidance of an air-to-air missile and was found to perform quite well.

To my mother

and to the memory of my father

Acknowledgements

I would like to express my sincere gratitude to my adviser Dr. Eugene M. Cliff for his guidance, support and constant encouragement throughout the course of this research.

I wish to thank the members of my dissertation committee for their time and effort expended in my behalf.

I would like to express my deep regret for the sudden passing of Dr. Henry J. Kelley. It was a great honor and unique experience to carry out research under the valuable guidance of Hank Kelley, who passed away before the completion of this work. Hank will be remembered as a great researcher, teacher and friend.

I would like to thank to RAFAEL - Armament Development Authority, Ministry of Defense of Israel, for helping me in my graduate studies.

This research was supported in part by Air Force Armament Laboratory, Guidance and Control Branch, Eglin AFB., FL., under contract F08635-86-K-0390, (Dr. J. Cloutier, project officer) and in part by DARPA under (ACMP) contract F49620-87-C-0116.

Finally, I wish to thank my family my wife, , my daughter and my son for their constant support throughout these years together.

Table of Contents

Chapter 1: Introduction

The problem of intercepting a moving target has a long history. In the first known study (1732) the **Hound-Hare Curve,** best known as the **Pure Pursuit** guidance, was presented by Bouguer, a French scientist in the Royal Academy of Science. Bouguer formulated the problem as a pursuit-evasion game for two ships, where the evading ship sails on a straight line and the pursuing (pirate's) one employs a pure pursuit guidance strategy. From this beginning until War World II the guidance problem was studied, mainly with a mathematical interest. During WWII there was a great interest in guidance schemes and several important guidance techniques were developed. Among these were several variations of **pure pursuit, command to line of sight, collision course** and the well known **proportional navigation** [1]. Proportional navigation guidance was developed during WWII in the U.S. by Yuan [2], Newell [3] and Spitz [4]. Murtaugh and Criel [5] in their study closed the classic approach era to proportional navigation and guidance in general. Since then, most of the research effort have been aimed

towards the investigation of the optimal guidance problem; Kishi [6], Bryson [7-8], Kreindler [9], [10-11] and many other have published in this area.

Today, almost all operational short range air-to-air missiles use proportional navigation guidance or one of its modifications to accomplish the intercept. Most other missiles employ these schemes at the terminal phase. Some missiles currently under research and development employ more advanced guidance laws based on optimal control theory.

In medium and long range intercepts the guidance is usually divided into two principal phases: midcourse phase and a terminal guidance phase. The midcourse phase starts just after launch and ends after seeker lock-on is realized, then, the terminal phase starts. As noted above, proportional navigation is usually used during the end game.

In recent years there has been considerable interest in the midcourse optimal guidance problem. Much of the recent work has focused on **reduced-order models** with an objective of synthesizing near-optimal closed-loop midcourse guidance laws. Cheng and Gupta [12], employ singular perturbation theory and engineering approximations to derive an "Advanced Midcourse Guidance for Air-to-Air Missiles". The performance of this guidance law is compared to an existing linear-optimal guidance scheme and to a proportional navigation guidance. It is **not** compared to an exact solution for an optimal guidance problem. Menon and Briggs [13] address the same problem. They use singular perturbation theory to get order reduction to the energy model, and based on this model they derive an on-board midcourse guidance law. Ref. [14] reports a study of

midcourse guidance including logic for re-starting a pulse-rocket motor. Again singular perturbation theory and engineering approximations allow order reduction.Based on this model an on-board midcourse guidance law and ignition control logic are derived, and a performance comparison between the optimally ignited boost-coast-sustain motor and a boost-sustain motor is presented. In all of these studies [12-14] the optimal solutions for the point-mass ('exact') model **are not** presented and hence there no 'bench mark' for comparing the near-optimal solutions.

This was a key motivation for the work presented here. A major purpose of this work is to study the optimal midcourse guidance problem with the **point-mass** model of medium and long range missiles featuring **boost-coast-sustain** propulsion. We are also interested in formulating on-board near-optimal guidance schemes.

In the study of medium and long range intercepts the range performance of the missile is a key issue [15]. More specifically, one is interested in the family of maximum-range trajectories parameterized by time-of-flight and by final energy (range-time-energy problem). Although the problem of best-range guidance has a long history [16-17], results for point-mass modelled vertical plane motions of missiles are **not** found in the literature (except for Ref. [15] that was done as part of this work). The best-range guidance problem is a typical optimization problem and may be 'solved' via, Pontryagin's Minimum Principle [18] approach, which leads to a two-point-boundary-value problem (TPBVP). These are very delicate numerical problems. In the usual approach one implements a version of

Newton's method which requires that one provide initial estimates for all dependent variables (states and co-states) for certain values of the independent variable. In many cases the domain of attraction for the solution point is quite small.

The solution to an optimal control problem is commonly found in an open-loop form. On-board real-time guidance generally requires the optimal solution to be expressed in closed-loop form. Optimal feedback guidance approximations may be obtained by employing singular perturbation and/or neighboring extremal ideas. A brief review of reduced-order modelling and neighboring optimal techniques is the objective of the following paragraphs.

From the beginning of optimal flight studies, there has been great interest in approximations featuring simplified vehicle models. Reduced-order modelling is very attractive to the analyst in solving optimal control problems. It is motivated by the considerable difficulties encountered in computing optimal trajectories with the detailed system model and by the possible use in the synthesis of near-optimal closed-loop control laws. As indicated before, an application of the Minimum Principle leads to a TPBVP involving several unknown parameters. A reduction in system order decreases the number of unknown parameters and as a result simplifies the numerical computations.

Such a reduction in system order can be obtained via singular perturbation techniques [19]. This approach takes advantage of the time-scale separation of the state variables, by separating the dynamics into fast and slow modes with corresponding 'inner' and 'outer' solutions. The solution of the reduced-order

system is modified near one or both end-points by a 'boundary-layer' correction, also calculated via a system of differential equations of lower order than that of the original system. Such corrections may also be needed at 'turning-points', internal to the interval of interest.

In recent years singular perturbation techniques have been extensively used in optimization problems and in particular in flight optimization [10,12-14,20-43]. The concept of singular perturbation techniques in problems of flight and trajectory optimization was introduced by Kelley [20-26] and applied in different formulations by Breakwell [27-28], Ardema [29-32], Calise [33-37], Shinar [38-40] and many others. The earliest and most well-known approximation in flight optimization is that of the energy-state. The energy model began as an ad hoc approximation [44-46] and found a theoretical basis in singular perturbation theory by Kelley [20-26].

The problem of guidance in the neighborhood of an optimal nominal trajectory has been studied by Kelley [47] who developed a procedure for synthesizing linear feedback for optimal guidance. Similar approach to neighboring optimal control was also presented by Breakwell and Bryson [48]. In Ref. [49] Kelley introduced higher order feedback approximations. Techniques to improve the convergence in neighboring optimum guidance are presented by Powers in Ref. [50]. The basic idea there is to use a min-distance norm to modify the lookup parameter (index). An approach to intercept on-board calculations which employs Euler solutions for point-mass vehicle model but makes use of singular-perturbation theory ideas in terms of hierarchical trajectory-family structure were sketched by Kelley

and Well [51] and was implemented by Weston [52] and Visser [53]. With this background, it is the goal of this work to explore the optimal and on-board near-optimal midcourse guidance for the class of medium and long range missiles.

First, an optimal midcourse guidance is examined for an air-to-air missile featuring boost-coast-sustain propulsion. A vertical plane, point-mass model is studied with load factor as a control variable and coast time as a parameter. The basic problem considered here is to find the load-factor history and coast time to maximize the final range for given final time and final energy. Time-range-energy optimal trajectories are computed, open-loop, via the usual necessary conditions and a **multiple-shooting** computational approach [54]. A requirement on terminal velocity magnitude is examined for its effect on firing range.

Next, we study of the optimal midcourse guidance problem with several reduced-order models such as:

- Singular perturbation with γ as fast variable;
- Point mass model with approximation of the induced-drag;
- Energy model.

Optimal trajectories, computed with these models and the point-mass model, are compared.

Finally, a new approach, to on-board real-time calculations for midcourse near-optimal guidance, is derived. Extremal fields and neighboring extremals theory ideas are used together with pre-calculated Euler solutions and feedback gains to establish a closed-loop guidance scheme. First, the scheme is derived for a fixed (specified) final time case, next, its validity is extended to incorporate final time

perturbations. The optimal reference trajectories (nominal) and the closed-loop gains are obtained using the **point-mass model.** The indexing is done in terms of current time, but final time changes are allowed. This approach assumes that at certain time intervals, the predicted intercept point is computed, and then used as new terminal condition for the missile. It is also assumed that a terminal guidance law such as proportional navigation or more advanced guidance scheme is employed by the missile to accomplish the end game. The scheme is applied to two-dimensional midcourse optimal guidance of an air-to-air missile featuring boost-coast-sustain propulsion.

The following chapters are organized accordingly. In chapter 2 the equations of motion for the point-mass model are presented and the optimal control problem is formulated. Chapter 3 contains a derivation of the necessary conditions via, Pontryagin's Minimum Principle and extremal trajectories are obtained using the point-mass missile model with the multiple-shooting numerical approach. The reduced-order models are described and studied in chapter 4. In chapter 5 we consider the near-optimal guidance. An approach to on-board real-time calculations for an optimal guidance approximation is derived and examined via numerical simulations. Summary, concluding remarks and recommendations for further study are drawn in chapter 6. The appendix presents aerodynamic and propulsive modelling for our missile-example.

Chapter 2: Problem Formulation

In this chapter system equations for the point-mass model of a missile's motions in the vertical-plane are presented. Next, the optimal control problem is formulated as a range performance problem.

2.1 System Model

In general we consider the following nonlinear system:

$$\dot{X} = f(X, U, t) \tag{2.1}$$

in a time interval $[t_o, t_f]$ with the initial conditions $X(t_o) = X_o$, a target set $X(t_f) \in \Theta_f$ and a control constraint set $U(t) \in \Omega$.

In our missile-example we have:

$$X = [x, h, \gamma, E]^T \text{ and } U = n \text{ ;} \tag{2.2}$$

In these equations x is range , h is altitude , γ is the usual path-angle to the horizontal , E is the specific-energy and n is the load-factor.

The point-mass equations for the vertical-plane motions are described by:

$$\dot{x} = V \cos \gamma \tag{2.3}$$

$$\dot{E} = \frac{V}{W}(T - D) \tag{2.4}$$

$$\dot{h} = V \sin \gamma \tag{2.5}$$

$$\dot{\gamma} = \frac{g}{V}(n - \cos \gamma) \tag{2.6}$$

The energy is the sum of potential and kinetic energy. It is introduced to replace the speed V as a state variable, hence, the symbol V denotes the velocity and is given by:

$$V = \sqrt{2g(E - h)} \tag{2.7}$$

This replacement of variables was first introduced by Kaiser [44], the common reason for this change is to obtain a better separation in time scales of the variables; E is relatively slow varying variable compared with either V or h . It is clear that system's characteristics are not changed with this choice of variables.

The aerodynamic and propulsive modelling (functions T and D) are detailed in the appendix. Here we note the functional dependence, viz:

$$T = T(t,h) \tag{2.8}$$

and

$$D = D(h,E,n). \tag{2.9}$$

The propulsion is of boost-coast-sustain type, thus the explicit dependence on time. The thrust is shown as a function of time in Figure A in the appendix. Note that since the thrust history is specified, the weight [$W(t)$] is also a specified function of time.

The control variable in system's model is the load-factor [n] and is limited by the following two constraints:

Structural limit:

$$|n| \leq n_{\max} \tag{2.10}$$

Aerodynamic limit:

$$|n| \leq C_{L\max}(M)\bar{q}\frac{S}{W} \equiv n_L(E,h) \tag{2.11}$$

2.2 Problem Formulation

The general optimal control problem to be considered is to minimize a performance index with a control vector function $U(t) \in \Omega$ and with the produced trajectory $X(t)$ that satisfies the initial conditions X_o and the target set $X(t_f) \in \Theta_f$.

As already indicated, in the study of long range intercept the range performance of the missile is a key issue (see [15] for example). More specifically, one is in-

terested in the family of maximum-range trajectories parameterized by time-of-flight and by final energy (range-time-energy problem).

Hence, the problem considered here is to find the load-factor history $[n(\bullet)]$ and a coast time interval $[t_c]$ to maximize the final range $[x(t_f)]$ while satisfying certain boundary conditions for given final time $[t_f]$.

In fact, several versions of the problem with differing end-conditions, are considered. In all formulations the following (common) requirements are imposed:

initial point	final point	
$x(0) = 0$	$\gamma(t_f)$ – free	
$h(0) = h_o$ (specified)	$h(t_f) = h_f$ (specified)	
$E(0) = E_o$ (specified)	$E(t_f) \geq E_f$ (specified inequality)	(2.12)

Note that since the final altitude is specified, the inequality on the final energy implies a lower bound on final velocity.

The basic problem (p1) is to maximize the final range with the common boundary conditions (above) and

$\gamma(0) = 0$ (specified) and	t_f – specified.	(2.13)

We may view the values of E_f and t_f as parameters and thus problem p1 leads to a two-parameter family. Of particular interest are those members where t_f is left open (i.e. unspecified). This one-parameter family of problems is denoted p2.

Finally, we shall investigate a modified problem, wherein the initial path-angle is open and the final time specified

$$\gamma(0) - \text{ open and} \qquad t_f - \text{ specified.} \tag{2.14}$$

This two-parameter family of problems is denoted p3.

In chapter 5, while computing the feedback gains for the neighboring optimal guidance scheme, we consider a related optimal problem; a new, slightly different from problem p1, that provides the same control time-history as the basic problem. The objective in this new problem is to maximize the final energy for a specified range, the same maximum range that was found in the basic problem, while the other requirements remain same as above (problem p1).

Chapter 3: Optimal Trajectory

This chapter contains a study of optimal trajectories for midcourse guidance of an air-to-air missile that was introduced in the previous chapter. First, the existence of optimal solutions is discussed and necessary conditions based on Pontryagin's Minimum Principle [18] are derived. Next, a comprehensive study of the time-range-energy optimal problem is done.

3.1 Necessary Conditions

As indicated above our approach is to apply the Minimum Principle. Accordingly the variational-Hamiltonian is defined, the adjoint equations are derived, minimization of the Hamiltonian takes place and extremal solutions are obtained. It should be noted that the Minimum Principle is a statement of necessary conditions for optimality that allow one to narrow down the set of controls which may be optimal. A control satisfying the necessary conditions is called an ex-

tremal control; it is a candidate for optimality. Thus, an optimal control must be extremal, but an extremal control is not necessarily an optimal one.

Once the set of all extremal controls has been deduced there are, at least, two ways to proceed. If a sufficiency theorem is available, one could attempt to verify that some of the extremal candidates are optimal (perhaps only locally). Alternatively, if the set of candidates is small, it is tempting to evaluate the performance along each, and then simply to compare the results. For this approach to be rigorous one must also know that an optimal solution exists.

The approach taken here is the latter one. Since the extremal solutions are unique (at least we are only able to find one), this must be the optimal solution, provided such solution exists. To establish existence the following theorem is used:

Consider the following nonlinear process

$$\dot{X} = f(X, U, t) \tag{3.1}$$

in a time interval $[t_o, t_f]$ *with the initial conditions* $X(t_o) = X_o$ *, a target set* $X(t_f) \in \Theta_f$ *a control constraint set* $U(t) \in \Omega$ *and the cost for each* $U(t) \in \Omega$ *is* $C(U)$. *Assume that there exists a uniform bound for all responses* $X(t)$ *to controllers* $U(t) \in \Omega$ *and that the velocity set*

$$V(X, t) = \{f(X, U, t) \mid U \in \Omega(X, t)\} \tag{3.2}$$

is convex for each fixed (X,t).

Then there exists an optimal controller $U^*(t)$ *on* $[t_o, t_f]$ *in* Ω *minimizing* $C(U)$.

This existence theorem is actually an adaptation of the existence theorem in Lee and Markus ([63], theorem 4, chapter 4, pp. 259-262) The key issue in this theorem is the convexity of the velocity set (also called the hodograph space [64-65]). Although, for most problems the proof of existence of an optimal control is difficult, it can be shown for the problem in our study by applying the hodograph space technique (see for example Marec [64] or Vinh [65]) that helps to verify convexity. The hodograph space is usually used in conjunction with the Minimum Principle to find optimal solutions or at least to find if optimal solution exists.

With this background we are able to establish the velocity set for the problem in study and to verify convexity. First, the state X and time t are fixed, then, the control domain $\Omega(X, t)$ is transformed to the velocity set. Doing so one gets the maneuverability domain which is the instantaneously useable domain in the hodograph space. While constructing this hodograph space one might observe that the control appears only in the equations for $\dot{E}$ and $\dot{\gamma}$ (see equations (2.1) - (2.9)). Thus, the hodograph space for this problem consists basically of the drag polar expressed in the $\dot{E}$, $\dot{\gamma}$ plane. To be more specific $\dot{E}$ is an affine function of the drag ($\dot{E} = a + b\, D(n)$ where a and b are constants) and $\dot{\gamma}$ is an affine function of the lift. It is clear that such a domain is not convex, hence, according to the existence theorem, optimal solutions may not exist. However, one may overcome this difficulty by relaxing the controls [63-65], which means allowing chattering controls. This is the same as adding points to the maneuverability domain to obtain the convex hull (the smallest convex domain that contains the original do-

main). Chattering controls are high consumers of energy, hence, such controls are not in the interest of this study and consequently avoided. The occurrence of chattering controls and their relation to the energy co-state will be discussed later in this section.

Now we present a short discussion on the way of including the coast parameter t_c in our optimal problem setting. The coast parameter can be included in several different ways. In one approach t_c can be treated as a state-variable by formally augmenting a trivial differential equation, $\dot{t}_c = 0$. The right-hand side of the system (equations (2.3) through (2.6)) depends on the 'state' t_c through the thrust and the weight (i.e. $T(h, t, t_c)$ and $W(t, t_c)$). This approach for including free-parameters in the optimal control-setting is discussed in [18,pp. 190], for example. In this case , however, the system ((2.3)-(2.6)) depends on t_c in a **discontinuous** way. Additionally, the admissible values for t_c are restricted [$t_c \geq 0$] so that some type of constraint may be needed. For these reasons the approach used here is simply to analyze the solutions for a range of t_c values and read-off the minimizer from this sub-family.

The general variational-Hamiltonian is defined as follows:

$$H(\lambda_X, X, U, t) = \lambda_X \bullet f(X, U, t) \tag{3.3}$$

where λ_X is the co-state variable vector. The variational-Hamiltonian for our example is defined as follows:

$$H(\lambda_X, X, U, t) = \lambda_x V(h, E) \cos\gamma + \lambda_E \frac{V(h, E)}{W(t, t_c)} [T(h, t, t_c) - D(h, E, n)]$$

$$+ \lambda_h V(h, E) \sin\gamma + \lambda_\gamma \frac{g}{V(h, E)} [n - \cos\gamma] \tag{3.4}$$

where

$$\lambda_X = [\lambda_x \ \lambda_E \ \lambda_h \ \lambda_\gamma]^T \tag{3.5}$$

Next, we present a brief derivation of the necessary conditions for the missile-example. The co-state variables are governed by the adjoint equations, viz:

$$\dot{\lambda}_X = -\frac{\partial H}{\partial X} \tag{3.6}$$

For the missile-example case we get

$$\dot{\lambda}_x = 0 \tag{3.7}$$

$$\dot{\lambda}_E = -[\lambda_x \cos\gamma + \lambda_h \sin\gamma - \lambda_\gamma \frac{g}{V^2}(n - \cos\gamma) + \lambda_E \frac{(T - D)}{W}] \frac{\partial V}{\partial E}$$

$$+ \lambda_E \frac{V}{W} \frac{\partial D}{\partial E} \tag{3.8}$$

$$\dot{\lambda}_h = -\left[\lambda_x \cos\gamma + \lambda_h \sin\gamma - \lambda_\gamma \frac{g}{V^2}(n - \cos\gamma) + \lambda_E \frac{(T-D)}{W}\right] \frac{\partial V}{\partial h}$$

$$-\lambda_E \frac{V}{W}\left(\frac{\partial T}{\partial h} - \frac{\partial D}{\partial h}\right) \tag{3.9}$$

$$\dot{\lambda}_\gamma = \lambda_x V \sin\gamma - \lambda_h V \cos\gamma - \lambda_\gamma \frac{g}{V} \sin\gamma \tag{3.10}$$

The Minimum Principle requires that an optimal control (here the optimal load factor, n^*) must minimize the variational-Hamiltonian, which leads to:

$$\min_{U\in\Omega} H(\lambda_X, X, U, t) = \min_{|n| \le \min(n_{max}, n_L)} \left[\lambda_\gamma \frac{g}{V} n - \lambda_E \frac{V}{W} D(h, E, n)\right] \tag{3.11}$$

In principle, one uses this condition to solve for an extremal control, n^*. For the drag-polar given in the appendix, the result is:

$$n^* = -sign(\lambda_\gamma)\left[\frac{g}{\rho V^2 D_i}\left|\frac{\lambda_\gamma}{\lambda_E}\right|\right]^{\frac{1}{p-1}} \tag{3.12}$$

Of course, one should check that the extremal control satisfies the constraints and that the control actually minimizes the Hamiltonian function. The latter condition can be verified by using the hodograph space which in the present example, can be identified with the $\dot{E}, \dot{\gamma}$ plane. In this plane the the maneuverability domain is based on the convex hull that contains the drag polar. In the hodograph space different values of the Hamiltonian for fixed $\lambda\gamma$ and λ_E are re-

presented by straight lines. The line that minimizes the Hamiltonian and is tangent to the maneuverability domain can be obtained only for a negative λ_E.

The final aspect of the Minimum Principle is the boundary conditions on the co-states [transversality conditions]. While certain of these conditions will be different for the various problems [p1, p2 and p3] , a number of them are common:

$$\lambda_x(t_f) = -1$$

$$\lambda_y(t_f) = 0$$

$$E(t_f) = E_f \quad \text{or} \quad \lambda_E(t_f) = 0 \tag{3.13}$$

The $E - \lambda_E$ boundary condition is complicated because of the **inequality** nature of the condition. In practice one solves the problem with the specified value of $E(t_f)$ and then checks the corresponding co-state $\lambda_E(t_f)$. If this is negative then the solution is extremal, else one must re-solve with $\lambda_E(t_f) = 0$ (natural) boundary condition. This will arise if the specified bound E_f is less than the **natural** value [i.e. $E(t_f)$ with $\lambda_E(t_f) = 0$], so the inequality end-condition is not active. Chattering solutions may be obtained for **equality** constraint on the final energy with a specified bound E_f less than the natural value, for such a case one gets $\lambda_E(t_f) > 0$.

3.2 Numerical Results

The two-point boundary value problem described above is solved numerically using the computer code **BOUNDSCO** [54]. The code implements a **multiple-shooting** algorithm in which the independent-variable interval [0 , t_f] is broken into sub-intervals. For our missile-example problem the interval knot-points were placed at end-of-boost, beginning and end-of-sustain and several points between them and between end-of-sustain and the final-time. The algorithm requires that one provide initial estimates for all dependent variables [states and co-states] at the left end of each sub-interval. These are then iteratively adjusted so that the specified end-conditions are met at zero and at t_f and so that dependent variables are continuous at the knot-points. In our missile-example application it was difficult to obtain estimates for the variables that were within the 'domain of attraction' for the algorithm. In fact, solutions obtained for a reduced-order model (presented later in 4.2), where induced-drag is approximated with a constant load factor, were used as an initial estimates for the point-mass model.

A set of results for this problem without a coasting phase ($t_c = 0$) is presented in Figures 1 through 5. Shown in Figures 1 and 2 are graphs of an extremal trajectory for the basic problem p1 with the following boundary conditions: $t_f = 150\ sec.$, $h_o = 20\ Kft.$, $E_o = 52.8\ \ Kft.$, $\gamma_o = 0$, $h_f = 20\ Kft.$ and $E_f = 140\ Kft.$ These produce an initial and final speed of $1450\ ft/sec.$ and $2767\ ft/sec.$, respectively. Note from Figure 1 that the extremal trajectory exhibits a fair amount of lofting; the peak altitude is over 100 Kft. As shown in Fig. 1e the load factor is

initially quite large but exhibits a rapid decrease after the end of the sustain phase (~10*sec.*). For much of the trajectory the flight is nearly ballistic. There is an interesting transient near the end of the flight; at t_f the co-state λ_γ must vanish (transversality) and so one has $n^*(t_f)$ equal zero. For this case the final condition on energy is binding, that is, one finds that $E(t_f) = 140\ Kft(= E_f)$.

These calculations were repeated for a range of values of the final time parameter, t_f and the final energy E_f. The representative results for this two-parameter family are shown in Figure 3.

Also of interest is the problem (p2) with final time open. This is actually a one-parameter family with parameter E_f. Note that for a given E_f the solution to this problem (p2) will be the peak of the curve generated by t_f-family of problem p1. Displayed in Figure 4 are the results for a range of values of E_f.

As noted, one of the more interesting features of the extremal trajectories is the amount of lofting and the attendant early, rapid change in path angle (cf Fig. 1c). At the beginning of this study we thought that this feature might lead to an idealization suitable for the closed-loop synthesis (see also chapter 3). Shown in Figure 5 are results of the problem with free initial path-angle (p3) for a range of t_f values with $E(t_f)$ open. From a comparison of the range obtained in p1 and p3 one may notice that, a greater range might be obtained with a pre-maneuver made by the launching aircraft, even if the pre-maneuvering time is taken into account, this aspect has not been investigated further.

Shown in Figures 6 and 7 are graphs of an extremal trajectory for the basic problem, with a coasting phase. The coasting time and the following data are

used there: $t_c = 15\ sec.$, $t_f = 150\ sec.$, $h_o = 20\ Kft.$, $E_o = 52.8\ Kft.$, $\gamma_o = 0$, $h_f = 20\ Kft.$ and $E_f = 125\ Kft$. These produce an initial and final speed of $1450\ ft/sec.$ and $2600\ ft/sec.$, respectively.

Fig. 8 presents results with a range of coast-times for several specified final times (100, 150 and 200 sec.). It is clear that, at least for the range considered, the inclusion of a coast-arc reduces the range. Moreover, it appears that 'negative' coast-times may be of interest, provided one can make sense of the idea.

It is clear from Fig. 6d that the energy achieves a maximum-value at the end of the sustain phase. In general, one expects that for reasonable values of the sustain thrust level the energy would be increasing on the sustain arc, but, depending on the length of the coast-arc, the peak energy at the end-of-sustain may be only a local maximum. These observations lead one to speculate that a coast-arc might be necessary if the specified final energy was sufficiently high. The question is whether this feature arises for 'reasonable' values of the parameters E_f and t_f . Shown in Fig. 9 are results of a study of maximum-range against specified final energy for several values of t_c . In all these results $t_f = 150\ sec.$ For these parameter values the best performance is achieved with zero coast. From these results it is clear that, an inclusion of a coasting phase produces smaller maximum-range, which is in contradiction with the results obtained in Ref. [14]. To clarify these differences a study of the maximum-range problem, with the **energy model** (used in [14]) was done. In this case it was found that an inclusion of a coasting phase generates greater maximum-range, which is in agreement with the results in [14]. It is obvious from these results that the use of the energy model in missile flight

performance optimization gives bad approximation that might produce misleading results (see also chapter 4).

These results and a comparison between energy histories for two cases where $t_c = 0$ and $t_c > 0$ motivated a study of the case where the sustain phase is perturbed. Shown in Fig. 10c are graphs of energy histories, two of them present the cases described previously. Note that for the case with the coast- arc, the energy decreases very sharply and a 'big gap' is developed between the two energy graphs during the coast phase. Observing these results one expects that 'filling the gap' might improve the maximum-range performance. A study was done of several cases where the sustain phase is changed. In all of these cases the total impulse is kept constant, while the sustain thrust and duration are perturbed by ΔT_s and Δt_s respectively. Cases where ΔT_s gets positive and negative values (while Δt_s gets values with the opposite sign) were studied. In each case studied the thrust in the sustain phase was kept constant in time. Figures 10 present an example from this study and compare the following three cases:

- the nominal **boost-sustain** propulsion ($t_c = 0$) ;
- **boost-coast-sustain** propulsion ($t_c = 5$ *sec.*);
- **boost-sustain** propulsion ($t_c = 0$) with a sustain phase $\Delta t_s = 5$*sec.* longer.

Note that in the last case the sustain phase ends in the same time as in the coasting (second, $t_c = 5$) case. These two cases represent an 'equivalent' thrust-time distribution. In Fig. 10b and 10c the range and altitude vs. time are presented. These results show that, lowering the sustain thrust level instead of including a coast phase, produces larger maximum-range. An explanation to this

might be found in Figures 10a and 10c. One can notice that at the end-of-sustain phase, the non- coasting missile performs better than the coasting one, it has higher altitude and greater energy. It was also found, in other examples (not shown here), that, an increase of the sustain thrust (accompanied by a decrease of the duration in a way that keeps the total impulse constant), reduces the range.

Chapter 4: Reduced Order Models

Since the beginning of optimal flight and in particular trajectory optimization, there has been great interest in approximations featuring simplified vehicle models. Reduced-order modelling is very attractive to the analyst in solving optimal control problems. It is motivated by the considerable difficulties encountered in computing optimal trajectories with the detailed system model and also by possible use in the synthesis of near-optimal closed-loop control laws. As mentioned earlier, an application of the Minimum Principle leads to a TPBVP involving several unknown dependent variables. A reduction in system order simplifies the numerical computations; it also reduces the number of unknown parameters that have to be guessed while employing iterative methods.

Such a reduction in system order may be obtained via the singular perturbation method [19], a technique that employs a time-scale separation of the state variables into fast and slow state variables. The singular perturbation method is applied in two out of three of the reduced-order approximations studied in this

chapter, while in the third an approximation of the induced-drag is used. A brief introduction to the singular perturbation approach is presented in section 4.1.

One of the interesting features of the extremal trajectories, shown in the previous chapter, is the amount of lofting and the attendant early, rapid change in path angle. The idea that this feature might lead to an idealization suitable for the closed-loop synthesis motivated the study (presented in 4.2) of a singularly perturbed model with γ as fast variable. Breakwell employed a similar approach in several studies of minimum-time airplane climb problems [27-28].

Another interesting property of the extremal trajectories is that after an initial high-g pullup and a rapid change in path-angle, the trajectories are almost ballistic. This behavior motivated the investigation of a point-mass model with an approximation of the induced-drag (presented in section 4.3). This study is similar to the study of the minimum-time airplane climbs, presented in Refs. [27] and [28], but with some modifications.

The earliest and most well-known approximation in flight optimization is that of the energy-state. The energy model began as an ad hoc approximation [44-46] and found a theoretical basis in singular perturbation theory by Kelley in [20-26]. Energy-state has played an important role in the development of singular perturbation theory applied to optimal control problems. The energy-model is studied in section 4.4.

With this background, it is the objective of this chapter to investigate the best-range guidance using reduced-order models. A study of best-range guidance problem employing the following reduced-order models is presented:

- Singular perturbation with γ as fast variable.
- Point mass model with an approximation of the induced-drag;
- Energy model - γ and h as fast variables.

Extremal trajectories are computed for these reduced-order models, and compared to the 'exact' (point-mass model) trajectory.

4.1 An introduction to the singular perturbation theory

In this section we present a brief introduction to the singular perturbation theory. Most of the material in this introduction is based on the following References: Kelley [26], Ardema [30] and Visser [41].

As indicated before, application of the necessary conditions leads to the TPBVP that in many applications is of great complexity. A reduction of system order simplifies the computations. Such reduction can be obtained by employing the singular perturbation technique. This approach takes advantage of the time-scale separation of the state variables, by separating the dynamics into fast and slow modes with corresponding 'inner' and 'outer' solutions. The solution of the reduced-order system is modified near one or both end-points by a 'boundary-layer' correction, also calculated via a system of differential equations of lower order than that of the original system.

The method of singular perturbations was originally developed [19] to be used with initial-value problems described by ordinary differential equations and in-

volving a small parameter ε in such way that if the parameter becomes zero, the order of the dynamic system is reduced.

To present some of the basic features of singular perturbation theory we consider as an introductory example the following nonlinear initial-value problem

$$\frac{dx}{dt} = f(x, y, t); \quad x(\varepsilon, t_o) = x_o$$

$$\varepsilon \frac{dy}{dt} = g(x, y, t); \quad y(\varepsilon, t_o) = y_o$$

where x and y are scalar functions and $\varepsilon > 0$ is a 'small' scalar parameter. If ε has its actual value the system is termed 'exact' and if $\varepsilon = 0$ the system is called 'reduced'. In the terminology of singular perturbation theory x is called the slow variable and y is called the fast variable.

It is clear that for $\varepsilon = 0$ the initial condition for y cannot be satisfied. The most obvious way to meet the boundary condition on y is to allow a discontinuity at $t = t_o$. From optimal control theory it is known that control variables can be discontinuous. The occurrence of jumps in the fast state variables may suggest that fast states can play the role of controls in the reduced system.

The loss in boundary condition can be accounted for by boundary layer solutions. In the boundary layers stretched time-scales are used, allowing the fast variable to change rapidly, while the slow variable is 'frozen'. The boundary layer solutions are good representations of the exact solutions near the end-points, while the reduced solution is a good representation of the exact solution far away from the end-points.

To obtain solutions of a singularly perturbed optimal control problem a procedure called Matched Asymptotic Expansion (MAE) is employed. In this method, separate solutions are obtained for inner and outer regions by using asymptotic expansion techniques. These solutions are matched in an overlap region of common validity. The most common asymptotic expansion is to expand all the variables in asymptotic power series in ε. Expansion of the state variables for the inner and outer layers in our introductory example can be described as follows:

$$x^o(\varepsilon, t) = x_0^o(t) + \varepsilon x_1^o(t) + \varepsilon^2 x_2^o(t) + \varepsilon^3 x_3^o(t) + \cdots$$

$$y^o(\varepsilon, t) = y_0^o(t) + \varepsilon y_1^o(t) + \varepsilon^2 y_2^o(t) + \varepsilon^3 y_3^o(t) + \cdots$$

$$x^i(\varepsilon, \tau) = x_0^i(\tau) + \varepsilon x_1^i(\tau) + \varepsilon^2 x_2^i(\tau) + \varepsilon^3 x_3^i(\tau) + \cdots$$

$$y^i(\varepsilon, \tau) = y_0^i(\tau) + \varepsilon y_1^i(\tau) + \varepsilon^2 y_2^i(\tau) + \varepsilon^3 y_3^i(\tau) + \cdots$$

here the superscripts ^{o} and ^{i} represent the outer and inner solutions respectively, τ is the stretched time in the boundary layer and the subscripts $_{0,1,\ldots}$ stand for the order of the solution. In this work only the zero-th order solutions is used.

4.2 Singular perturbation with path-angle as a fast variable

As indicated earlier, the extremal trajectories exhibit a fair amount of lofting and a rapid change in path-angle at the initial phase of flight. The idea that it might

lead to an idealization suitable for the closed-loop synthesis motivated the study presented in this section.

4.2.1 System model

For a vehicle modelled with γ as a fast variable the singular perturbation vertical-plane model may be described by:

$$\dot{x} = V\cos\gamma \tag{4.1}$$

$$\dot{E} = \frac{V}{W}(T - D) \tag{4.2}$$

$$\dot{h} = V\sin\gamma \tag{4.3}$$

$$\varepsilon\dot{\gamma} = \frac{g}{V}(n - \cos\gamma) \tag{4.4}$$

Range as a performance index, the system equations (4.1)-(4.4) and the boundary conditions of problem p1 (see equation (2.12)) define a singularly perturbed optimal problem. In this problem γ is the fast variable and x, E and h are the the slow variables.

4.2.2 Necessary Conditions

A brief derivation of the necessary conditions, for the missile-example, is presented next. Our approach is to apply Pontryagin's Minimum Principle.

The variational-Hamiltonian is defined as before:

$$H(\lambda_X, X, U, t) = \lambda_x V(h, E)\cos\gamma + \lambda_E \frac{V(h, E)}{W(t, t_c)}[T(h, t, t_c) - D(h, E, n)]$$

$$+ \lambda_h V(h, E)\sin\gamma + \lambda_\gamma \frac{g}{V(h, E)}[n - \cos\gamma] \tag{4.5}$$

the adjoint equations are expressed as follows:

$$\dot{\lambda}_x = 0 \tag{4.6}$$

$$\dot{\lambda}_E = -[\lambda_x \cos\gamma + \lambda_h \sin\gamma - \lambda_\gamma \frac{g}{V^2}(n - \cos\gamma) + \lambda_E \frac{(T - D)}{W}]\frac{\partial V}{\partial E}$$

$$+ \lambda_E \frac{V}{W}\frac{\partial D}{\partial E} \tag{4.7}$$

$$\dot{\lambda}_h = -[\lambda_x \cos\gamma + \lambda_h \sin\gamma - \lambda_\gamma \frac{g}{V^2}(n - \cos\gamma) + \lambda_E \frac{(T - D)}{W}]\frac{\partial V}{\partial h}$$

$$-\lambda_E \frac{V}{W}\left(\frac{\partial T}{\partial h} - \frac{\partial D}{\partial h}\right) \tag{4.8}$$

$$\varepsilon\dot{\lambda}_\gamma = \lambda_x V \sin\gamma - \lambda_h V \cos\gamma - \lambda_\gamma \frac{g}{V}\sin\gamma \tag{4.9}$$

The way one can get the adjoint equations is presented in [41] (and in many other publications).

Minimization of the variational-Hamiltonian, leads to:

$$\min_{U\in\Omega} H(\lambda_X, X, U, t) = \min_{|n| \le \min(n_{max}, n_L)} \left[\lambda_\gamma \frac{g}{V} n - \lambda_E \frac{V}{W} D(h, E, n)\right] \tag{4.10}$$

The final aspect of the Minimum Principle is the boundary conditions on the co-states. The transversality conditions for the slow variables are same as presented earlier (see chapter 3 equation (3.13)) which means $\lambda_x(t_f) = -1$ and $E(t_f) = E_f$ or $\lambda_E(t_f) = 0$.

4.2.3 The outer solution

The reduced-order solution for the drag-polar given in the appendix is obtained by setting $\varepsilon = 0$ in (4.4) and in (4.9). Doing so one gets three algebraic equations, (4.4), (4.5) and (4.10), that have the following outer solution:

$$n^o = \cos\gamma^o \tag{4.11}$$

$$\gamma^o = \tan^{-1}\left(-\frac{\lambda_h^o}{1 + \frac{\lambda_\gamma^o}{g}}\right) \tag{4.12}$$

$$\lambda_x^o = -1 \tag{4.13}$$

$$\lambda_\gamma^o = \lambda_E^o p \frac{g}{W} \mid n^o \mid^{p-1} \tag{4.14}$$

Here again, the super script $^\circ$ represents the outer solution. Equations (4.1) through (4.3) and equations (4.6) through (4.8) combined with the solutions (4.11) - (4.14) and with the boundary conditions define a reduced-order TPBVP. This problem can be solved numerically using the multiple-shooting scheme. However, it appears that the control variable can be obtained only through an additional iteration procedure, using iteratively equations (4.11) - (4.14), to solve for the variables n, γ and λ_γ for given h, E, λ_h and λ_E.

4.2.4 The inner solution

The boundary layer equations are obtained by introducing a stretching transformation into the state and the co-state equations. This allows the fast variables to change rapidly while the slow variables are 'frozen' and receive the end-points values of the outer solution. Thus, the slow variables remain constant in the boundary layer.

For the drag-polar given in the appendix the extremal control is:

$$n^i = -sign(\lambda_\gamma^i) \left[\frac{g}{\rho (V^o)^2 D_i^o} \mid \frac{\lambda_\gamma^i}{\lambda_E^o} \mid \right]^{\frac{1}{p-1}} \tag{4.15}$$

here again, the super script ^{i} represents the inner solution. Equations (4.4) and (4.9) combined with the solutions (4.15) and with the boundary conditions introduce a reduced-order TPBVP for the boundary layer.

In the boundary layer control law, the frozen end-points conditions of the slow variables can be replaced by the current value of the slow variables, which makes the control law a feedback law. This feedback law is used in the numerical example presented in 4.2.6.

4.2.5 Composite solution

In the case of problem p1 the initial path-angle is specified, but, the initial path-angle obtained as a solution of the outer layer cannot be the same, hence, an initial boundary layer exists and is found as a solution of TPBVP with γ specified on both end-points. It can be also shown that a final boundary layer exists. This observation is based on the following facts:

- the path-angle at the final time is free, which means $\lambda_{\gamma}(t_f) = 0$;
- $\lambda_{\gamma}(t) \neq 0$, for the outer solution.

The final boundary layer is a TPBVP with $\lambda\gamma$ specified on both end-points. To construct a composite solution the variables γ and $\lambda\gamma$, in the inner and outer layers at both end-points must be matched.

4.2.6 Numerical results

The combined inner-outer solutions to the problem are obtained numerically through two iteration processes. The first process solves at each integration step for n^o, λ_γ^o and γ^o from equations (4.11)-(4.14). The second solves the matched inner outer problem which also is a TPBVP.This is done using the multiple-shooting computational approach [54], and employing the boundary layer extremal control law, based on the current value of the slow variables. As a result of these two computational processes it is very difficult to obtain numerical solutions with this scheme, although, this singular-perturbation problem has less states.

As a result of these difficulties and since the final boundary layer does not affect the outer solution and hence the initial boundary layer, only the initial boundary layer is calculated and matched to the outer solution in our numerical example.

Results for problem p1 computed with this reduced-order model, are shown and compared to other models (including the point-mass model), in Figures 11. It can be observed in Figures 11b and 11c that, in the initial boundary layer this model performs quite well. The resulting path-angle and load-factor are close to those of the point-mass model. However, the outer solution is not so good. It is clear from these results that this model is **not** good enough to be used as an approximation of the exact optimal trajectory.

4.3 Point-mass model with an approximation of the induced-drag

After an initial high-g pullup and a rapid change in path-angle the extremal trajectories are almost ballistic. This behavior motivated the study of the point-mass model where the induced-drag is modelled with a constant load factor. In this approximation the constant load factor might get different values, varying from zero to the load factor limits.

4.3.1 System equations

For a missile modelled as a point-mass with an approximation of the induced-drag using a constant load factor (n_c) , the system equations may be described by:

$$\dot{x} = V \cos \gamma \tag{4.15}$$

$$\dot{E} = \frac{V}{W} [T - D_o - D_i(h,E,n_c)] \tag{4.16}$$

$$\dot{h} = V \sin \gamma \tag{4.17}$$

$$\dot{\gamma} = \frac{g}{V} (n - \cos \gamma) \tag{4.18}$$

In these equations the functional dependence of the induced drag is changed by using a constant parameter n_c instead the control variable n, while the functional dependence of D_o , T, V and W remains the same as before.

The system equations, the boundary conditions of problem p1 and range maximization as a performance index introduce a new optimal control problem.

4.3.2 Necessary Conditions

The variational-Hamiltonian is defined as before:

$$H(\lambda_X, X, U, t) = \lambda_x V(h, E)\cos\gamma + \lambda_E \frac{V(h, E)}{W(t, t_c)}[T(h, t, t_c) - D(h, E, n_c)]$$

$$+ \lambda_h V(h, E)\sin\gamma + \lambda_\gamma \frac{g}{V(h, E)}[n - \cos\gamma] \tag{4.19}$$

The co-state variables are governed by the following equations:

$$\dot{\lambda}_x = 0 \tag{4.20}$$

$$\dot{\lambda}_E = -[\lambda_x \cos\gamma + \lambda_h \sin\gamma - \lambda_\gamma \frac{g}{V^2}(n - \cos\gamma) + \lambda_E \frac{(T - D)}{W}]\frac{\partial V}{\partial E}$$

$$+ \lambda_E \frac{V}{W}\frac{\partial D}{\partial E} \tag{4.21}$$

$$\dot{\lambda}_h = -[\lambda_x \cos\gamma + \lambda_h \sin\gamma - \lambda_\gamma \frac{g}{V^2}(n - \cos\gamma) + \lambda_E \frac{(T - D)}{W}]\frac{\partial V}{\partial h}$$

$$-\lambda_E \frac{V}{W}\left(\frac{\partial T}{\partial h} - \frac{\partial D}{\partial h}\right) \tag{4.22}$$

$$\dot{\lambda}_\gamma = \lambda_x V \sin\gamma - \lambda_h V \cos\gamma - \lambda_\gamma \frac{g}{V} \sin\gamma \tag{4.23}$$

Minimization of the variational-Hamiltonian, leads to:

$$\min_{U\in\Omega} H(\lambda_X, X, U, t) = \min_{|n| \le \min(n_{max}, n_L)} [\lambda_\gamma \frac{g}{V} n] \tag{4.24}$$

4.3.3 The singular and non-singular sub-arcs solutions

Since the control variable (n) appears linearly in (4.24) and n is bounded, the extremal control solution can be obtained as follows:

$$\text{If } \lambda_\gamma \equiv 0 \quad \text{then} \quad -\min(n_{max}, n_L) < n < \min(n_{max}, n_L) \tag{4.25}$$

$$\text{If } \lambda_\gamma \not\equiv 0 \quad \text{then} \quad n = -\min(n_{max}, n_L)\ \text{sign}\ (\lambda_\gamma) \tag{4.26}$$

It appears here that λ_γ is a switching function, if it crosses zero at a certain time then the control jumps from one bound to the other and this time point is called **switching point.** In the case where $\lambda_\gamma = 0$ over a finite interval of time the control gets an intermediate value that lies between its bounds and is called a **singular control.** The part of the trajectory with the singular control is termed **singular arc** and the problem of determining the singular control is called **singular control problem** (for more details on this problem see Bell and Jacobson [58]).

An extremal control trajectory in the nonsingular region may be obtained by integrating the system equations (4.15) - (4.18) and using the control law (4.26). The singular arc must satisfy (4.25) on a finite interval of time, which means that all the time derivatives of λ_γ must be zero

$$\dot{\lambda}_\gamma \equiv \ddot{\lambda}_\gamma \equiv \dddot{\lambda}_\gamma \equiv \cdots \equiv 0 \tag{4.27}$$

To determine the singular control one has to differentiate the switching function (here λ_γ) with respect to time until the control appears explicitly with a coefficient which is not identical zero [57-58]. If $2q$ time derivatives are required, then the **order** of the singular arc is q, it can be shown that the singular control first appears only on even derivatives.

The singular control is found in this singular problem as follows. First, we substitute $\lambda_\gamma = \dot{\lambda}_\gamma = 0$ and $\lambda_x = -1$ into (4.23) and solve for γ.

$$\gamma = \tan^{-1}(-\lambda_h) \tag{4.28}$$

Next, we substitute $\lambda_\gamma = \dot{\lambda}_\gamma = 0$ and the solution of γ from (4.28) into expression from the second time derivative of λ_γ. The singular control appears explicitly in this second derivative hence, the order of singularity is **one** . The extremal control law for the singular sub-arc is given by the following expression:

$$n = \frac{V}{g}\cos^2\gamma\left[\left(-\frac{1}{\cos\gamma} + \lambda_E \frac{(T-D)}{W}\right)\frac{\partial V}{\partial h} + \lambda_E \frac{V}{W}\left(\frac{\partial T}{\partial h} - \frac{\partial D}{\partial h}\right)\right]$$

$$+ \cos\gamma \tag{4.29}$$

provided the value of n is between its boundaries.

Kelley in [55-57] introduced new necessary condition for singular optimal control. This is the generalized Legendre-Clebsch condition known also as Kelley-Contensou test [56]. Kelley-Contensou test was applied to the optimal solution obtained above and was found to satisfy the strengthened necessary condition

$$-\frac{\partial}{\partial n}\left[\frac{d^2}{dt^2}\left(\frac{\partial H}{\partial n}\right)\right] = \frac{g^2}{V\cos\gamma} > 0 \tag{4.30}$$

provided $\cos\gamma > 0$, a condition that is satisfied by the definition of the path-angle.

The joining of singular and non-singular arcs generally involves a jump in the singular control variables. This jump produces a **broken extremal** or a **corner,** in which Erdmann corner condition [18,59,60] must be satisfied. This condition requires that all the co-state variables be continuous at an junction point. Additionally, the McDanell-Powers junction conditions [61] apply at the junction of singular and non-singular arcs. One can prove, with the use of theorem 3 in [61], that the optimal control in our problem is discontinuous at the junction point. As already indicated, the degree of singularity in this problem is **one** . It can be also shown that, in the neighborhood of the junction, on the non-singular sub-arc, the following exists

$$\frac{d^2}{dt^2}\left[\frac{\partial H}{\partial n}\right] \neq 0 \tag{4.31}$$

Both, singularity degree and (4.31) are essential elements to prove existence of discontinuity at the junction point.

The system equations (4.16) - (4.19), co-state equations (4.20) - (4.22) combined with the solutions (4.25) - (4.26) and (4.28) - (4.29) and with the boundary conditions of the basic problem form a new TPBVP. In this new problem the singular and non-singular sub-arcs are joined.

4.3.4 Numerical results

The problem is solved numerically for several values of n_c , using the multiple-shooting method. Singular arc solutions are obtained easily, in fact, these solutions were used as initial guesses to find the first optimal trajectories with the point-mass model.

Results for this reduced-order model are shown and compared to other models in Figures 11. The following features are noticed in Fig. 11c: first, the load-factor receives at the beginning the aerodynamic limit value n_L and after a short period of time it reaches to the structural limit n_{max}; next, it jumps to a singular arc and remains on it until the final time; on the singular arc additional jumps occur due to the jumps in thrust at the end-of-boost and at the end-of-sustain, these jumps can be explained with the help of equation (4.30). It can be also observed in Figure 11c that there is no jump near the end-point which means that a nonsingular arc was not found near the end-point. This can be explained with the fact

that the path-angle is free at t_f or equivalently $\lambda_\gamma(t_f) = 0$, which is the same value of λ_γ on the singular arc.

4.4 Energy model

The earliest and most well-known approximation in flight optimization is that of the energy-state. This model has been appreciated since Kaiser's work [44], and found a theoretical basis in singular perturbation theory. In this model γ and h are the fast variable while x and E are the the slow variables.

The vertical-plane energy model can be described by:

$$\dot{x} = V\cos\gamma \tag{4.32}$$

$$\dot{E} = \frac{V}{W}(T - D) \tag{4.33}$$

$$\varepsilon\dot{h} = V\sin\gamma \tag{4.34}$$

$$\varepsilon\dot{\gamma} = \frac{g}{V}(n - \cos\gamma) \tag{4.35}$$

Range as a performance index, the dynamics equations (4.32)-(4.35) and the boundary conditions of problem p1 define a singularly perturbed optimal problem.

4.4.2 Necessary Conditions

A brief derivation of the necessary conditions, for the missile-example, is presented next. The variational-Hamiltonian was defined earlier in (4.5). The co-states must satisfy the following adjoint equations:

$$\dot{\lambda}_x = 0 \tag{4.36}$$

$$\dot{\lambda}_E = -\left[\lambda_x \cos\gamma + \lambda_h \sin\gamma - \lambda_\gamma \frac{g}{V^2}(n - \cos\gamma) + \lambda_E \frac{(T-D)}{W}\right]\frac{\partial V}{\partial E}$$

$$+ \lambda_E \frac{V}{W}\frac{\partial D}{\partial E} \tag{4.37}$$

$$\varepsilon\dot{\lambda}_h = -\left[\lambda_x \cos\gamma + \lambda_h \sin\gamma - \lambda_\gamma \frac{g}{V^2}(n - \cos\gamma) + \lambda_E \frac{(T-D)}{W}\right]\frac{\partial V}{\partial h}$$

$$-\lambda_E \frac{V}{W}\left(\frac{\partial T}{\partial h} - \frac{\partial D}{\partial h}\right) \tag{4.38}$$

$$\varepsilon\dot{\lambda}_\gamma = \lambda_x V \sin\gamma - \lambda_h V \cos\gamma - \lambda_\gamma \frac{g}{V}\sin\gamma \tag{4.39}$$

4.4.3 The outer solution

The reduced-order solution obtained by setting $\varepsilon = 0$ in (4.34), (4.35), (4.38) and (4.39). After doing so the following outer solution is obtained:

$$\gamma^o = 0 \tag{4.40}$$

$$n^o = 1 \tag{4.41}$$

$$\lambda_x^o = -1 \tag{4.42}$$

$$\lambda_h^o = 0 \tag{4.43}$$

$$\lambda_\gamma^o = \lambda_E^o \frac{(V^o)^2}{gW} \left(\frac{\partial D}{\partial n}\right)^o \tag{4.44}$$

Equations (4.32) through (4.33) and equations (4.36) through (4.37) combined with the solutions (4.40) - (4.44) and with the boundary conditions introduce a reduced-order TPBVP.

4.4.4 The inner solution

The boundary layer equations are obtained by introducing a stretching transformation into the state and the co-state equations. doing so indicates that the slow variables stay constant in the boundary layer. For the drag-polar given in the appendix the optimal control is:

$$n^i = -sign(\lambda_\gamma^i) \left[\frac{g}{\rho (V^o)^2 D_i^o} \left| \frac{\lambda_\gamma^i}{\lambda_E^o} \right| \right]^{\frac{1}{p-1}} \tag{4.45}$$

Equations (4.34) ,(4.35), (4.38) and (4.39) combined with the solution (4.45) and with the boundary conditions introduce a reduced-order TPBVP for the boundary layer.

4.4.5 Numerical results

Solutions to the outer problem may be obtained numerically through two iteration processes. The first one takes place at each integration step, h^o is solved to minimize the variational-Hamiltonian. The second solves the TPBVP using the multiple-shooting computational approach. Actually, it is much easier to exchange the multiple-shooting scheme with forward integration of the state-Euler equations, using the initial value of $\lambda_E(0)$ as a parameter; as a result, a family of extremals is obtained and a path that satisfies the energy requirement is found. Results for this model are shown and compared, to other models in Figures 11. It appears that the specified final energy in the missile-example, that was met by all three other models, cannot be met by any extremal obtained with the energy model. In this model the natural value of the final energy is much higher then the 'exact' one. Thus, in the energy model trajectory in the example shown in Figures 11 the inequality end-condition is active ($\lambda_E = 0$). The following four jumps are observed in Fig. 11a:

- Jump to the minimum altitude at $t = 0$;
- Jump at the end-of-boost;
- Jump at the end-of-sustain;

- Jump to the specified final altitude at t_f.

Although, boundary layer treatment for this jumps will smooth the trajectory, it is clear that such a trajectory is a bad approximation to the exact one. It is far away from being optimal and from engineering considerations it is unacceptable. These results lead to the conclusion that the energy model cannot be used to approximate optimal trajectories for the missile-example.

4.4 Comparison of the models

Using same boundary conditions, the following models are compared:

- Point mass ('exact');
- Singular perturbation with γ as fast variable;
- Point mass model with approximation of the induced-drag;
- Energy model.

Some time histories of several variables are compared in Figures 11: Figure. 11a presents the altitude, shown in Fig. 11b the path-angle and in Fig. 11c the optimal control is presented. From these results it is obvious that the energy model is a bad approximation. It is also clear that the other reduced-order models aren't good enough to approximate optimal trajectories for the boost-coast-sustain missile. Hence, optimal trajectories computed by using the point-mass model, are selected as the reference trajectories (**nominal**) for the closed-loop guidance scheme derived in the next chapter.

Chapter 5: Neighboring Optimal Trajectories

5.1 Fixed Final Time

In the previous chapters optimal open-loop solutions to the midcourse-guidance-problem based on four different models, have been obtained. In this chapter near-optimal trajectories, based on extremals computed using the point-mass model, are studied. We choose an optimal trajectory as a nominal reference trajectory and consider perturbations from it produced by small perturbations in the initial states $\delta X(t_o)$ and final conditions $\delta X(t_f)$ for a fixed final time. Kelley in [47] showed that the perturbed and the adjoint systems together form a linear, time-varying system and that the optimal problem of minimizing a performance index **"J is now abandoned in favor of minimizing the second-order approximation to J".**

The optimal control problem to be considered is based on linear, time-varying ordinary differential equations with a quadratic performance index. This prob-

lem is well known in the optimal control theory literature (see for example [62] or [66]) and belongs to an important class of optimal control known as Linear Quadratic (LQ) optimal control problems. It can be shown that for the LQ class of problems the optimal control law is a continuous linear time-varying function of the system states. The problem can be solved by using the Riccati differential equation, provided that the second partial derivative of the Hamiltonian (H_{UU}) is nonsingular for $[t_o, t_f]$ and that the Jacobi conjugate points condition is satisfied (for more details see [47]). The optimal control law one gets as a solution is a continuous linear feedback-type law and may be expressed as follows:

$$\delta U(t) = U_X(t)\delta X(t) + U_{Xf}(t)\delta X(t_f) \tag{5.1}$$

where δU is the optimal control vector function for the perturbed system, U_X and U_{Xf} are time-dependent functions known as the feedback gains. The near-optimal control law may be constructed in the following manner:

$$U(t) = U_{ref}(t) + \delta U(t) \tag{5.2}$$

here U is the near-optimal control vector function and U_{ref} is the reference control vector function.

5.2 Perturbed Final Time

In the previous section the fixed final time problem is presented and a feedback-type midcourse guidance neighboring the optimal trajectory is dis-

cussed. In this section the validity of the scheme is extended by incorporating also perturbations on the final time. We consider here the case where the final time is changed to a new specified time t_{fn}, where

$$t_{fn} = t_f + \delta t_f \tag{5.3}$$

here t_f is the nominal final time and δt_f is the known change in time.

A first order approximation for the terminal errors at t_{fn} is given by:

$$\delta X(t_{fn}) = \delta X(t_f) + f[X(t_f), U(t_f), t_f)\ \delta t_f \tag{5.4}$$

solving for $\delta X(t_f)$ one gets

$$\delta X(t_f) = \delta X(t_{fn}) - f[X(t_f), U(t_f), t_f)\ \delta t_f \tag{5.5}$$

next, substituting $\delta X(t_f)$ into the right hand side of the equation of δU we get

$$\delta U(t) = U_X(t)\delta X(t) + U_{Xf}(t)[\delta X(t_{fn}) - f[X(t_f), U(t_f), t_f)\ \delta t_f] \tag{5.6}$$

Now, one can compute the new feedback commands based on the given quantities $\delta X(t_{fn})$, δt_f and on f that is computed at t_f on the nominal trajectory. This procedure is the same as the previous one (the fixed final time scheme), but with modified final conditions. In the next sections, these schemes are implemented and tested on our midcourse-missile-guidance example.

5.3 Midcourse Guidance Law with Fixed Final Time

In the missile-guidance example the optimal law can be described by the following feedback guidance law:

$$n(t) = n_{ref}(t) + \delta n(t) \tag{5.7}$$

where $\delta n(t)$ is defined by:

$$\delta n(t) = N_x(t)\delta x(t) + N_h(t)\,\delta h(t) + N_\gamma(t)\delta\gamma(t) + N_E(t)\delta E(t)$$

$$+ N_{hf}(t)\delta h(t_f) + N_{Ef}(t)\delta E(t_f) \tag{5.8}$$

However, in optimal-guidance problem where the terminal range and altitude are specified it is more convenient to consider an 'equivalent' optimal control problem where the objective is to find a control function $n(\bullet)$ that maximizes the final energy $E(t_f)$ for a specified final range. The specified range for this new problem is the maximum range value that was found in the basic problem. The other boundary conditions remain the same. This new problem is equivalent to the basic one in the sense that it satisfies the same necessary conditions, provides the same control time-history and gives the same final energy. In this case the feedback part of the guidance law is:

$$\delta n(t) = N_x(t)\,\delta x(t) + N_h(t)\delta h(t) + N_\gamma(t)\delta\gamma(t) + N_E(t)\delta E(t)$$

$$+ N_{xf}(t)\delta x(t_f) + N_{hf}(t)\delta h(t_f) \tag{5.9}$$

There are several ways to calculate the feedback gains. In our approach we compute these gains by taking the partials of the control variable n with respect to the state variables and the final conditions with the time held constant. This is done by perturbing the state variables and the final conditions with positive and negative perturbations, re-solving numerically the TPBVP and using the central difference formula. The main reason for employing this computational method is that it uses the same numerical set up which was developed earlier to find optimal trajectories.

The six gains along the reference trajectory are shown as functions of time in Figure 12. Some observations concerning the behavior of those gains are notable. First, one can notice that the gains N_x and N_{xf} are identical, this is due to the fact that x is ignorable state. A state variable that does not appear on the right hand side of the dynamics equations and consequently does not appear in the Hamiltonian is termed an ignorable state. The state x does not appear on the right hand side of the dynamics equations, hence, one can translate any trajectory in the x direction without causing any change in the other state variables which means that x can be ignored. Next, it can be also noticed that N_h has almost the same values with opposite signs as N_{hf}. These gains are calculated using two different trajectories: a trajectory that starts at a perturbed initial altitude and ends at a nominal final altitude and a trajectory that starts at a nominal initial altitude and ends at a final perturbed altitude. For equal values (with opposite signs) of the initial and final perturbations, one may expect to get only small difference between the corresponding optimal controls and hence, to obtain almost

same gains values (with opposite signs). Finally, it can be observed that the gains are very large near the final time. Such behavior might cause difficulty when approaching the final time. This sensitivity of neighboring-optimal-guidance schemes close to the final time has been noted in the literature (see Refs. [49-53]). However, it is assumed here that a terminal guidance law, such as proportional navigation or more advanced guidance scheme, is employed to accomplish the end game.

5.4 Midcourse Guidance Law with Perturbed Final Time

In the previous section a fixed final time midcourse guidance law is presented. In this section the validity of the guidance scheme is extended by incorporating perturbations on the final time. We consider here the case where the final time, is changed to a new specified t_{fn} and with new specified perturbations on the final range and altitude ($\delta x(t_{fn})$ and $\delta h(t_{fn})$).

In this case the feedback part of the guidance law is:

$$\delta n(t) = N_x(t)\,\delta x(t) + N_h(t)\delta h(t) + N_\gamma(t)\delta\gamma(t) + N_E(t)\delta E(t)$$

$$+ N_{xf}(t)[\delta x(t_{fn}) - V(t_f)\cos\gamma(t_f)\delta t_f] + N_{hf}(t)[\delta h(t_{fn}) - V(t_f)\sin\gamma(t_f)\delta t_f] \quad (5.10)$$

This guidance law is the same as the previous one (the fixed final time law), but with modified final conditions. The various terms in (5.10) may be evaluated in several ways. In our simulations the computations are done as follows. The

nominal trajectory and the corresponding gains, indexed in terms of current time, are stored. The current states are measured and compared to the nominal states to find out the differences (perturbations), while the perturbations of the final states and of the final time come from some estimate of the new intercept point.

5.5 Simulation

The guidance scheme is tested in digital simulation runs by comparing trajectories generated by using the feedback law to optimal-control solutions. The optimal-control and reference trajectories are found by solving numerically the two-point boundary value problem using the computer code **BOUNDSCO.** A set of results for the best-range guidance problem was presented in chapter 3. Graphs of an extremal trajectory for the basic problem (p1) are shown in Figures 1 and 2. This path is selected as a nominal reference trajectory for the feedback scheme. The nominal reference trajectory has the following boundary conditions: $t_f = 150\ sec.$, $h_o = 20\ Kft.$, $E_o = 52.8\ Kft.$, $\gamma_o = 0$, $x_f = 438\ Kft.$ and $h_f = 20\ Kft.$ Note that x_f appears here instead of E_f; the final range has been specified while the final energy is free (to be maximized).

Several examples, in which the guidance scheme is tested in digital simulation runs, are shown in Figures 13 through 17. In all of these examples the perturbations used are much larger than those used for the computation of of the feedback gains. In all of these Figures three paths are presented. These are the open-loop state-Euler, the reference and the feedback law trajectories. The reference and

feedback trajectories are shown up to a point where the feedback commands become large (load factor higher than 2g).

Figure 13 presents graphs for a case with a perturbation on the initial range ($\delta x(0) = 5000\,ft$). The case with a perturbation on the initial altitude is shown in Figure 14 ($\delta h(0) = 5000\,ft$), while results with a perturbation on the initial energy is shown in Figure 15 ($\delta E(0) = 5000\,ft$). The trajectory shown in Figure 16 has a perturbation on the final altitude ($\delta h(t_f) = 5000\,ft$). Figure 17 is a trajectory with perturbations on the final time and the initial range ($\delta t_f = -2$ sec and $\delta x(0) = 5000\,ft$). These simulation results show that the feedback law follows the optimal solution very closely, even for large deviations from the states and the terminal conditions. However, it was found that when approaching the final time the commands become large. Divergence near the final time combined with discretization, of the feedback gains, were found to be the cause of this difficulties. As already mentioned, it appears that the class of neighboring-optimal-guidance schemes is sensitive near the final time and one should expect such difficulties. To accomplish the end game and overcome these difficulties a terminal guidance law should be employed.

Chapter 6: Summary and Conclusions

6.1 Best-range open-loop study

The study of time-range-energy optimal trajectories for an air-to-air missile with the point-mass model shows that there is a fair amount of lofting in these paths. After an initial high - g pullup the trajectories are almost ballistic. An indication that a greater range might be obtained with a pre-launch maneuver made by the launching aircraft can be noticed from the results obtained in the study of the optimal problem with the initial path-angle free (problem p3).

The results obtained in the case with a coast phase show that, an inclusion of a coasting phase produces smaller maximum-range. This result is in contradiction with the results obtained in Ref. [14]. The reason for differences is that the energy model, which was selected in [14], is a bad approximation when used with the class of time-range-energy optimization of air-to-air missiles featuring boost-coast-sustain propulsion. A study of several cases where the sustain phase is

perturbed was done. In all of these cases the total impulse is kept constant, while the sustain thrust and time are perturbed. The results of this study show that lowering the sustain thrust level instead of including a coast phase, produces larger maximum-range. It was also found that an increase of the thrust in the sustain phase, while maintaining the same total impulse, reduces the range.

6.2 Reduced-order models best-range open-loop study

A study of the following reduced-order models:

- Singular perturbation with γ as fast variable;
- Point mass model with approximation of the induced;
- Energy model;

and a comparison to the point-mass model was done. The results show that the energy model is a bad approximation for the application in this study; time-range-energy optimization of air-to-air missiles featuring boost-coast-sustain propulsion. It was also found that the other reduced-order models are not good enough to get approximations to the optimal trajectories for the boost-coast-sustain missile. As a result, optimal trajectories computed by using the point-mass model, are selected as the reference trajectories for the feedback guidance scheme.

6.3 Near-optimal Closed-loop study

In this study an approach to on-board real-time calculations for fixed final time is derived. Optimal control and neighboring optimal theories are combined to produce a closed-loop guidance algorithm. The validity of the guidance scheme is then extended by incorporating also perturbations on the final time. It was found that the guidance law for the perturbed final time is the same as the previous one (the fixed final time law), but with modified final conditions. The schemes are applied to a midcourse guidance for an air-to-air missile. Although a substantial numerical effort is required for synthesis of the feedback law, the actual on-board execution of the guidance scheme is rather simple.

Several simulation results comparing the closed-loop guidance scheme and the corresponding optimal trajectories are shown. It is found that the feedback law performs quite well, even for large deviations from the nominal states and final conditions.

6.4 Future Work

Further study of the best-range problem and application of the on-board real-time scheme derived earlier to three-dimensional flight is of interest. As indicated earlier, due the high gains near the final time, instability is caused. It is clear that such difficulty decreases the duration of the midcourse guidance phase which in some applications might be crucial. This motivates an investigation of different

indexing ideas that might improve the stability while approaching the final time. A study of the midcourse guidance problem with some state constraints and lower (active) control constraints might be of interest. These studies are motivated by the observation that the optimal trajectories tend towards very high altitudes, and have large path-angles and initial high load factors. In some applications these altitudes, path-angles and load-factors may be unacceptable.

Appendix: Aerodynamic and propulsive modelling

Drag coefficient

The drag coefficient is related to the lift-coefficient by the drag-polar

$$C_D(M,h,C_L) = C_{Do}(M,h) + C_{Di}(M)\,|C_L|^p.$$

With this form of the polar the drag-to-weight ratio may be written as

$$\frac{D}{W} = D_o + D_i\,|n|^p,$$

where

$$D_o = \frac{qS}{W}\,C_{Do}(M,h),$$

and

$$D_i = \left(\frac{qS}{W}\right)^{1-p} C_{Di}(M).$$

The altitude dependence in the zero-lift drag coefficient is expressed as

$$C_{Do}(M,h) = \hat{C}_{Do}(M)\left[1 + C\left(\frac{h}{\lambda}\right)^k\right] + C_{Dc}(M) f(T)$$

where C, λ and k are constants and $\hat{C}_{Do}$ and C_{Dc} are specified functions of Mach number. The C_{Dc} term accounts for a change in base pressure with the engine-off; the multiplicative term $f(T)$ is unity with the engine off and zero with it on. The functions C_{Do}, C_{Dc}, C_{Di}, ρ (air density) and a (sonic velocity) are constructed as cubic-spline interpolating polynomials.

Thrust

The propulsion is of **boost-coast-sustain** type. The thrust is modelled by giving the value as function of time, as follows and shown in Figure A.

$$\hat{T}(t) = \begin{cases} T_b & 0 \le t \le t_{be} \\ 0 & t_{be} < t \le t_{ce} \\ T_s & t_{ce} < t \le t_{se} \\ 0 & t_{se} < t \end{cases}$$

T_b and T_s are the boost and sustain thrust, respectively. The times t_{be}, t_{ce}, t_{se} are boost time, end-coast time and end-sustain time ($t_{be} \le t_{ce} < t_{se}$) . If ($t_{be} < t_{ce}$) there

is a coast interval t_c (where $t_c = t_{cs} - t_{be}$) between the end-of-boost and initiation of the sustain motor.

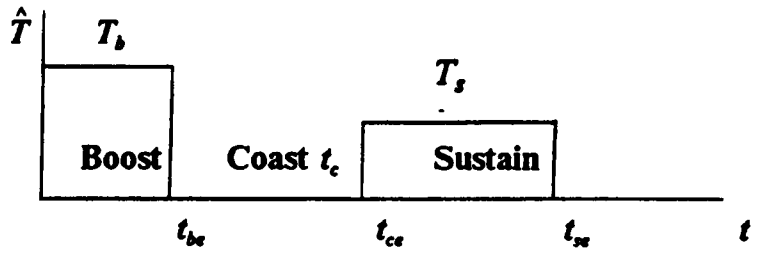

Figure A: Thrust vs. time

Weight change

When the thrust is non-zero the vehicle weight decreases at a constant rate

$$\dot{W}(t) = -W_i \qquad (i = b,s)$$

Load-factor constraints

The parameter n_{max} in the structural load-limit is constant,while the lift-coefficient limit is approximated by cubic-spline interpolation (i.e $C_{L\,max}(M)$).

List of Figures

Figures

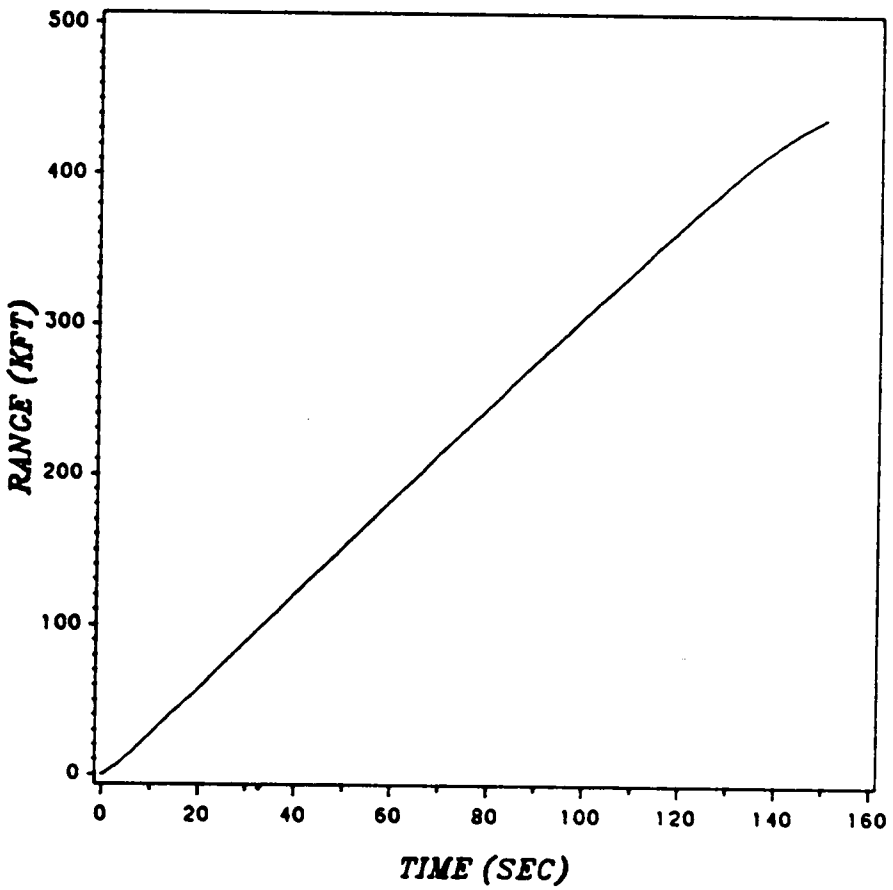

Figure 1a. Range time history.

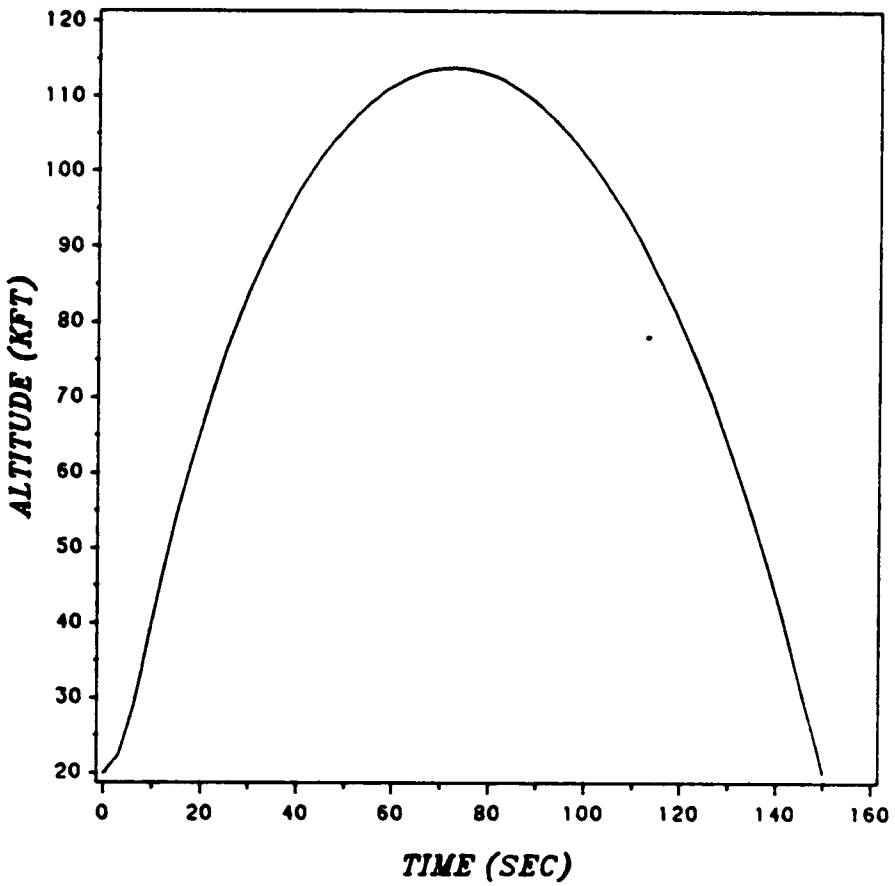

Figure 1b. Altitude time history.

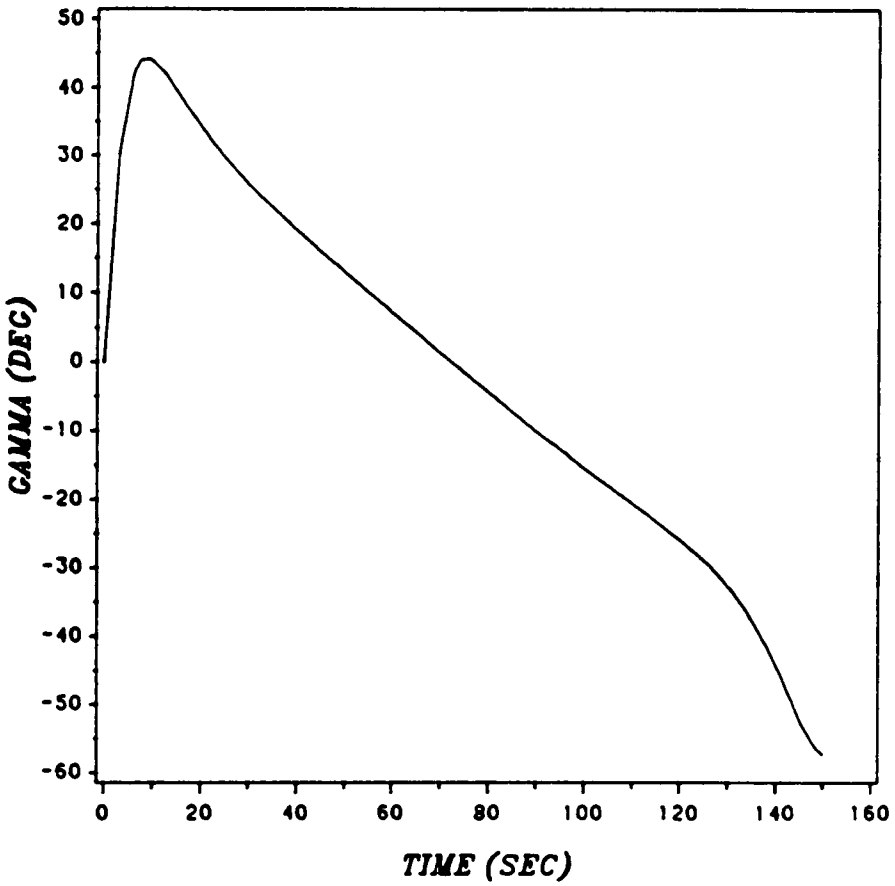

Figure 1c. Path-angle time history.

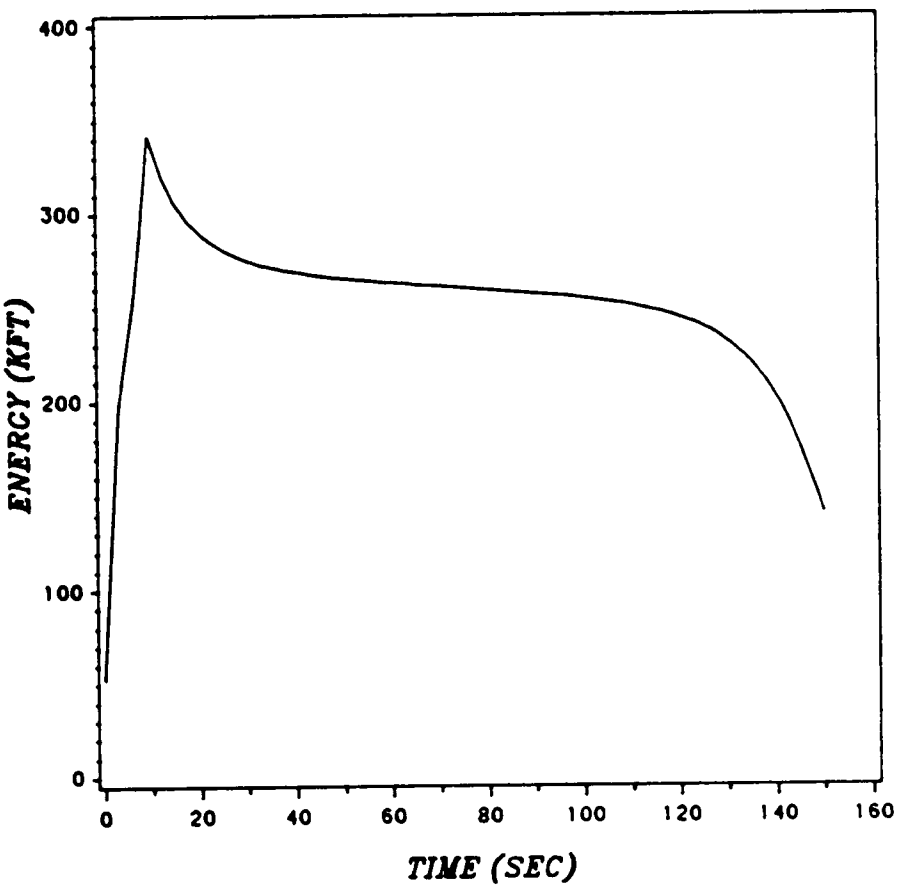

Figure 1d. Energy time history.

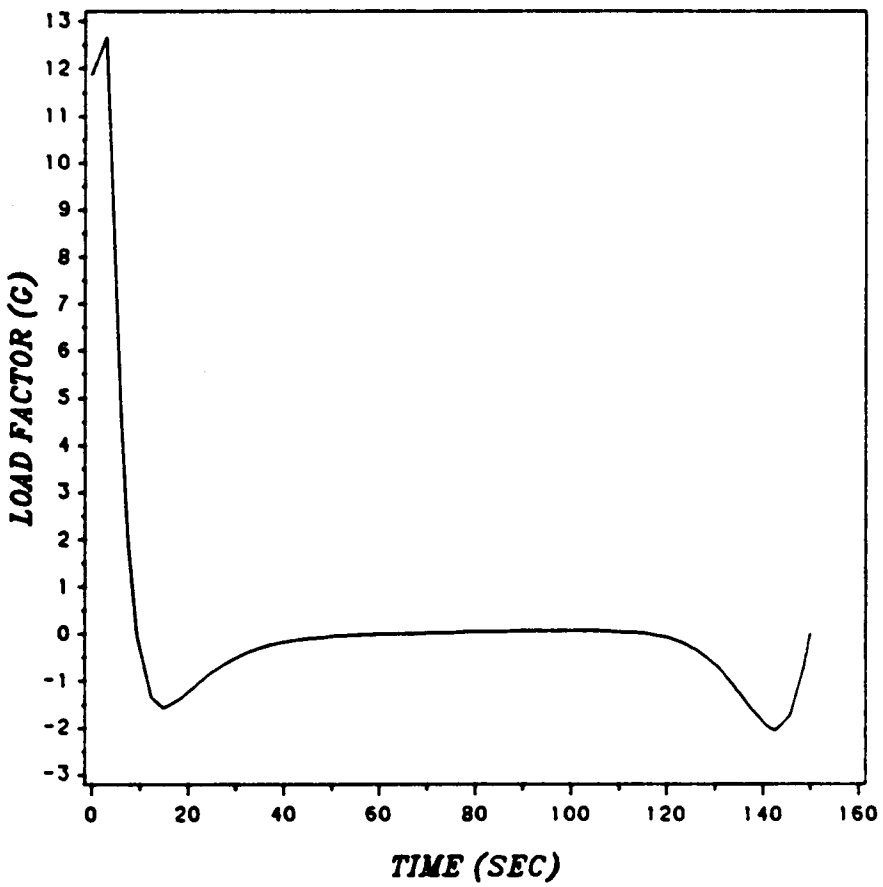

Figure 1e. Optimal control time history.

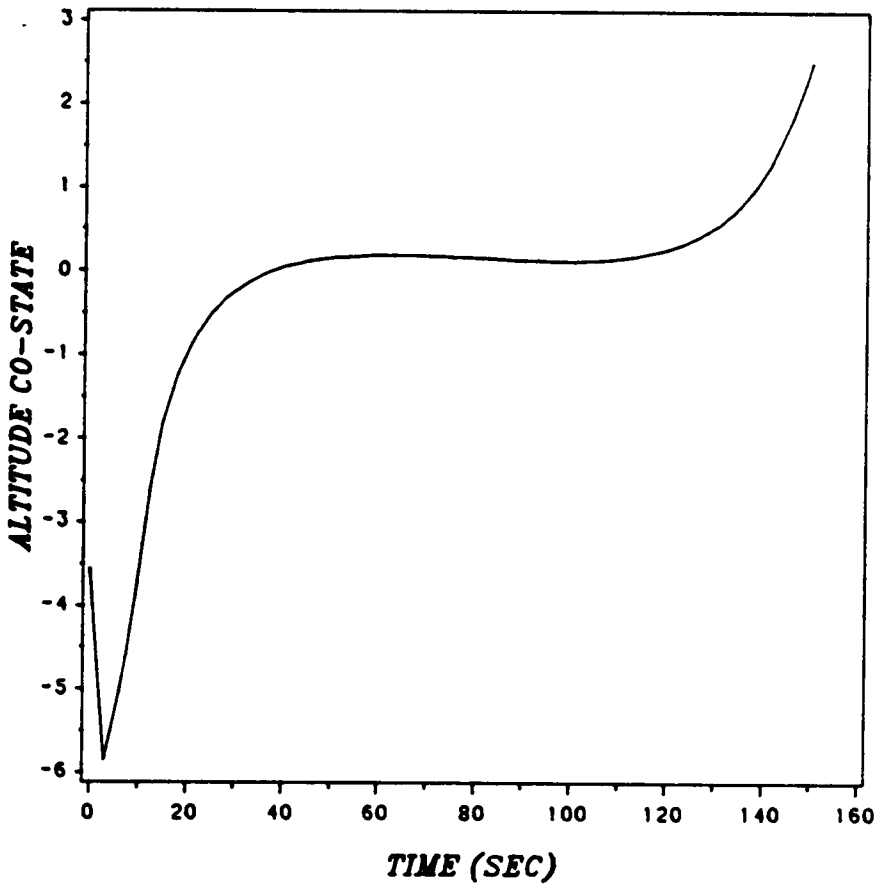

Figure 2a. Altitude co-state time history.

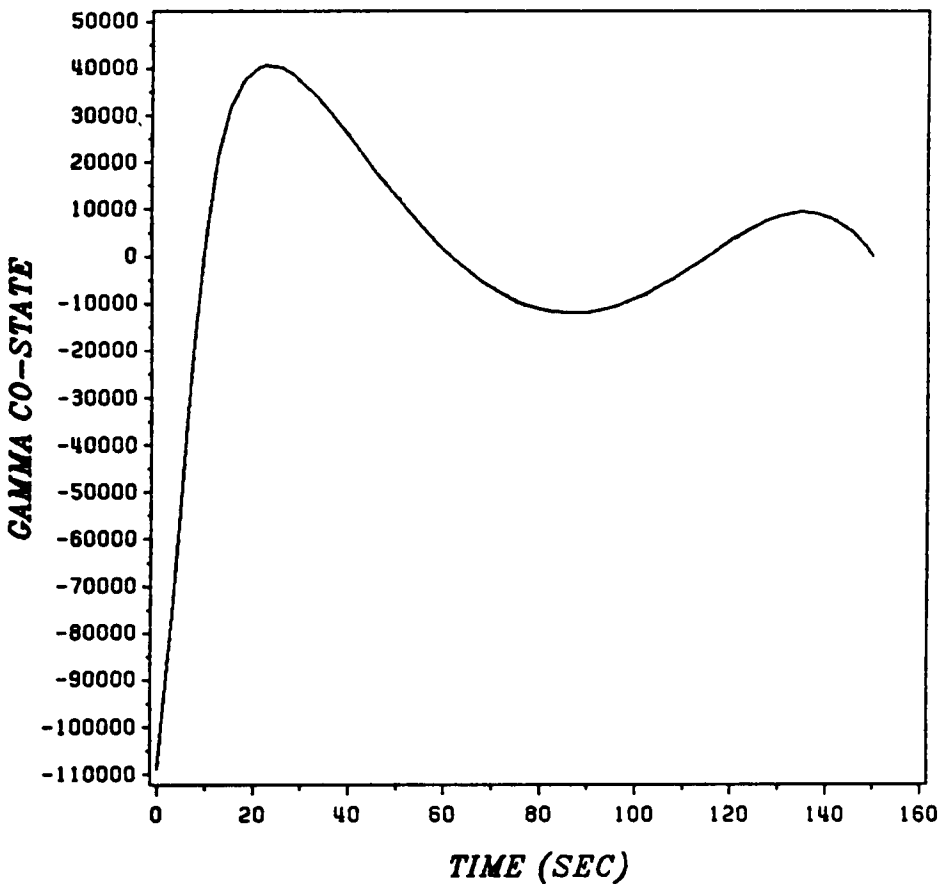

Figure 2b. Path-angle co-state time history.

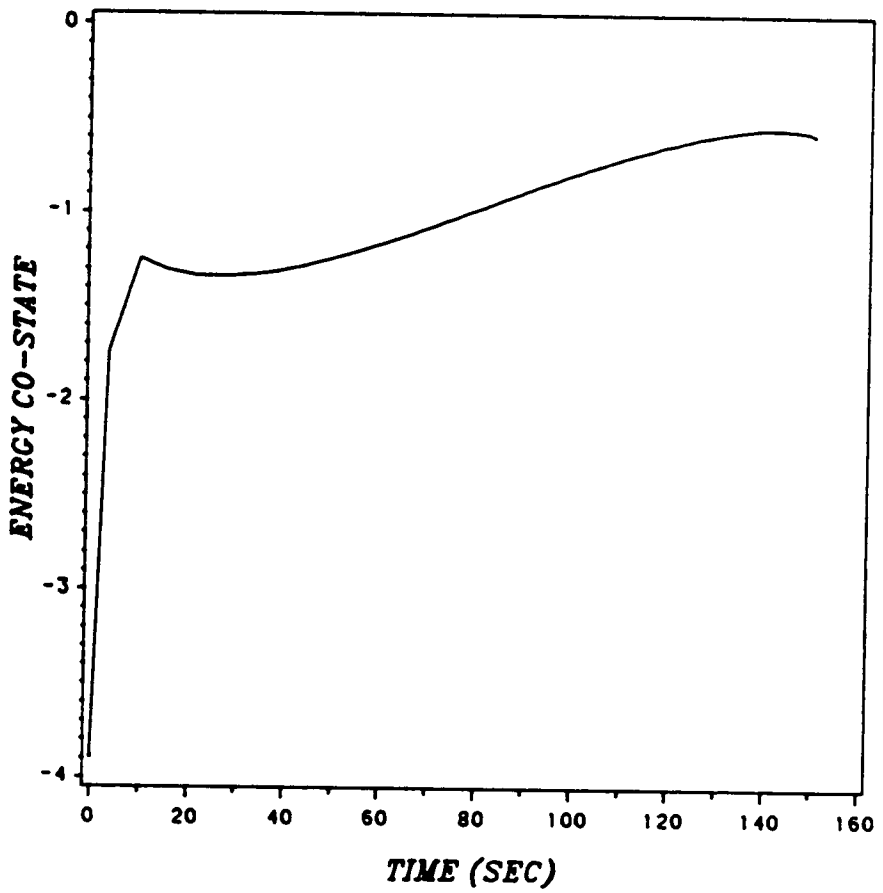

Figure 2c. Energy co-state time history.

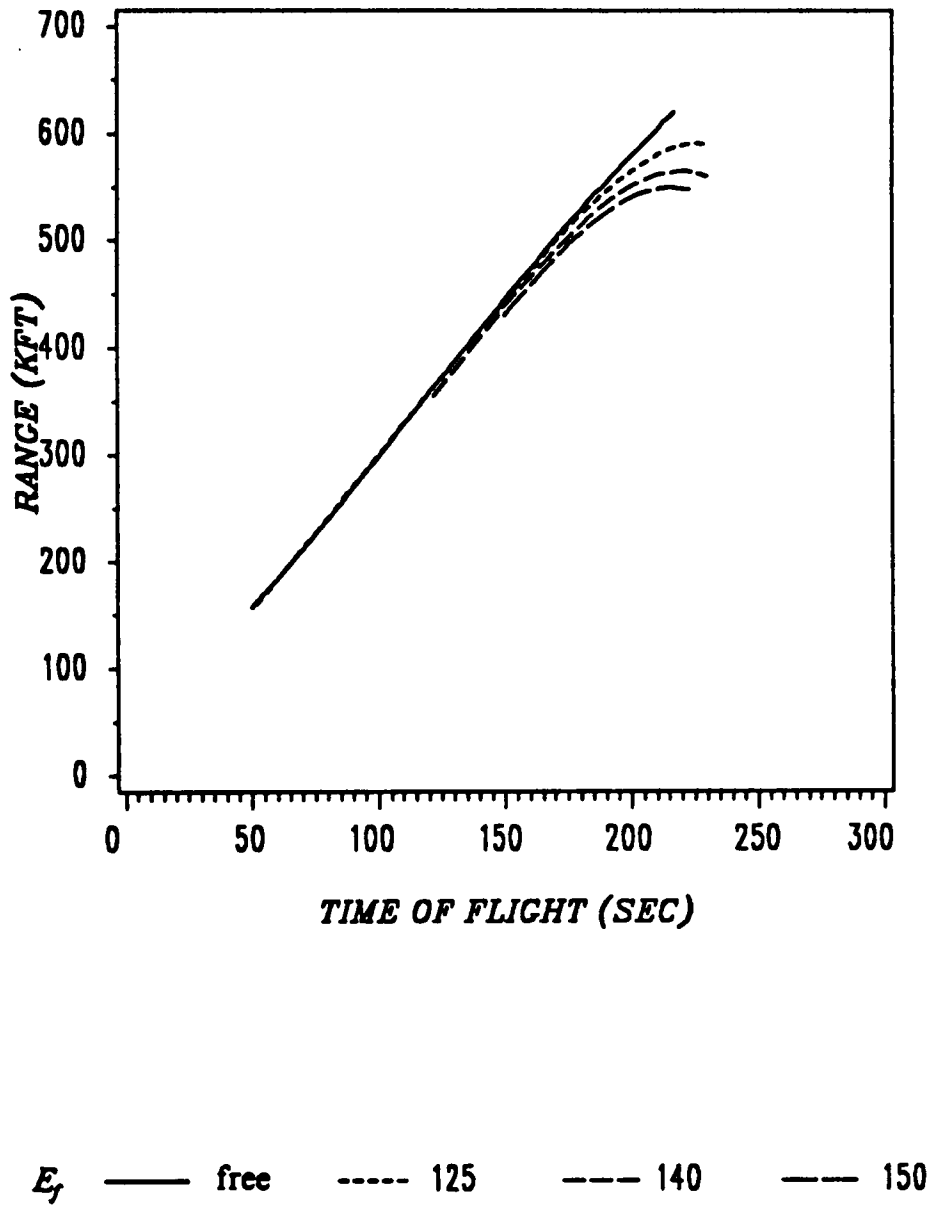

Figure 3. Range vs. time of flight.

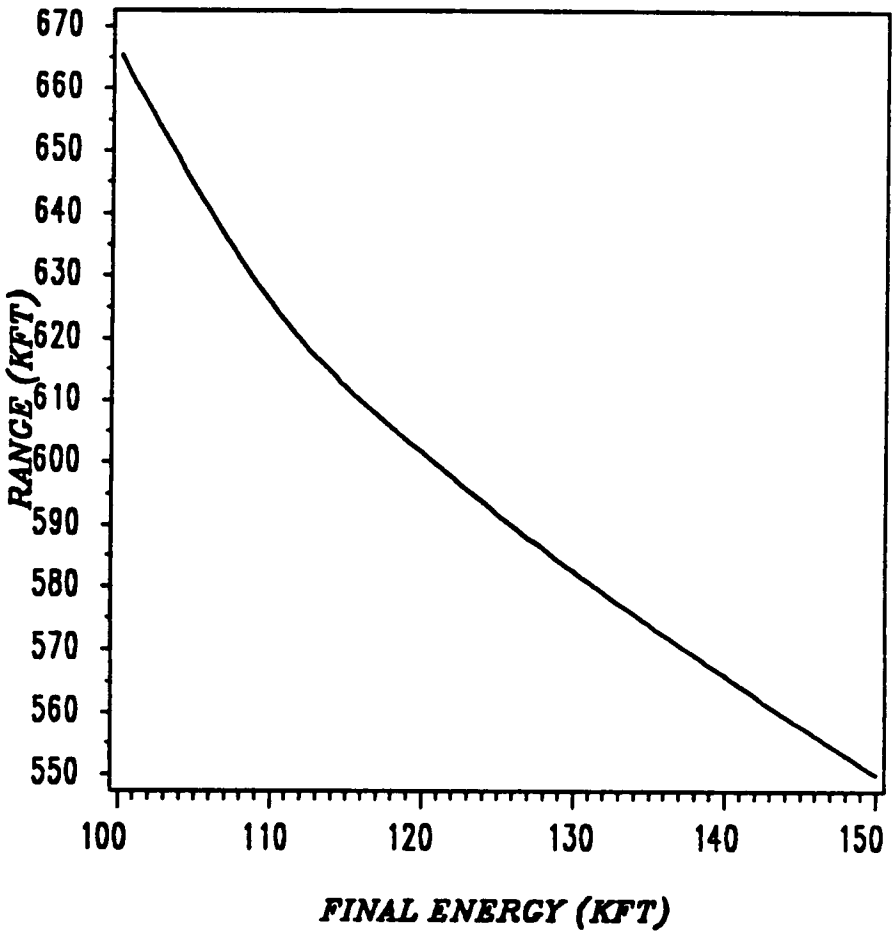

Figure 4. Range vs. final energy.

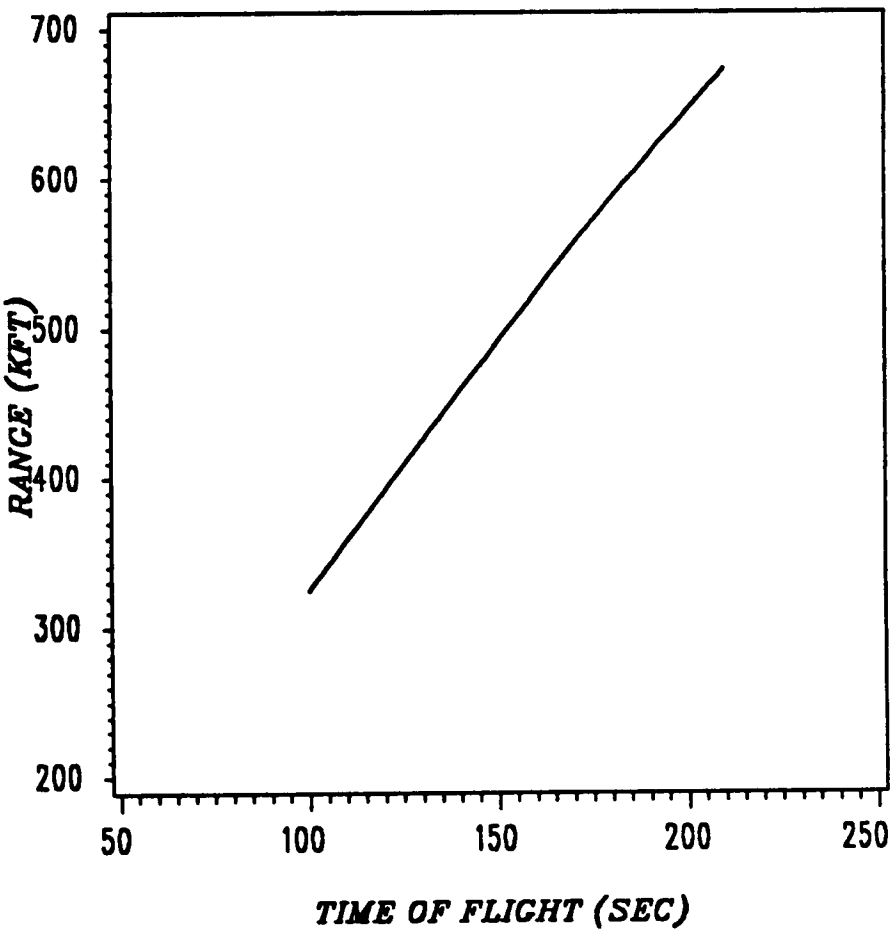

Figure 5. Range vs. time of flight: $\gamma(0)$ and $E(t_f)$ – open

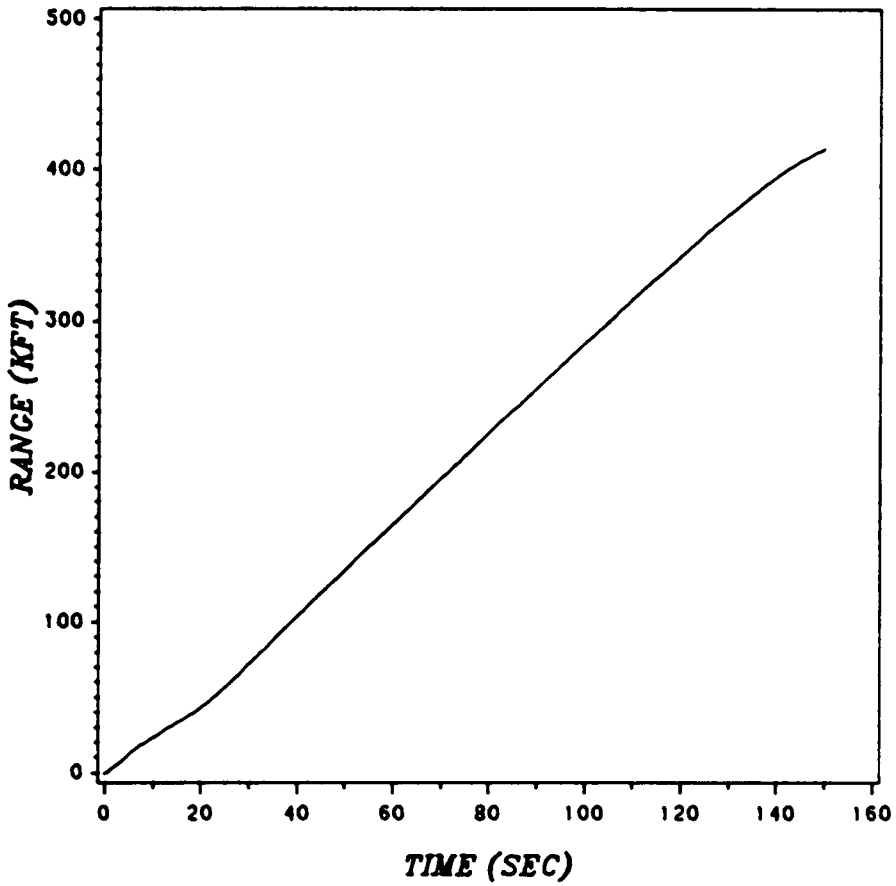

Figure 6a. Range time history.

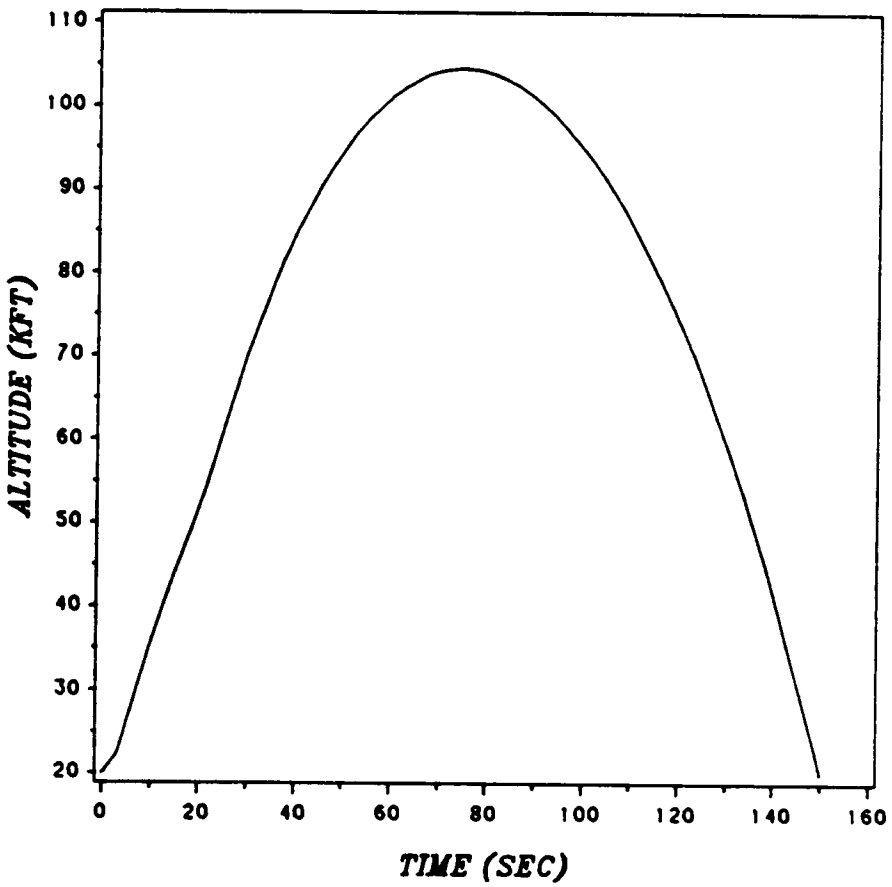

Figure 6b. Altitude time history.

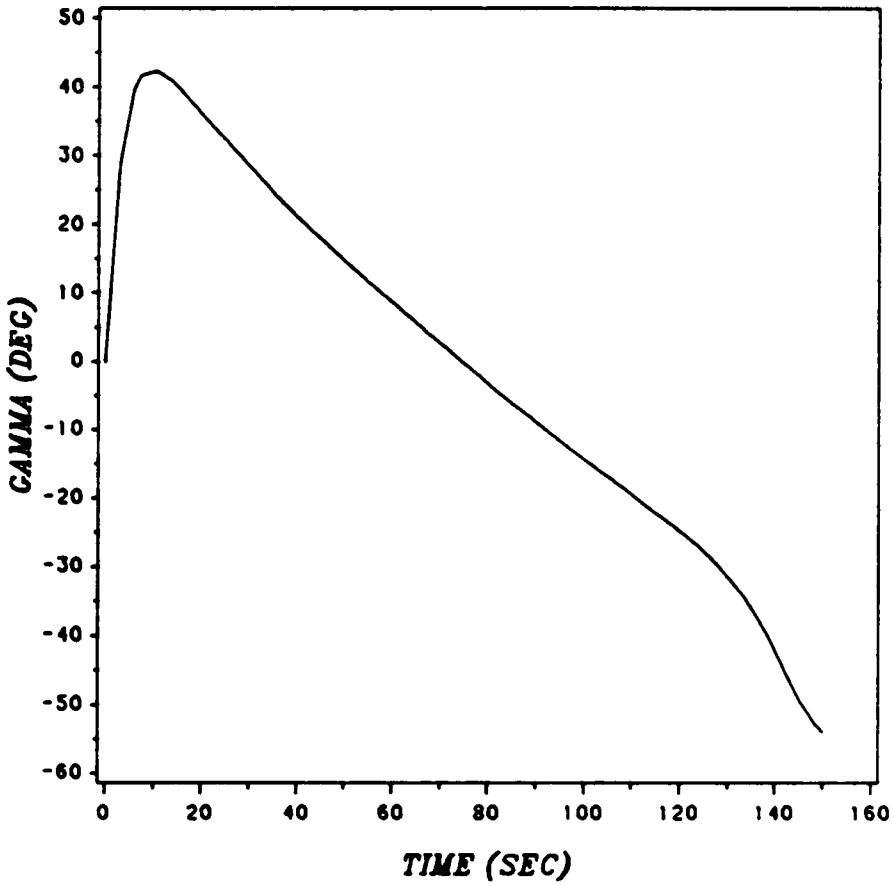

Figure 6c. Path-angle time history.

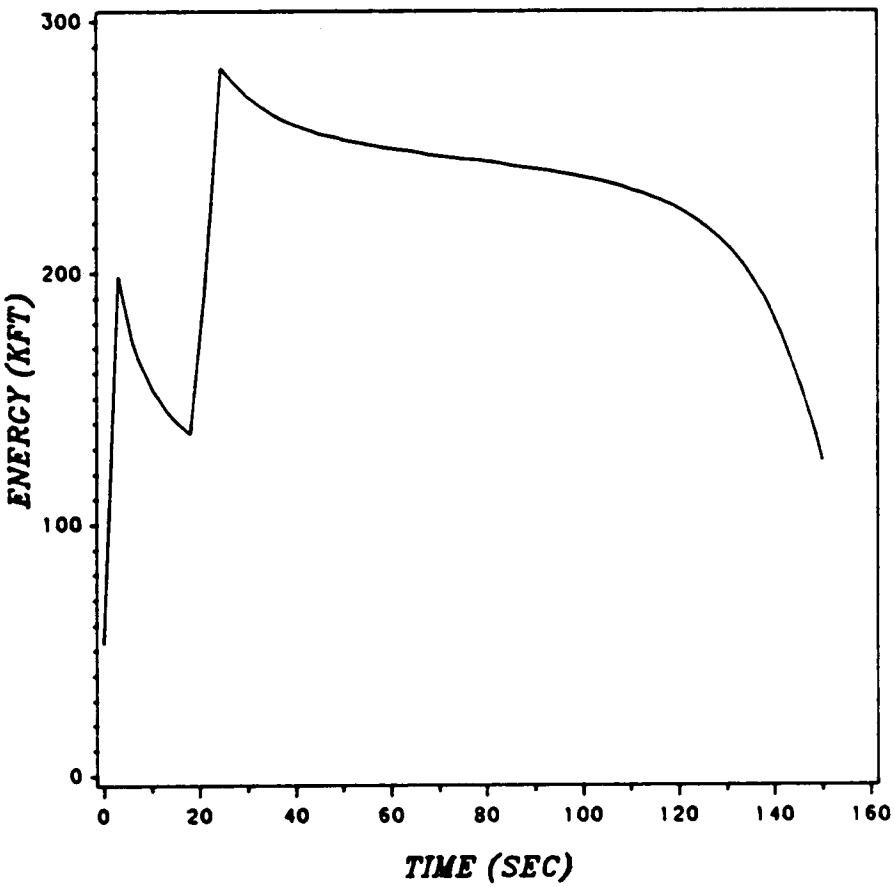

Figure 6d. Energy time history.

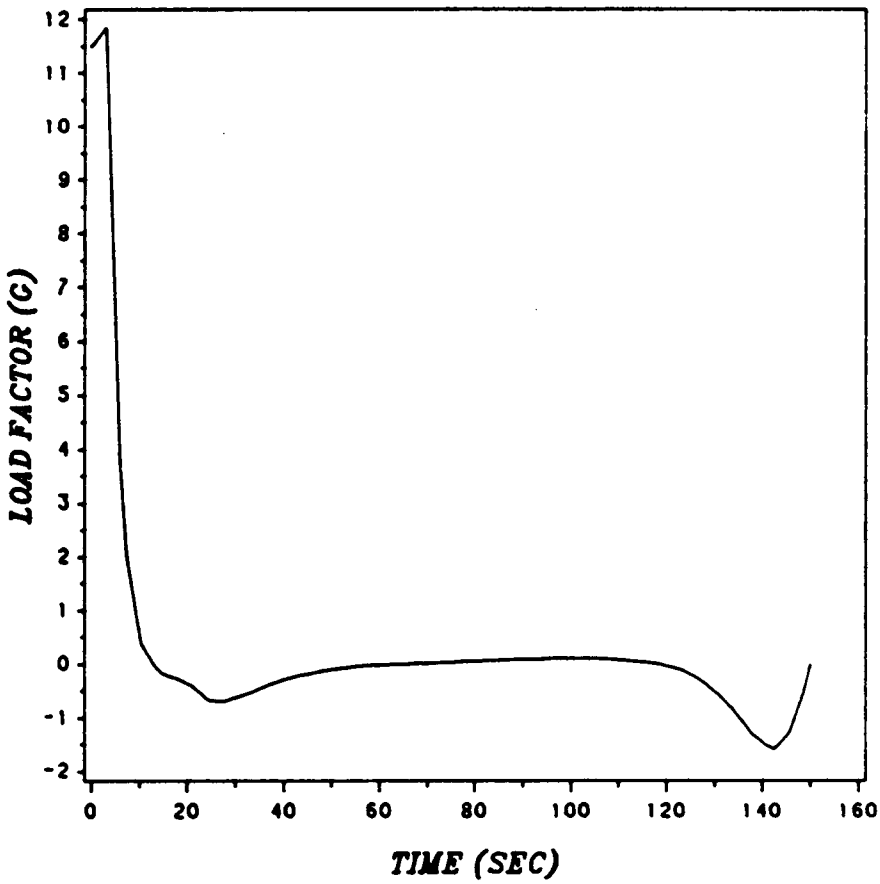

Figure 6e. Optimal control time history.

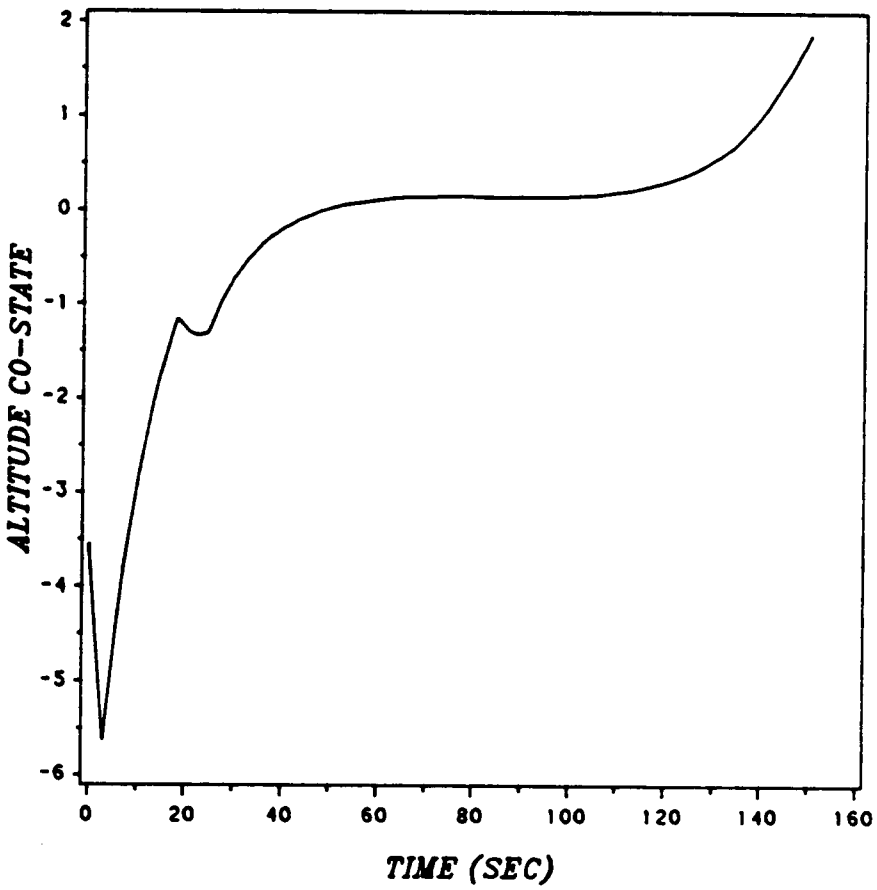

Figure 7a. Altitude co-state time history.

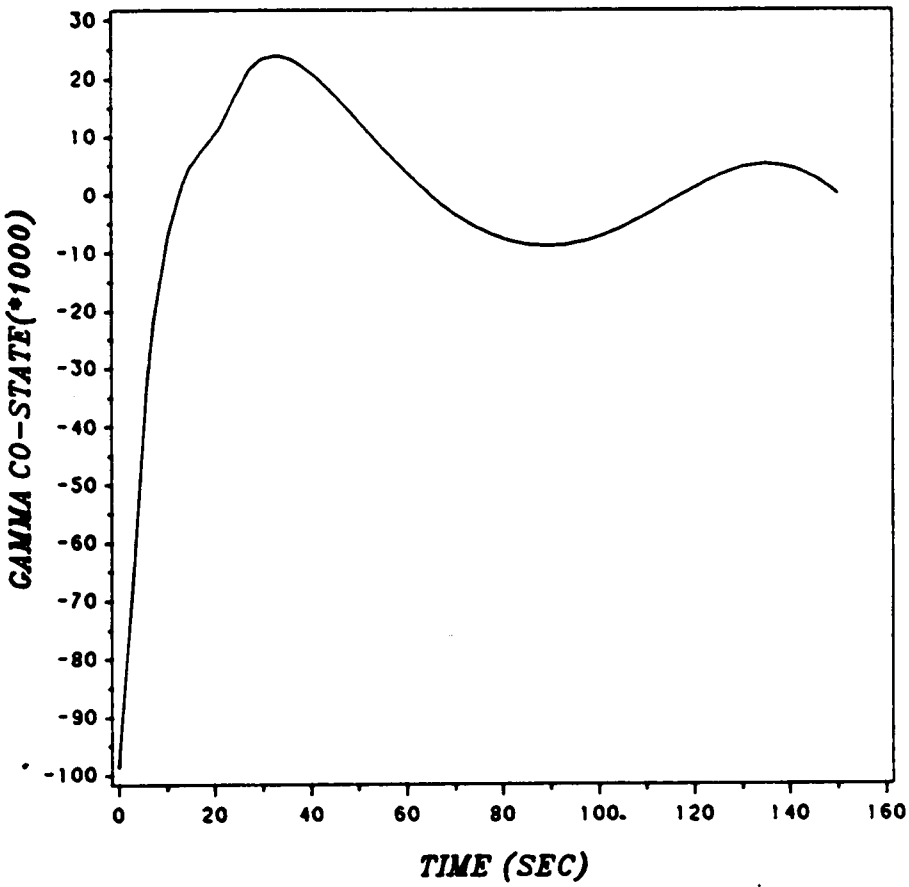

Figure 7b. Path-angle co-state time history.

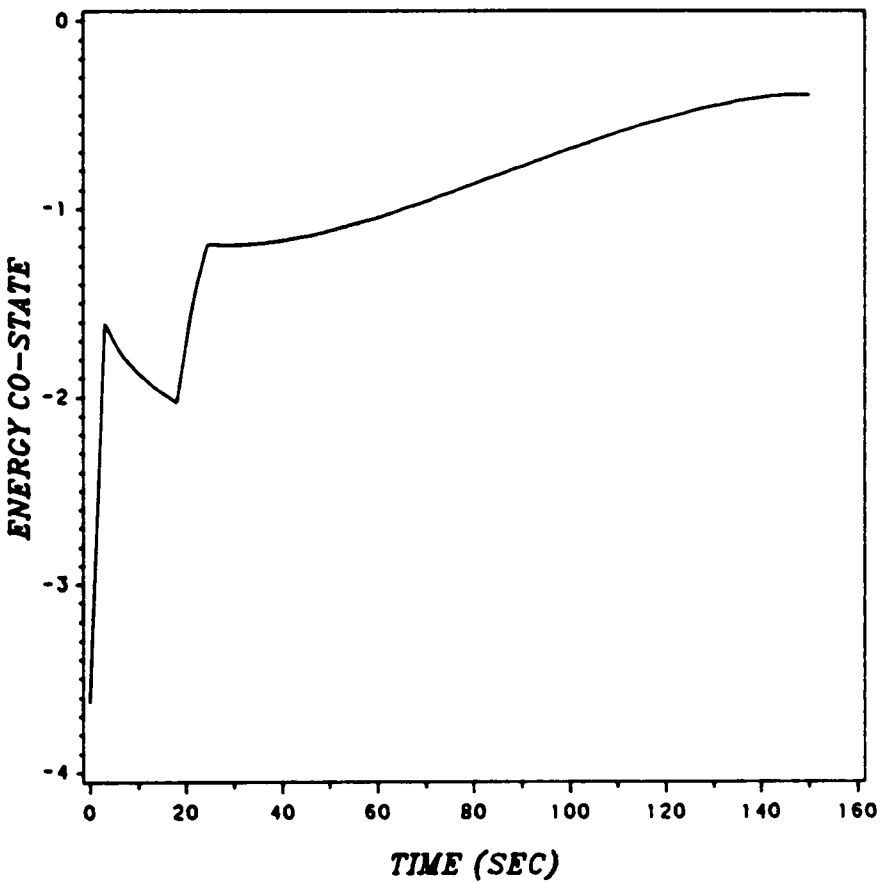

Figure 7c. Energy co-state time history.

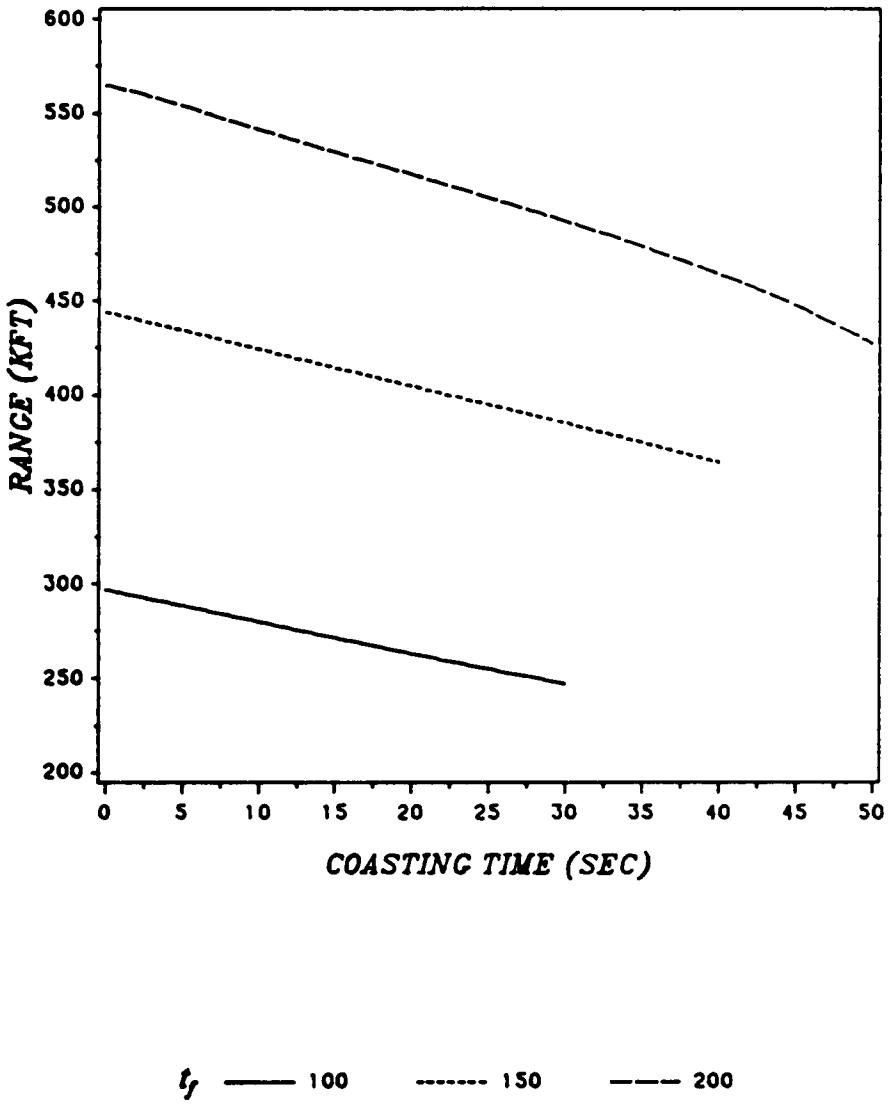

Figure 8. Range vs. coasting time.

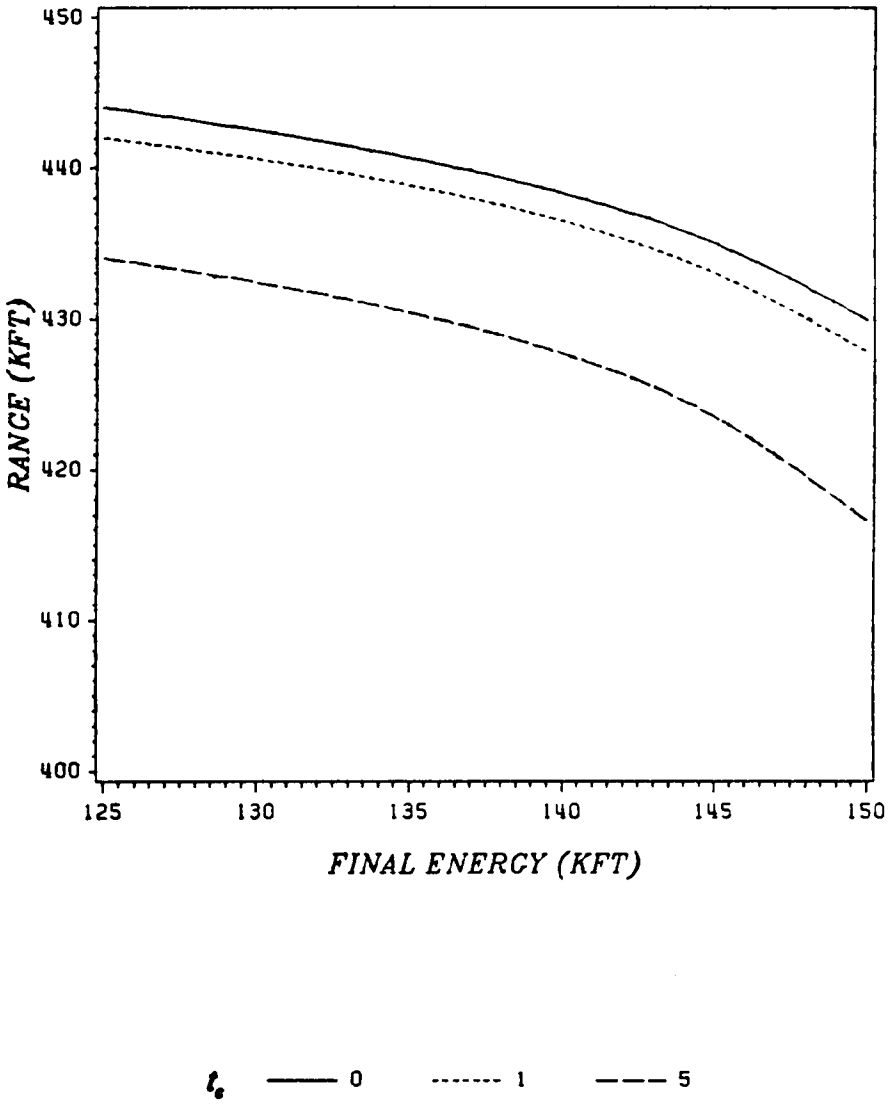

Figure 9. Range vs. final energy.

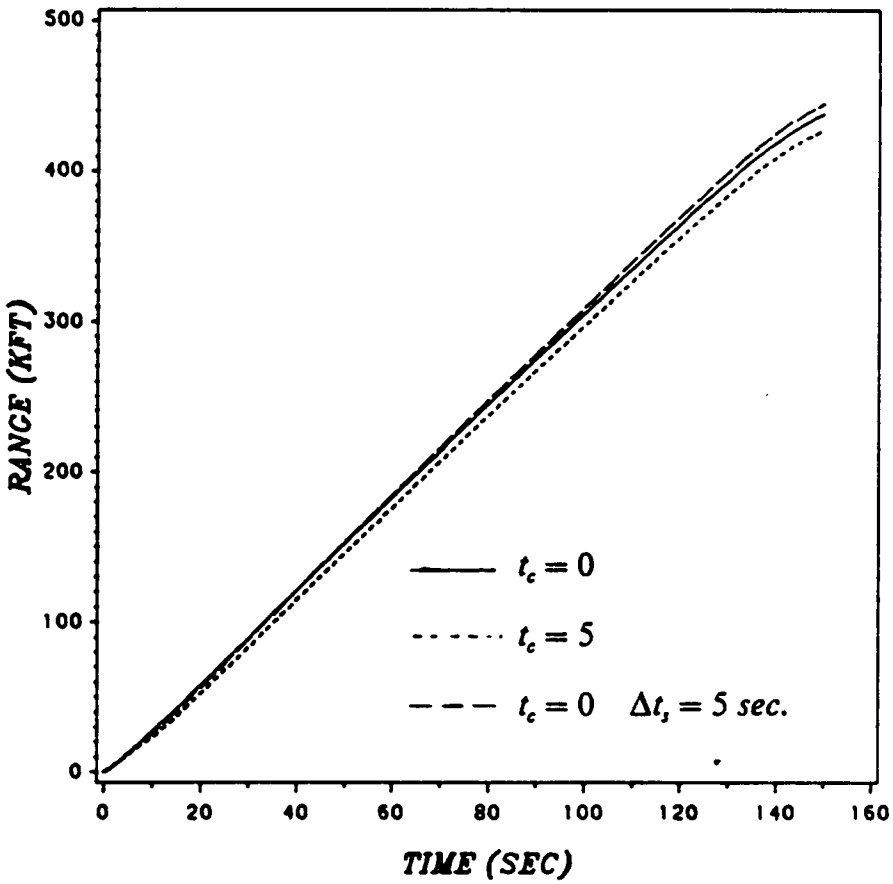

Figure 10a. Range time history.

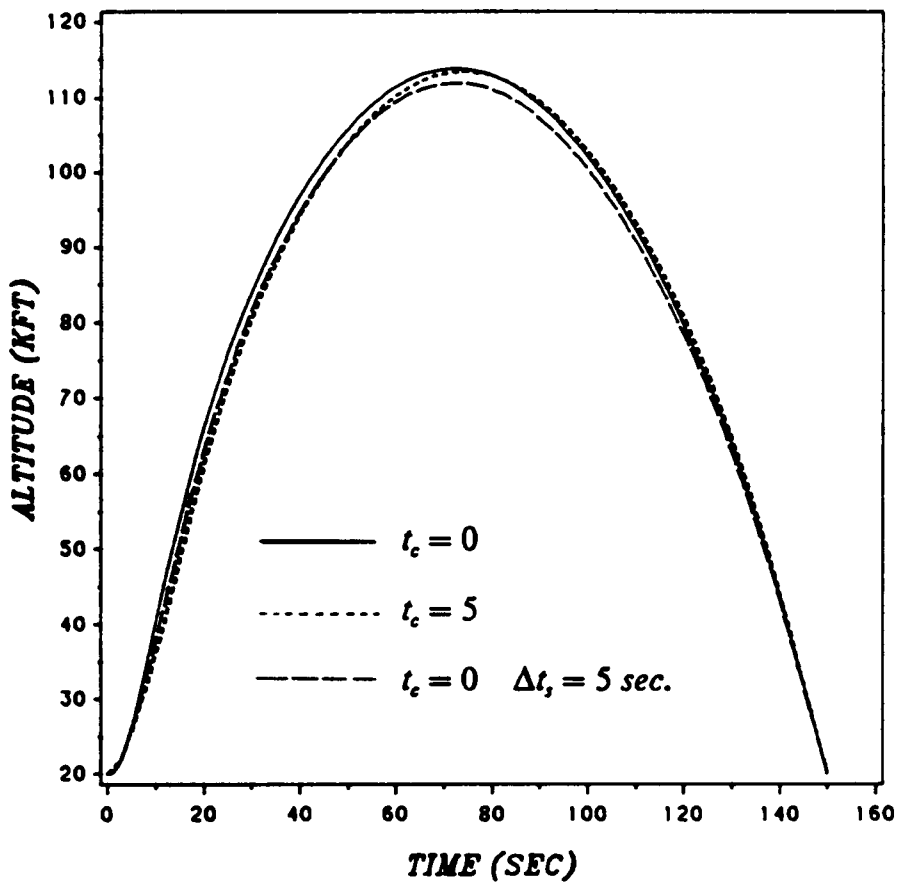

Figure 10b. Altitude time history.

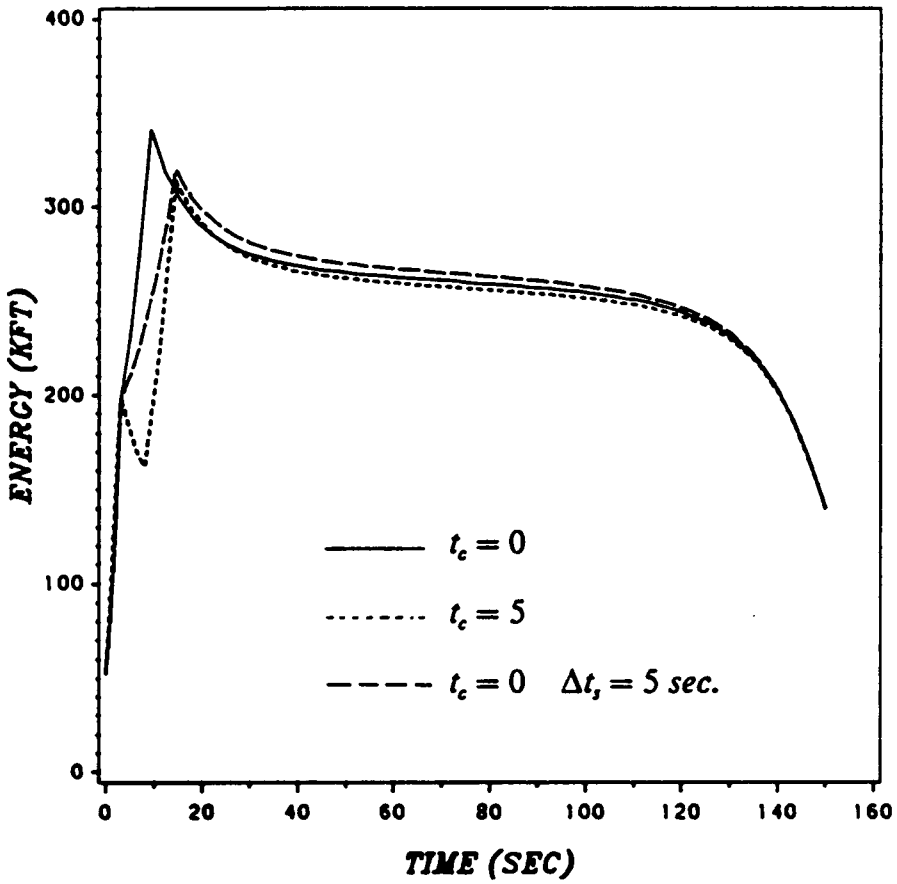

Figure 10c. Energy time history.

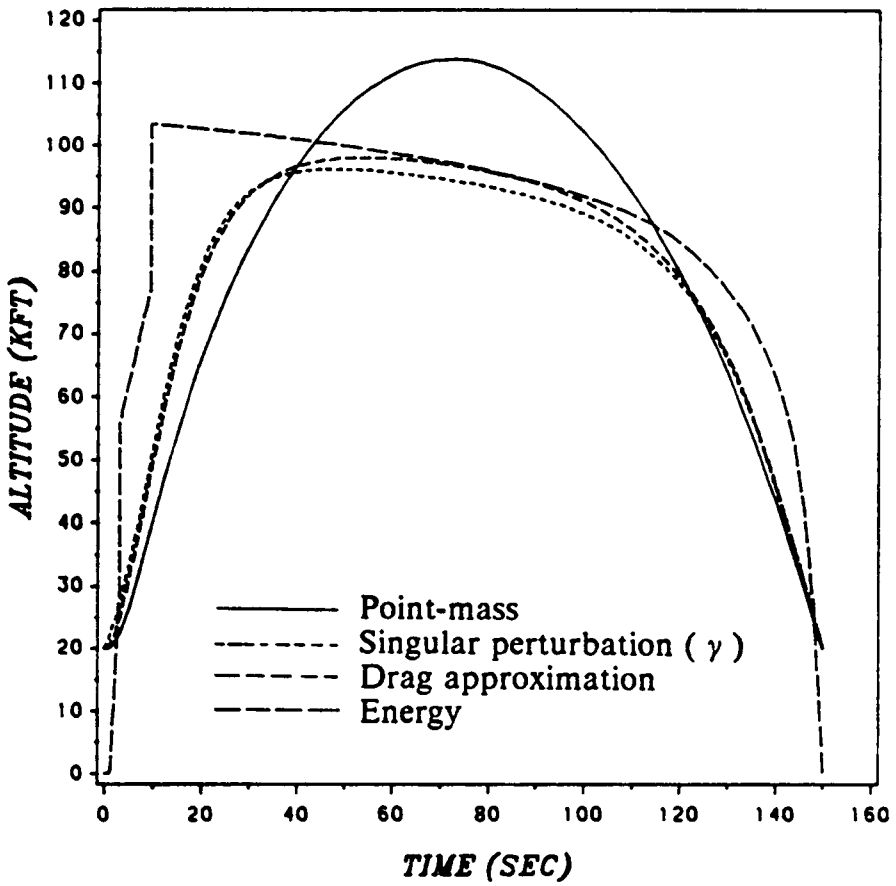

Figure 11a. Reduced-order models: Altitude time history.

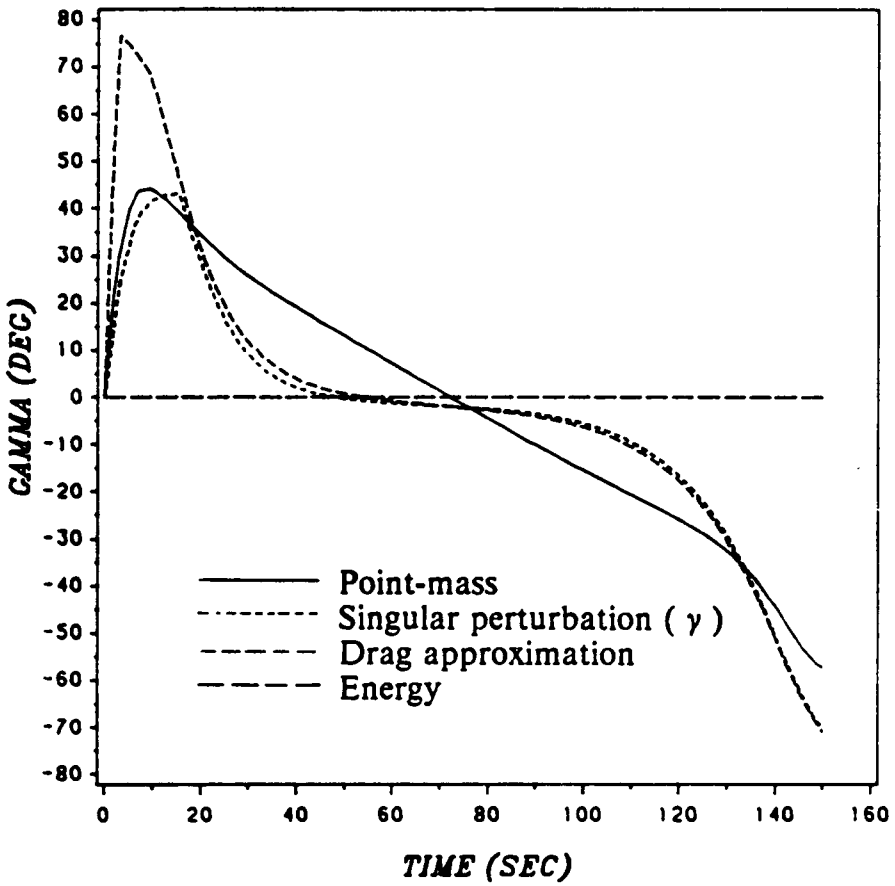

Figure 11b. Reduced-order models: Path-angle time history.

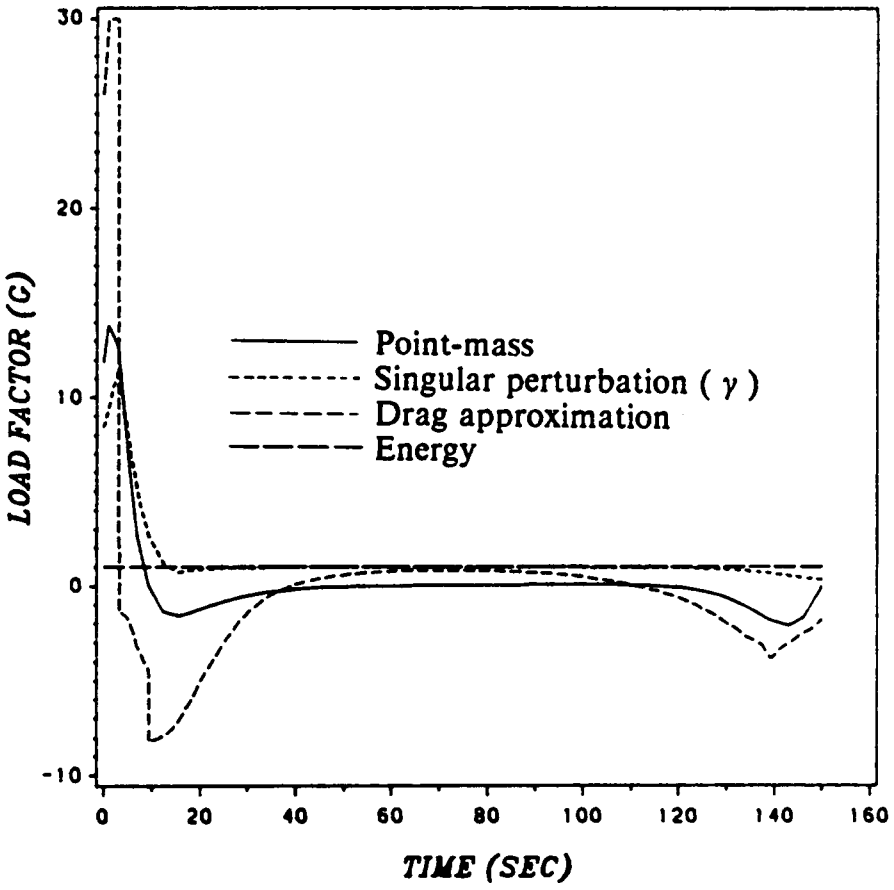

Figure 11c. Reduced-order models: Load-factor time history.

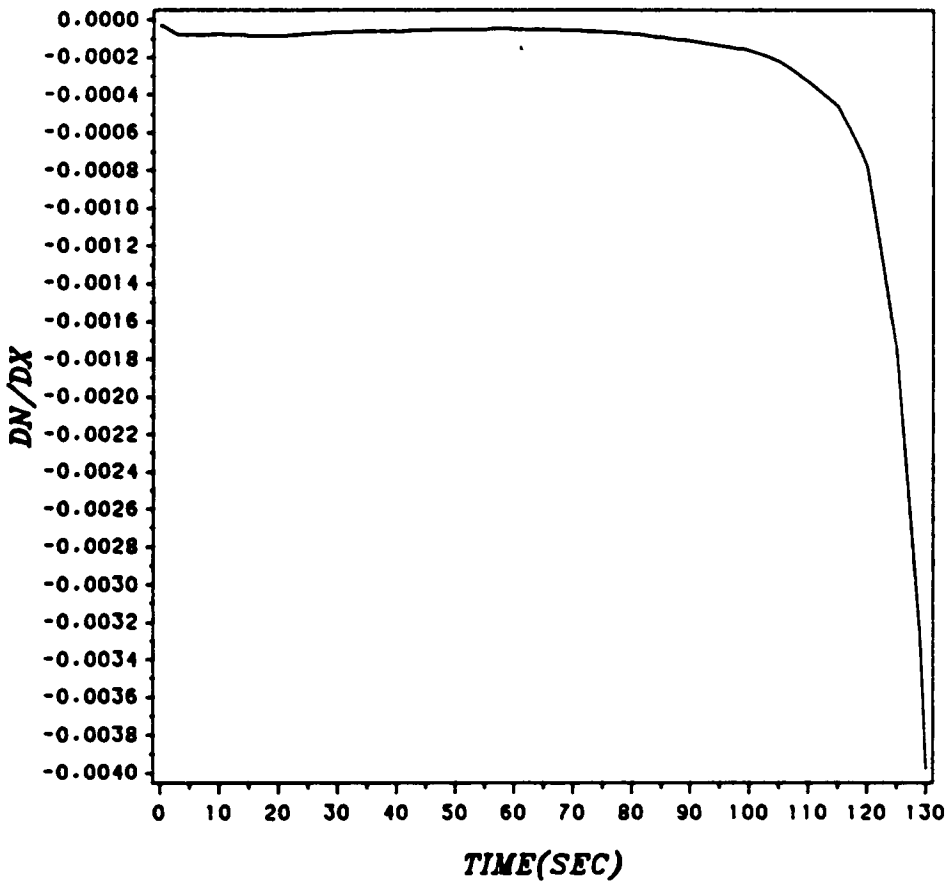

Figure 12a. Feedback gains: Range gain vs. time.

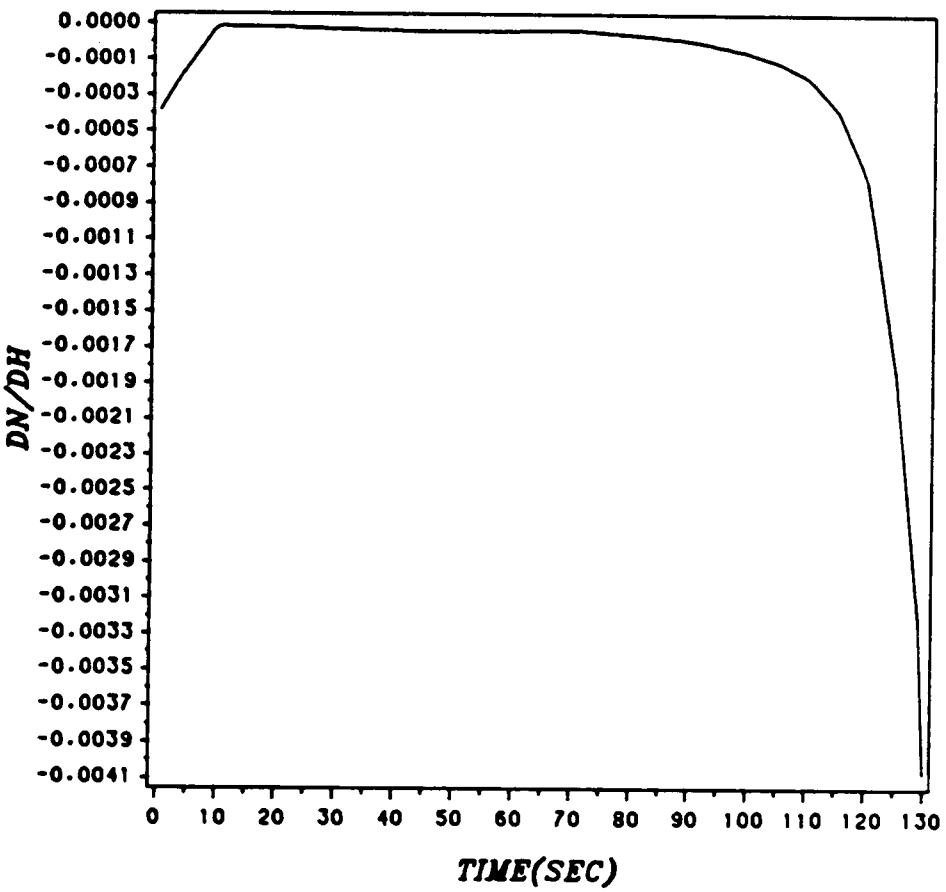

Figure 12b. Feedback gains: Altitude gain vs. time.

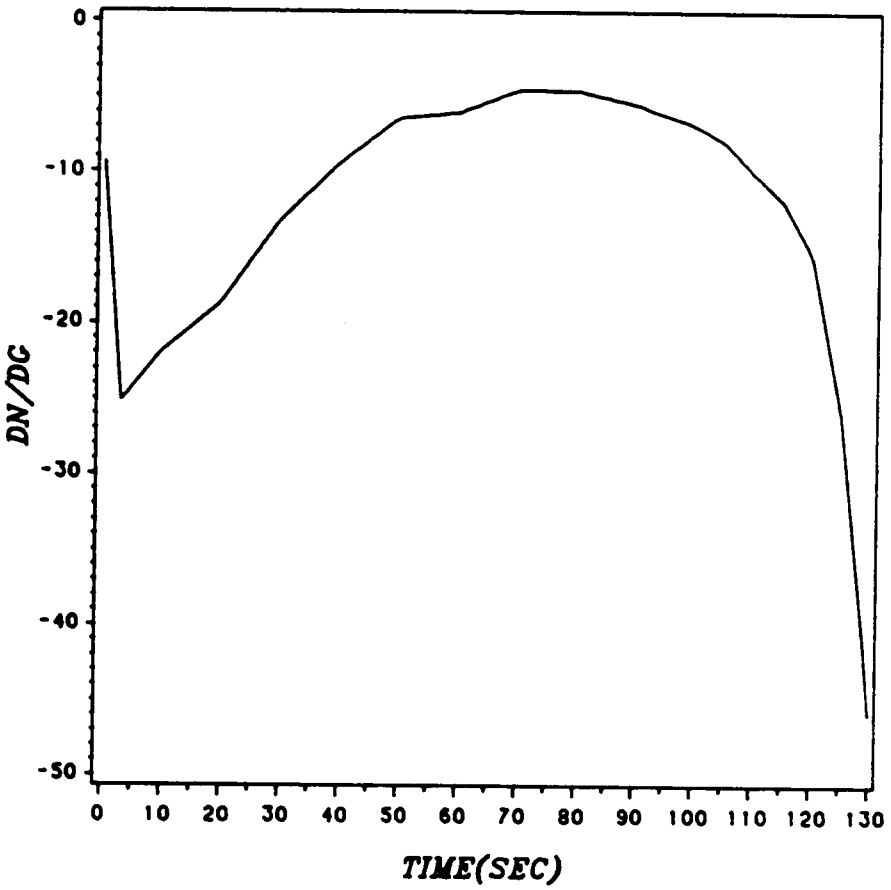

Figure 12c. Feedback gains: Path-angle gain vs. time.

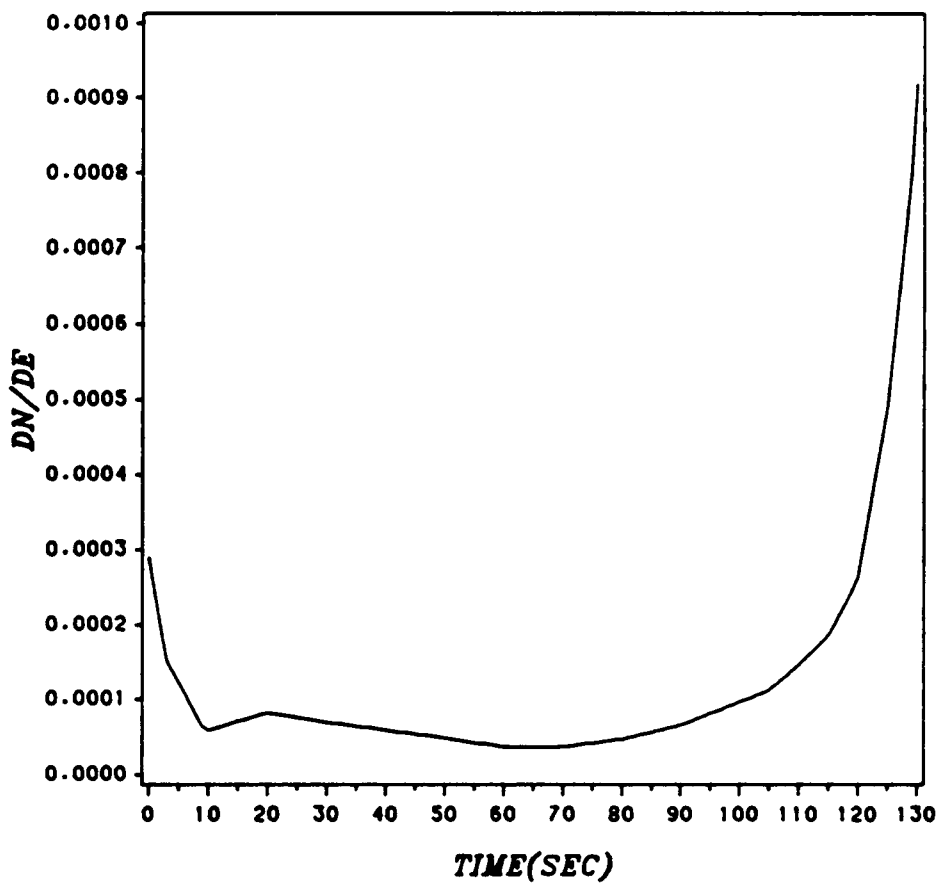

Figure 12d. Feedback gains: Energy gain vs. time.

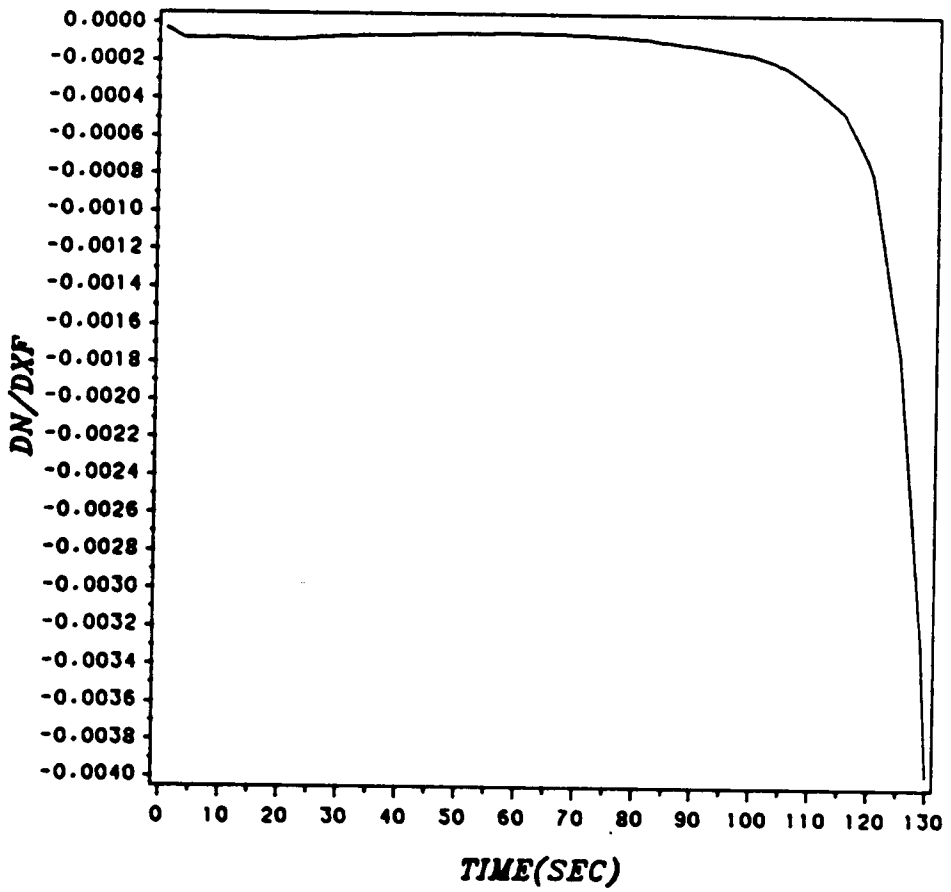

Figure 12e. Feedback gains: Final range gain vs. time.

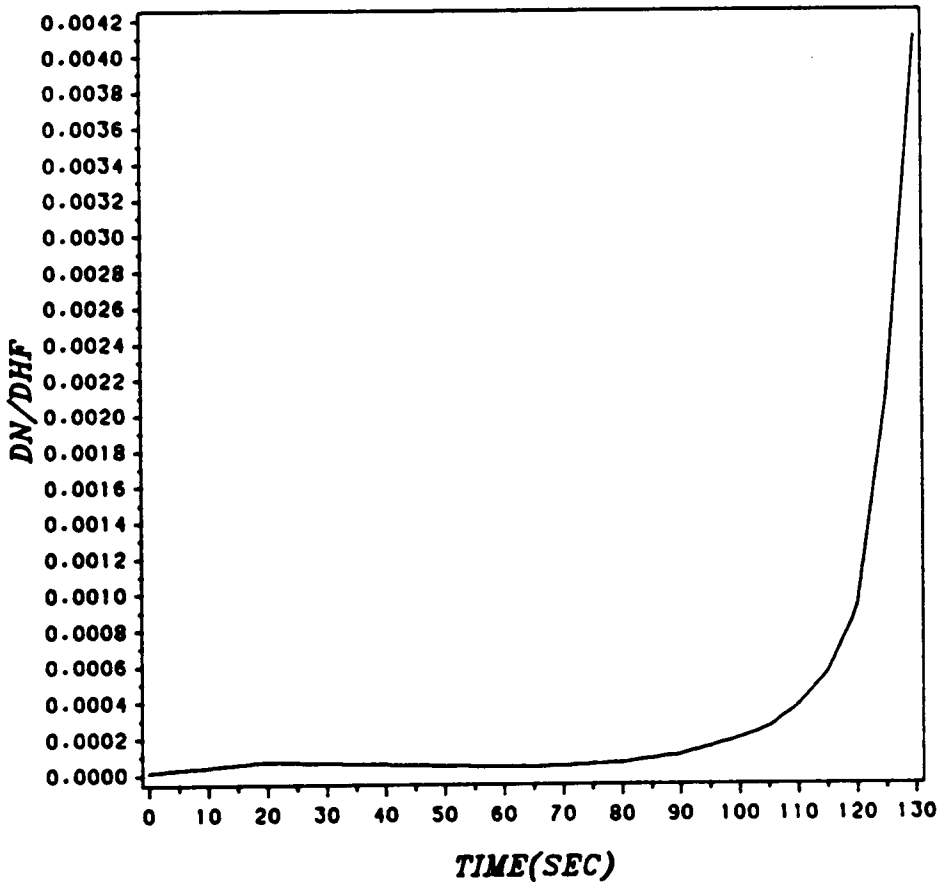

Figure 12f. Feedback gains: Final altitude gain vs. time.

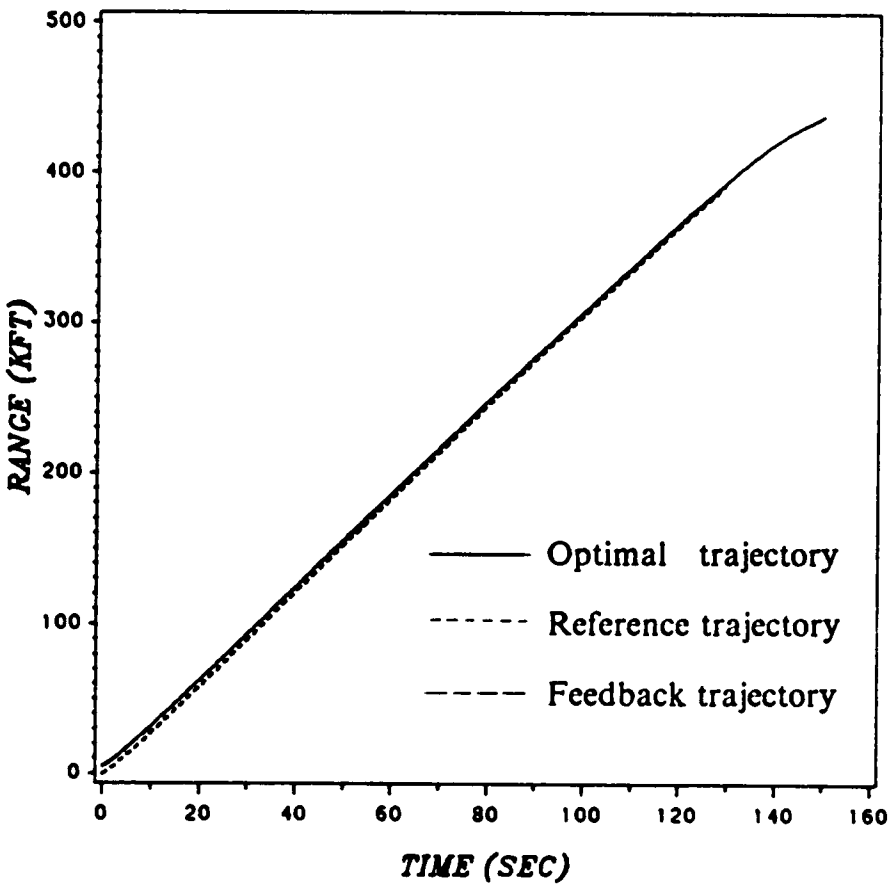

Figure 13a. Range history for example 1 - $\delta x(0) = 5000ft.$

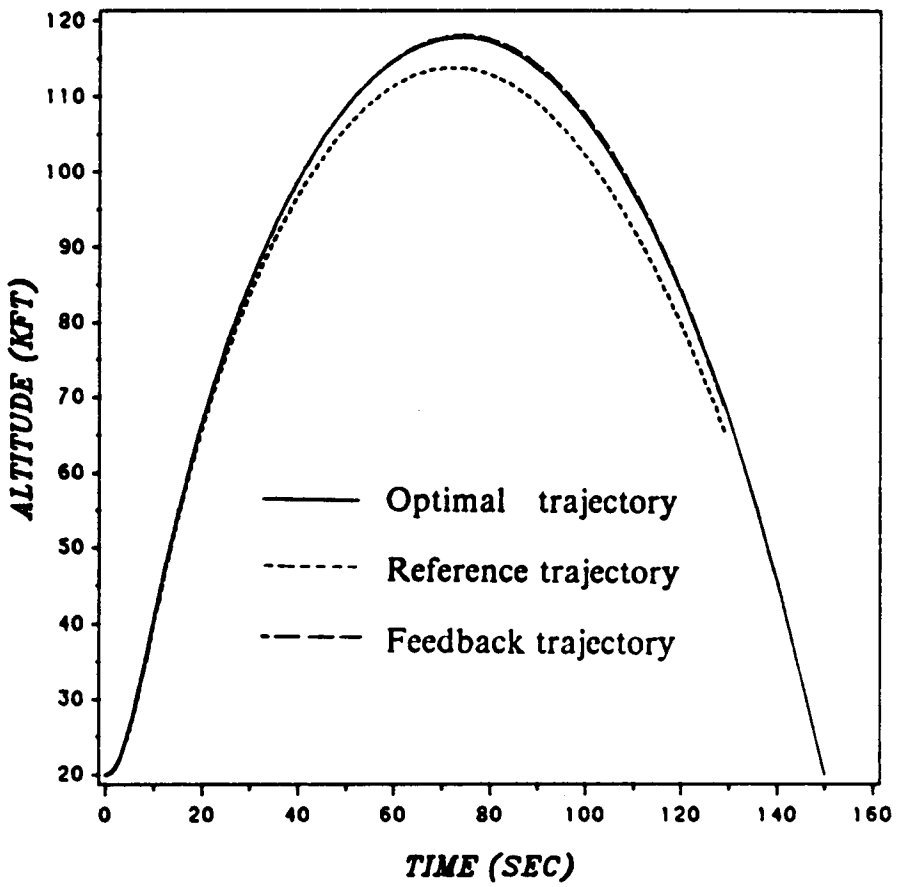

Figure 13b. Altitude history for example 1 - $\delta x(0) = 5000ft.$

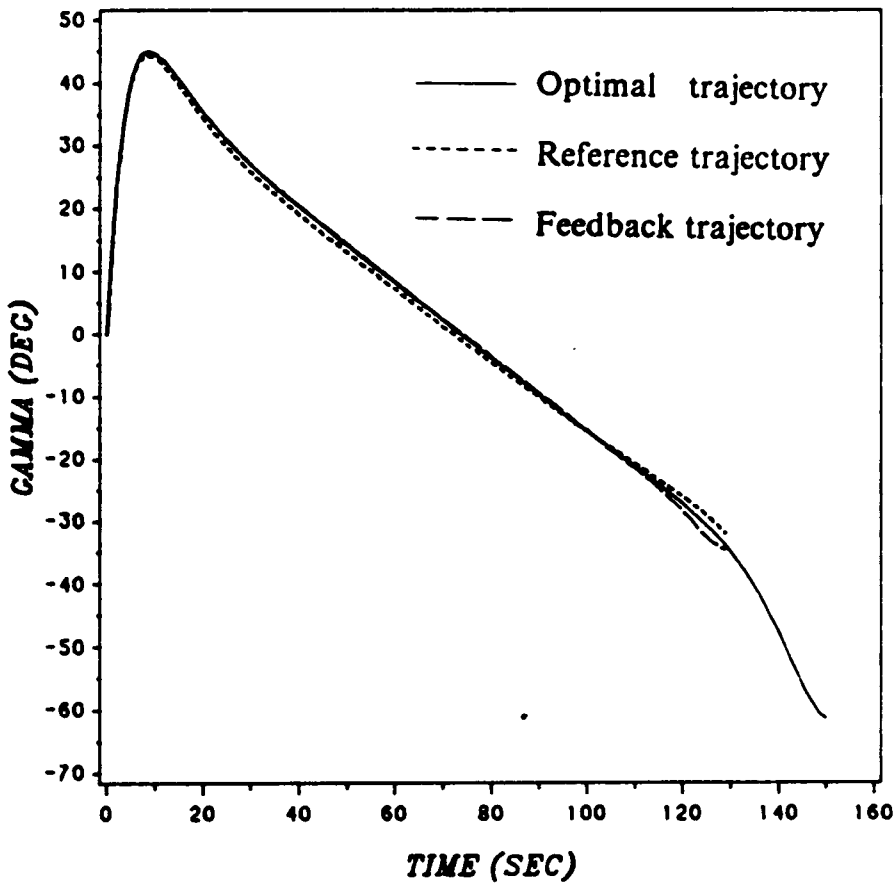

Figure 13c. Path-angle history for example 1 - $\delta x(0) = 5000ft$.

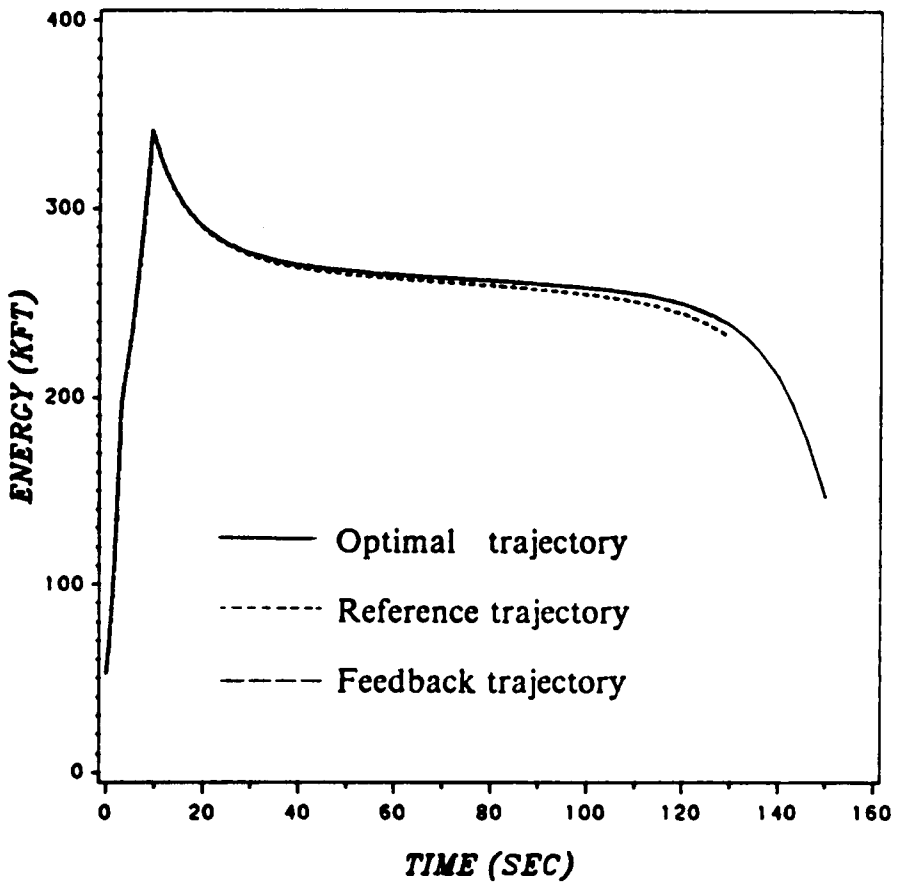

Figure 13d. Energy history for example 1 - $\delta x(0) = 5000ft.$

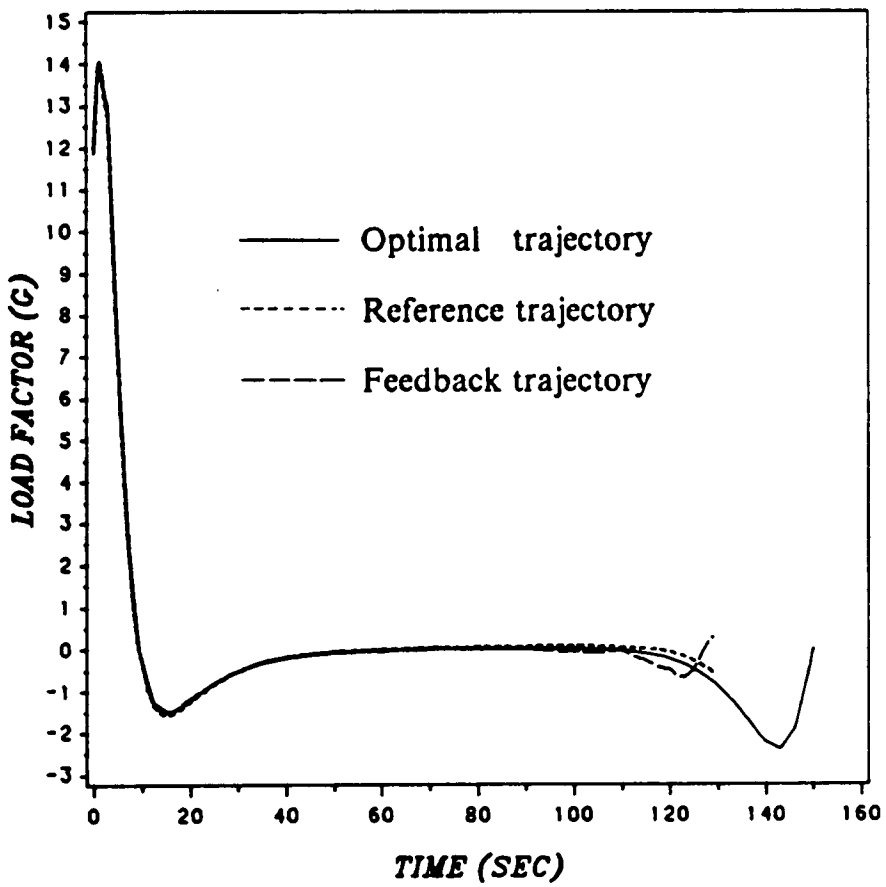

Figure 13e. Load-factor history for example 1 - $\delta x(0) = 5000ft.$

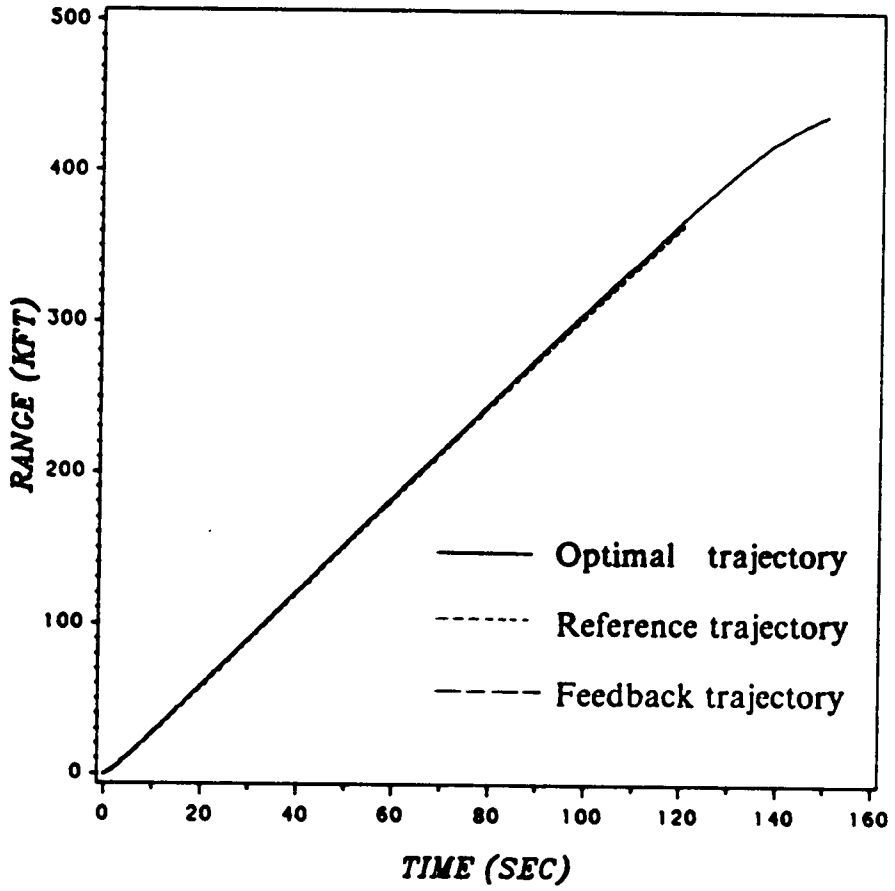

Figure 14a. Range history for example 2 - $\delta h(0) = 5000ft.$

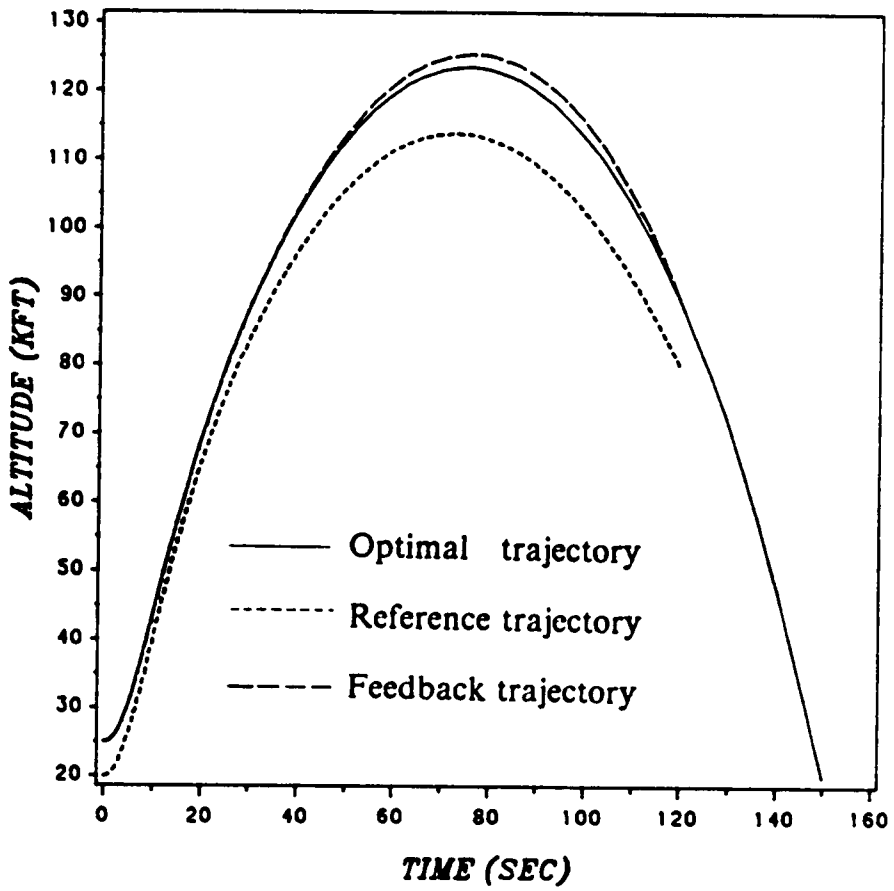

Figure 14b. Altitude history for example 2 - $\delta h(0) = 5000ft.$

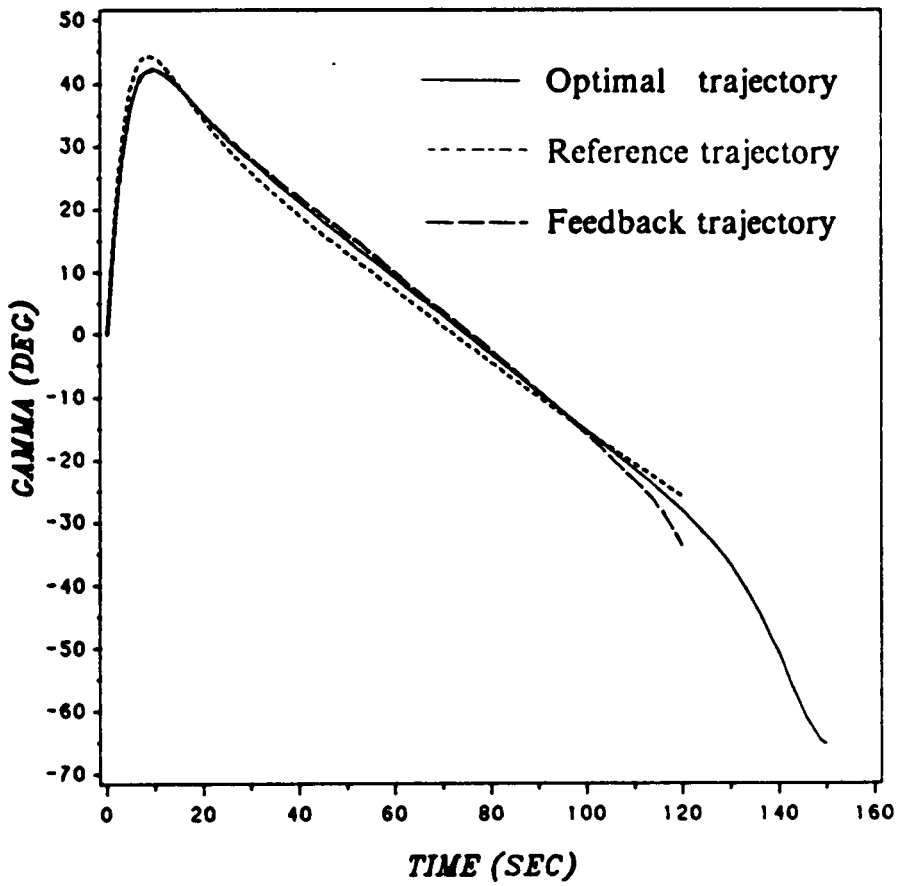

Figure 14c. Path-angle history for example 2 - $\delta h(0) = 5000ft.$

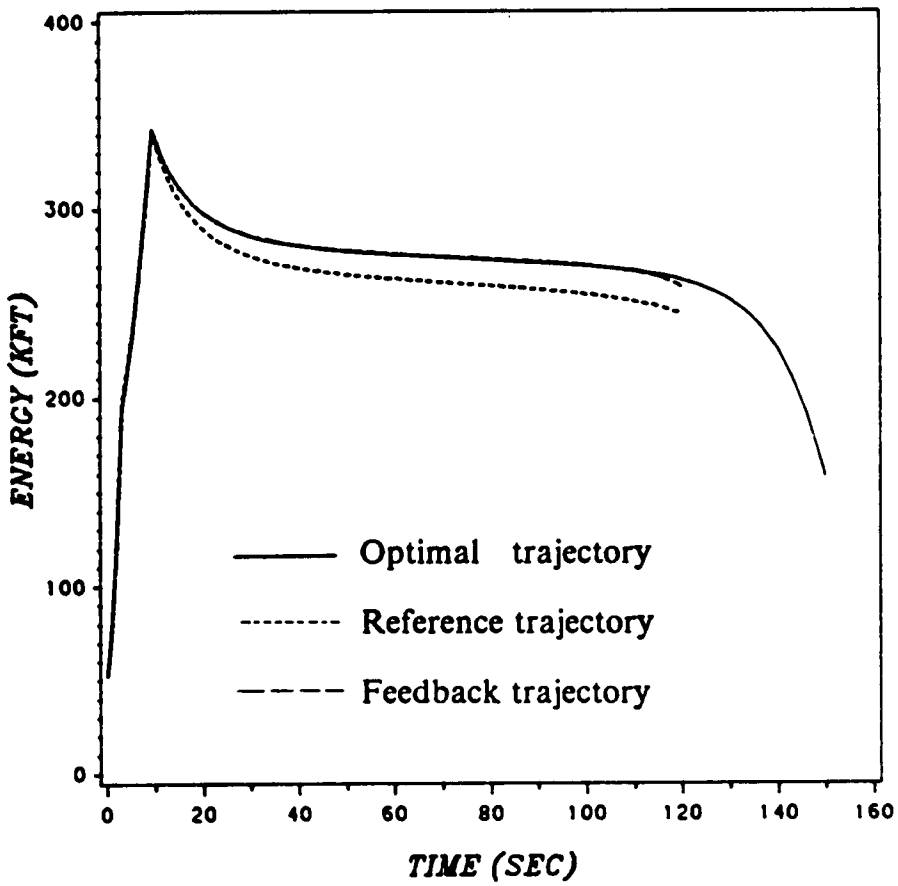

Figure 14d. Energy history for example 2 - $\delta h(0) = 5000ft$.

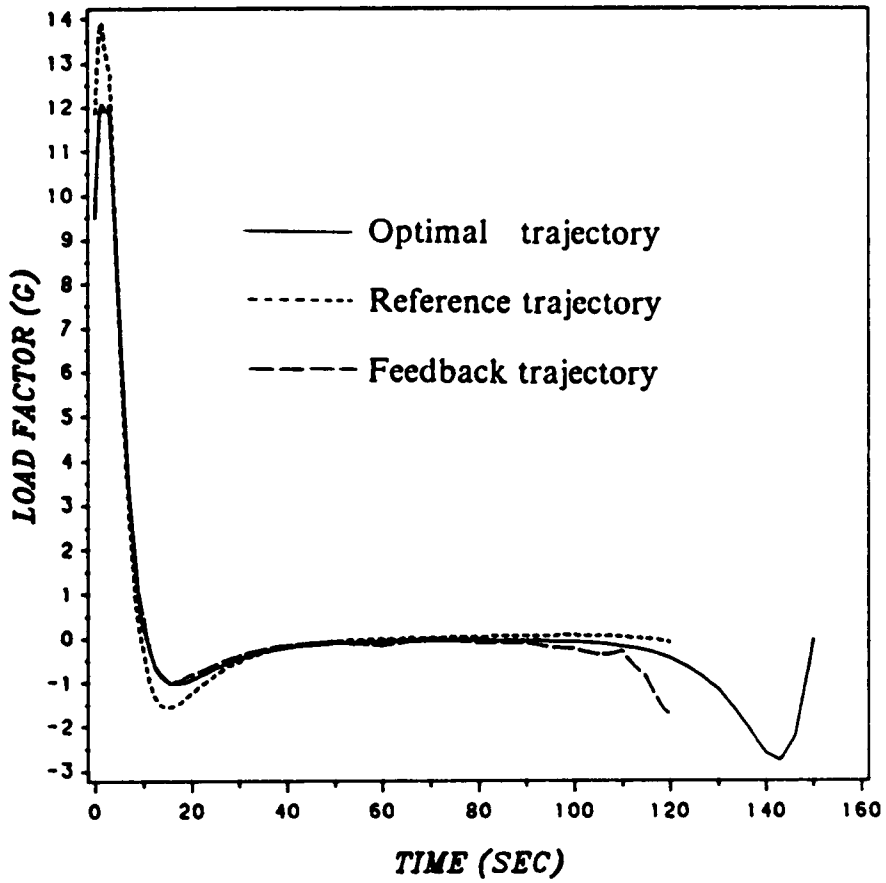

Figure 14e. Load-factor history for example 2 - $\delta h(0) = 5000ft.$

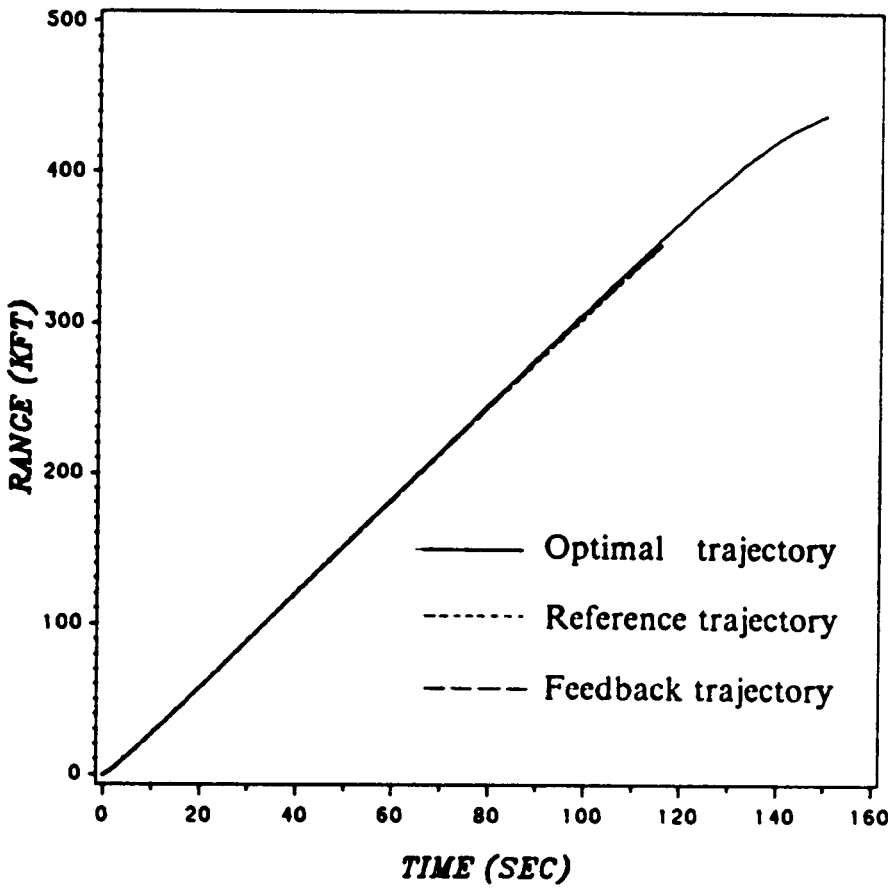

Figure 15a. Range history for example 3 - $\delta E(0) = 5000ft$.

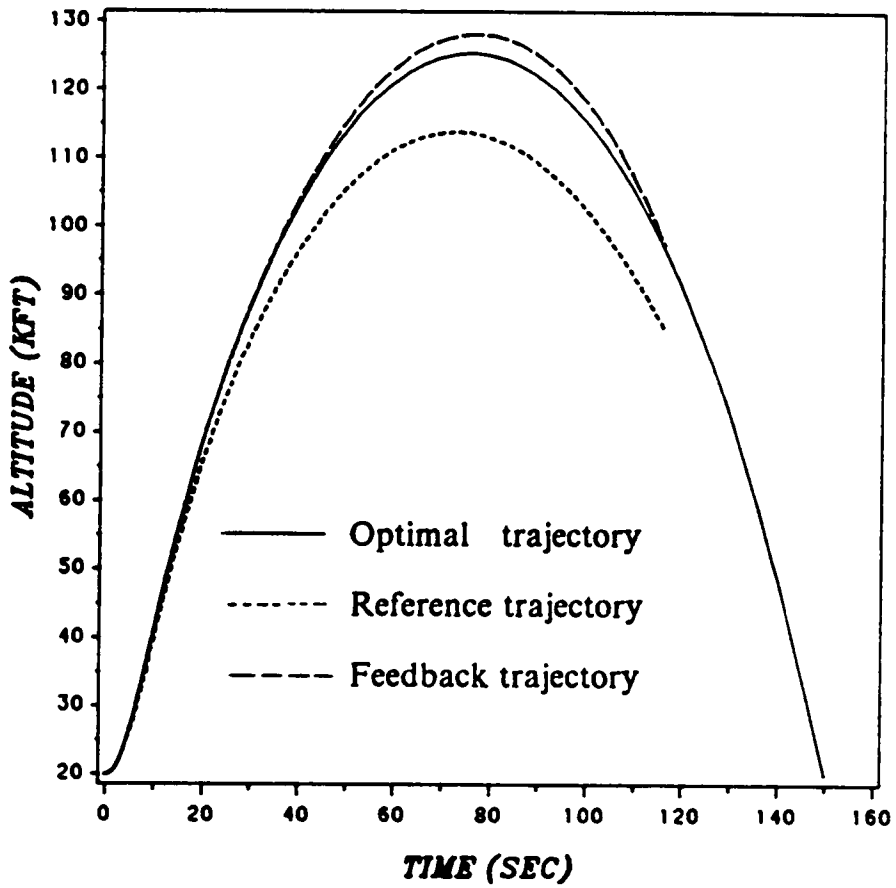

Figure 15b. Altitude history for example 3 - $\delta E(0) = 5000ft.$

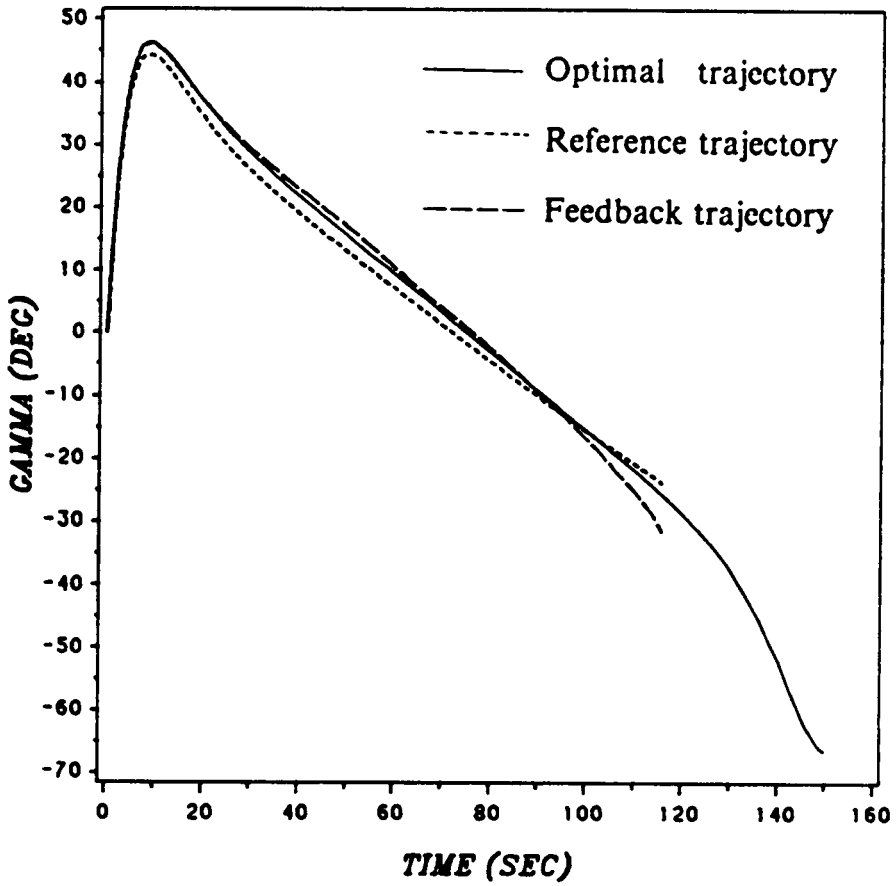

Figure 15c. Path-angle history for example 3 - $\delta E(0) = 5000ft.$

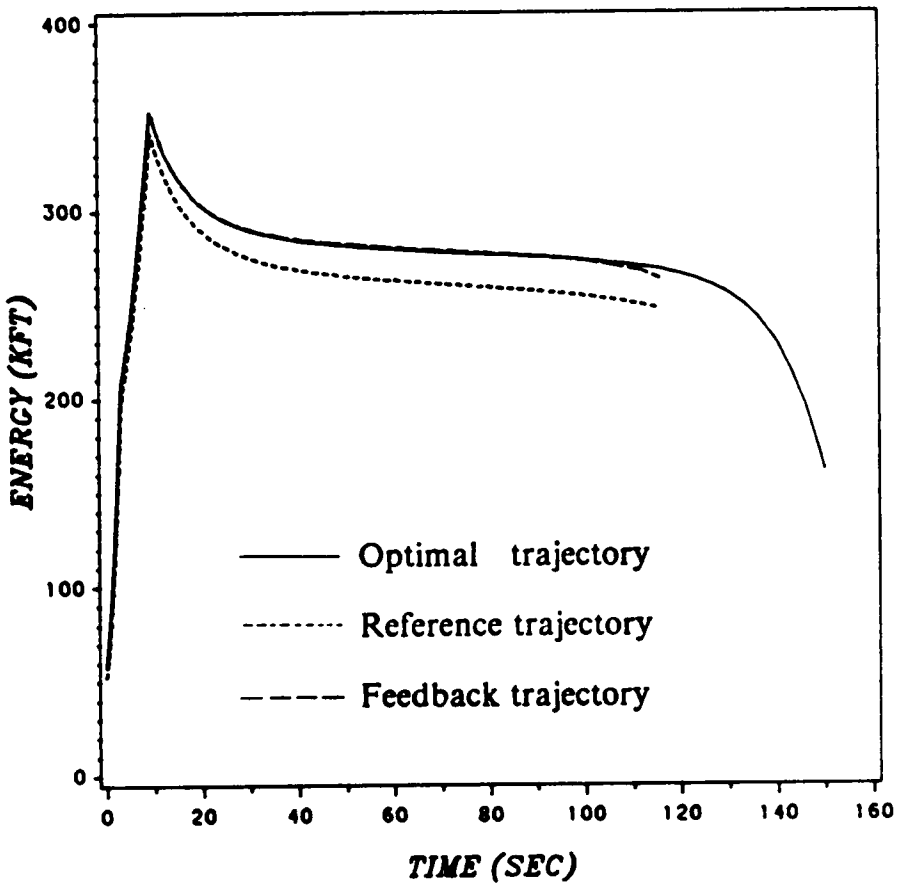

Figure 15d. Energy history for example 3 - $\delta E(0) = 5000ft.$

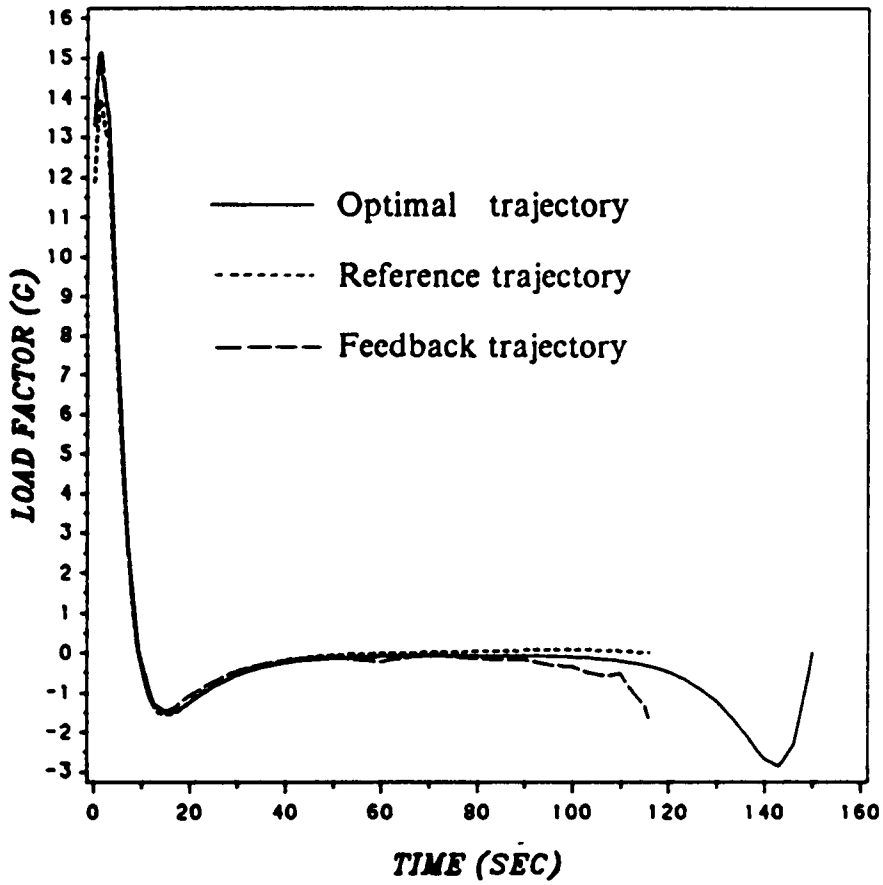

Figure 15e. Load-factor history for example 3 - $\delta E(0) = 5000ft$.

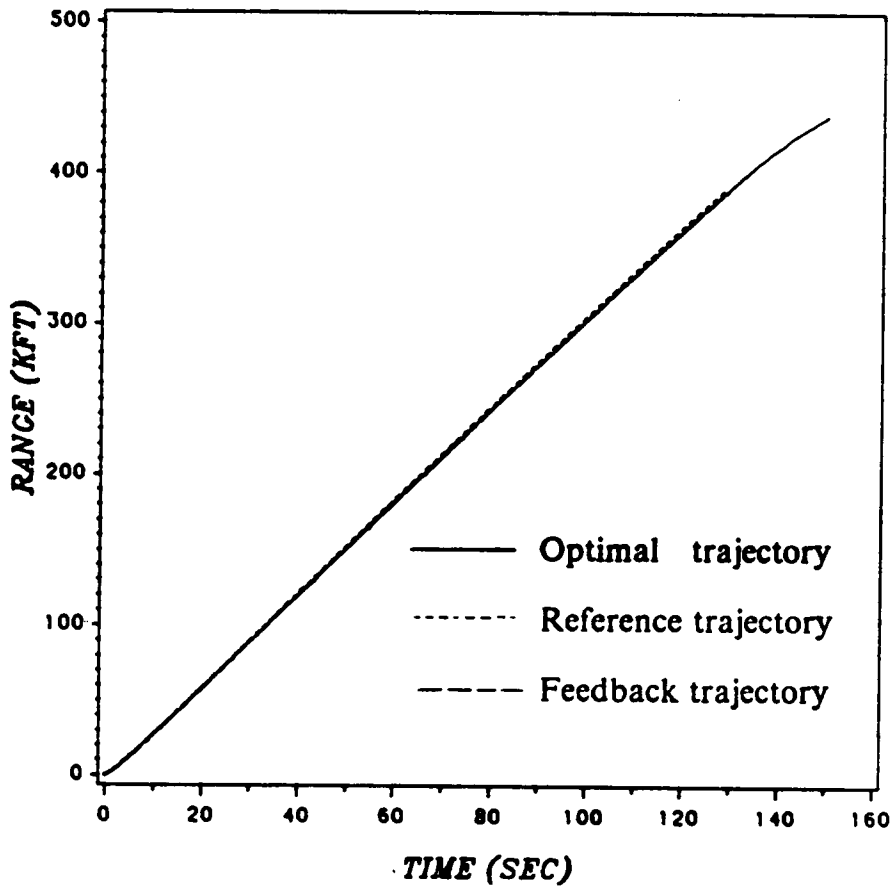

Figure 16a. Range history for example 4 - $\delta h(t_f) = 5000ft$.

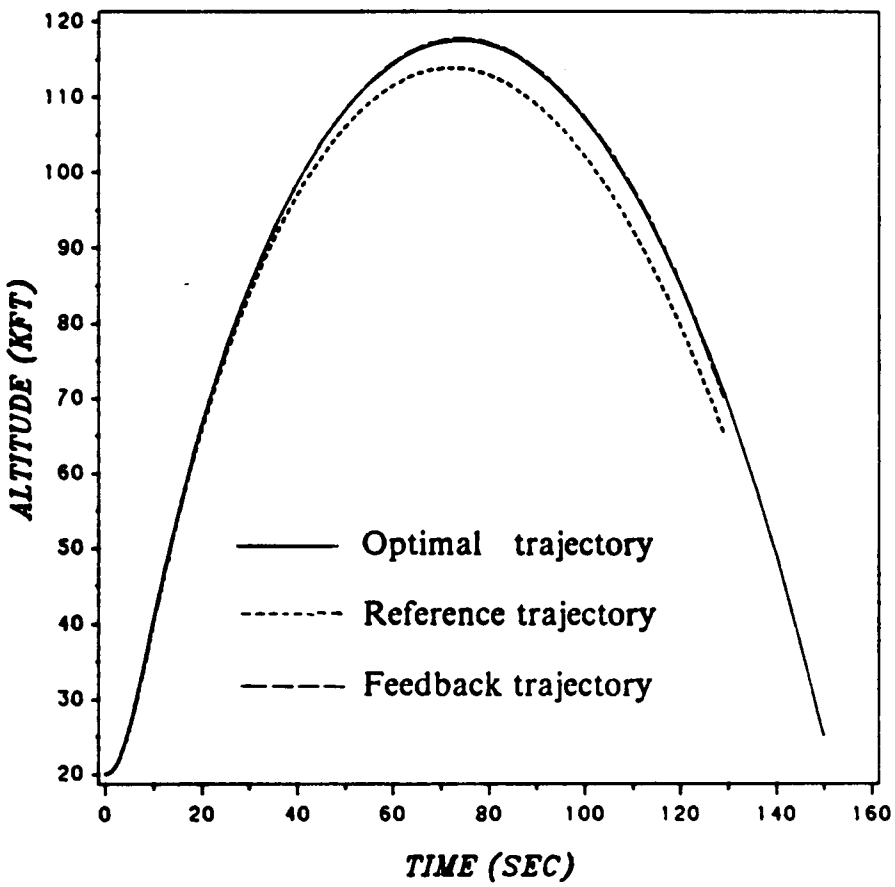

Figure 16b. Altitude history for example 4 - $\delta h(t_f) = 5000ft.$

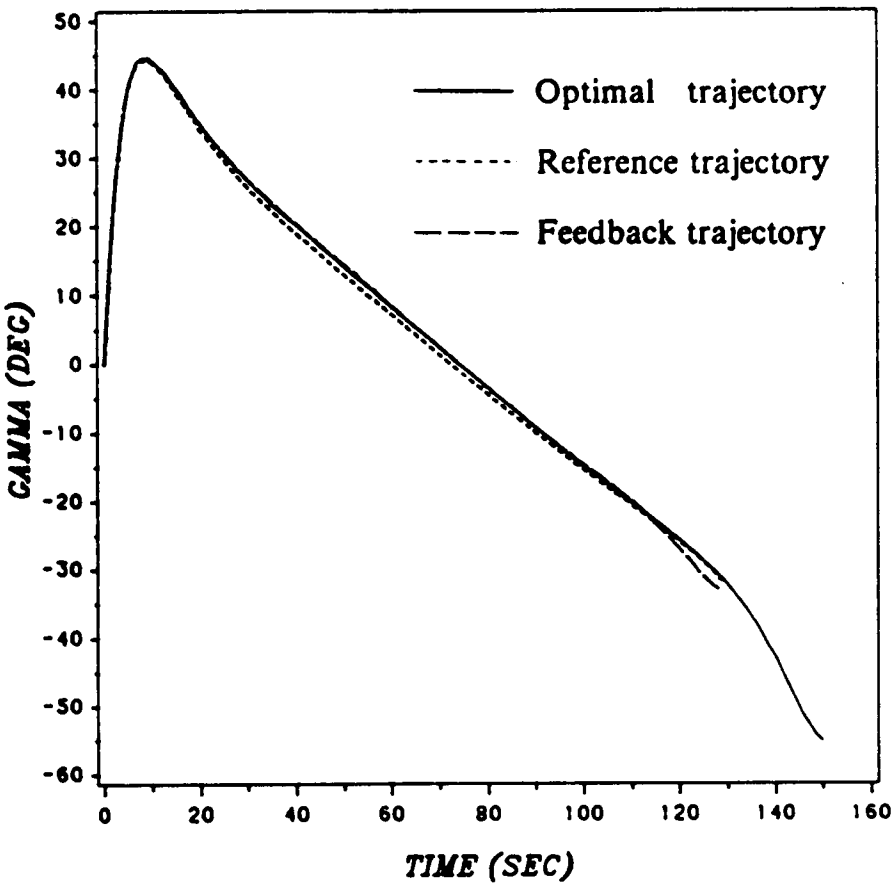

Figure 16c. Path-angle history for example 4 - $\delta h(t_f) = 5000ft$.

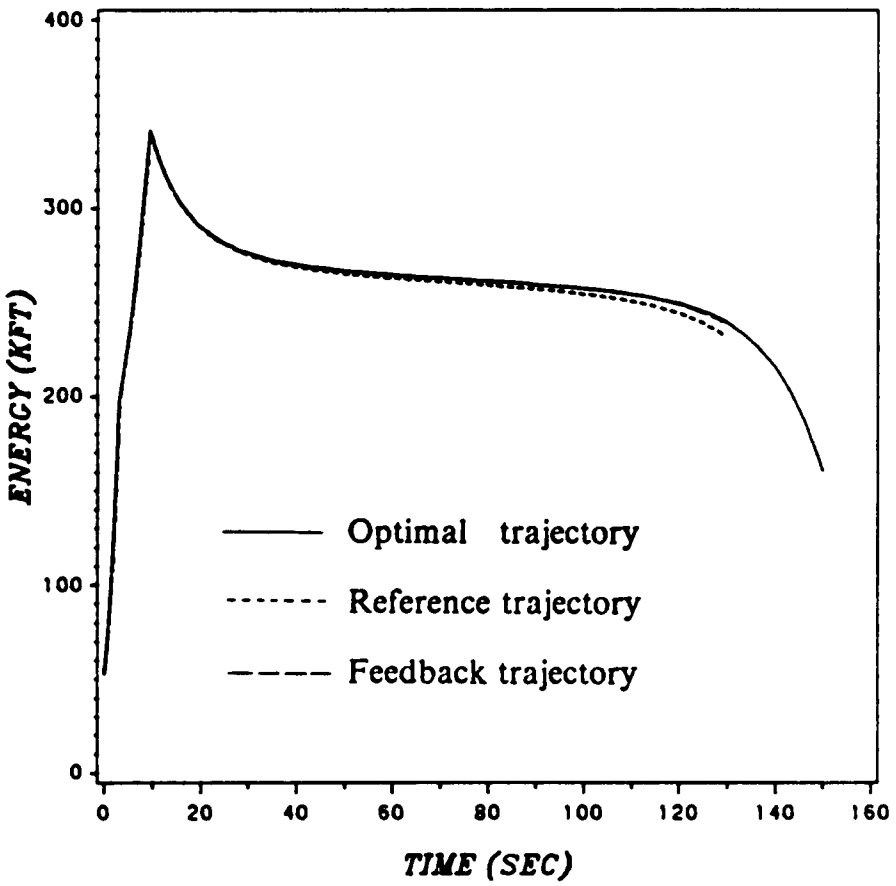

Figure 16d. Energy history for example 4 - $\delta h(t_f) = 5000ft$.

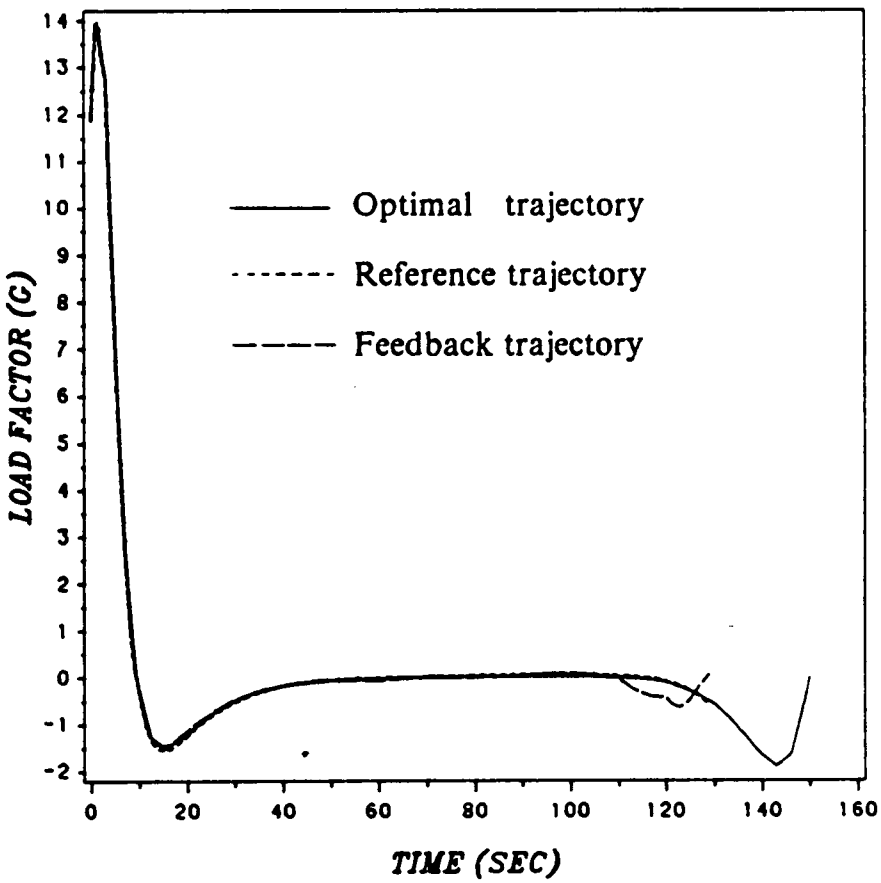

Figure 16e. Load-factor history for example 4 - $\delta h(t_f) = 5000ft.$

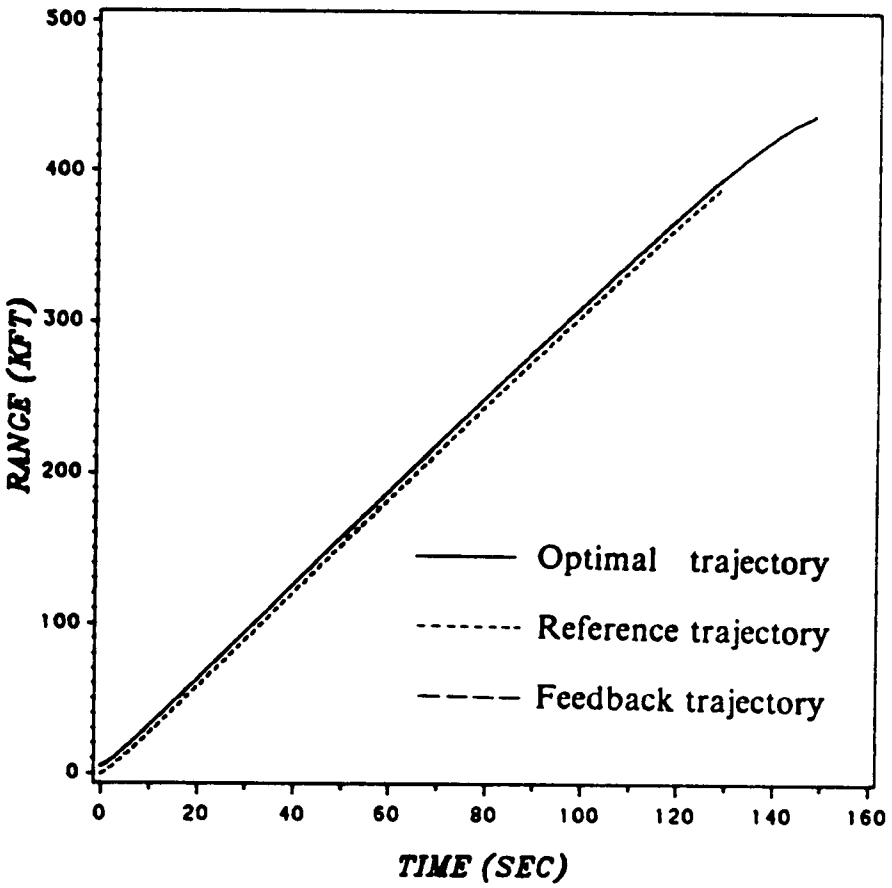

Figure 17a. Range history for example 5 - $\delta x(0) = 5000ft.$ $\delta t_f = -2sec.$

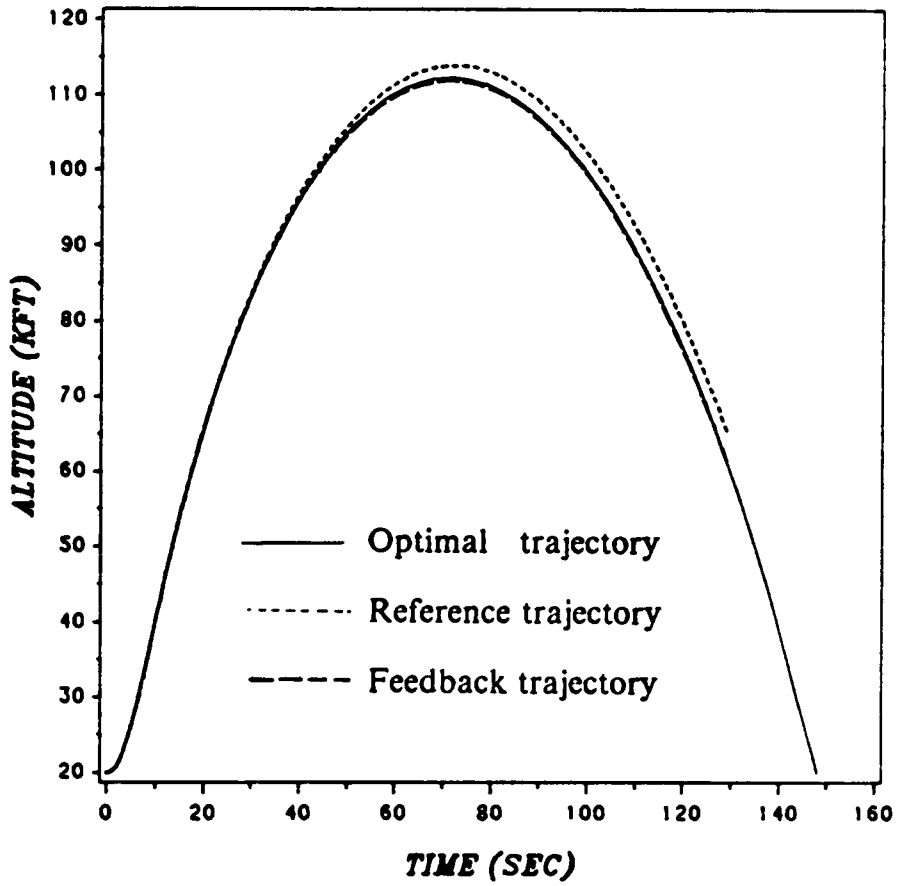

Figure 17b. Altitude history for example 5 - $\delta x(0) = 5000ft.$ $\delta t_f = -2sec.$

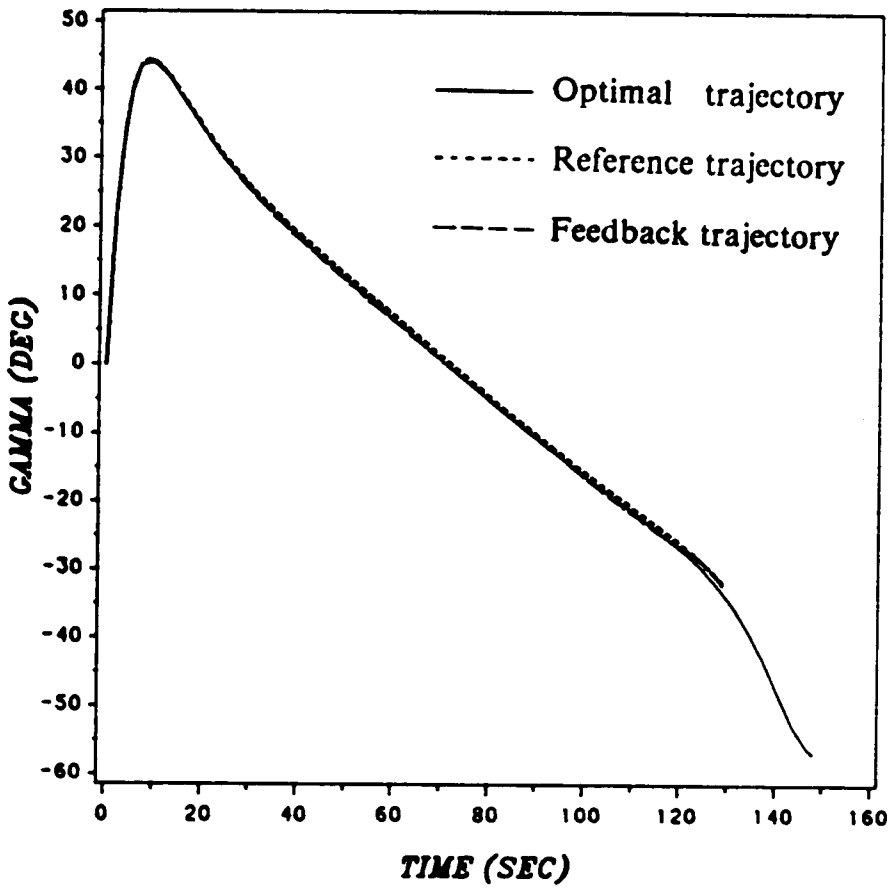

Figure 17c. Path-angle history for example 5 - $\delta x(0) = 5000ft.$ $\delta t_f = -2sec.$

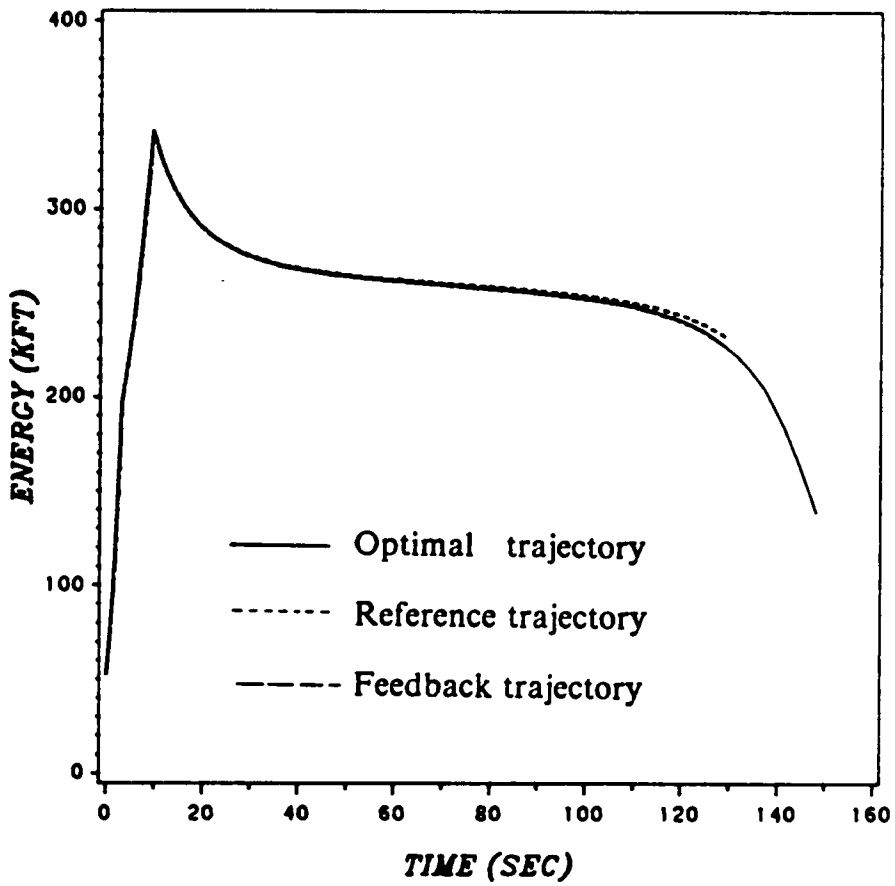

Figure 17d. Energy history for example 5 - $\delta x(0) = 5000ft.$ $\delta t_f = -2sec.$

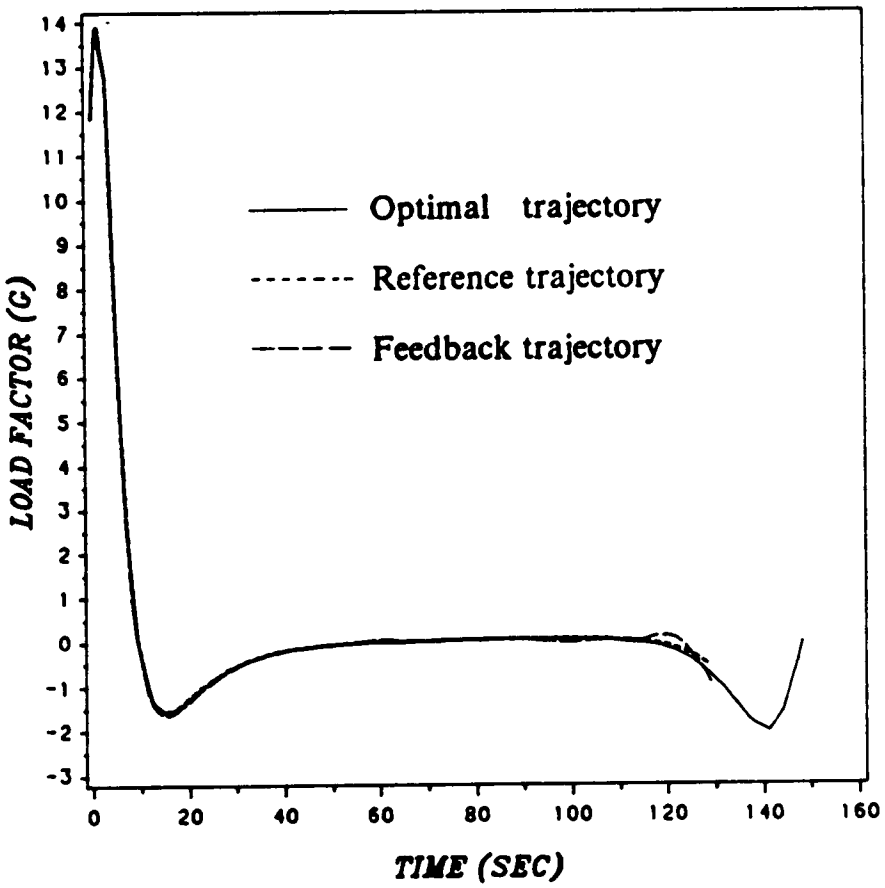

Figure 17e. Load-factor history for example 5 - $\delta x(0) = 5000ft.$ $\delta t_f = -2sec.$

References

1. Locke, A.S., Guidance, a volume in the series: Principles of Guided Missile Design, edited by Grayson Merrill, Van Nostard, Princeton, 1955.

2. Yuan, C.L., Homing and Navigational Courses of Automatic Target-Seeking Devices, *J. of Applied Physics,* Dec. 1948, pp. 1122-1128. Earlier, RCA Laboratories Report No. PTR-12C, 12.13.1943.

3. Newell, H.E., Guided Missile Kinematics, Report No. R-2538, Naval Research Laboratory, Washington, D.C., 5.22.1945.

4. Spitz, H., Partial Navigation Courses for a Guided Missile Attacking a Constant Velocity Target, Report No. R-2790, Naval Research Laboratory, Washington, D.C., 3.26.1946.

5. Murtaugh, S.A., Criel, H.E., Fundamentals of Proportional Navigation, *IEEE Spectrum,* Vol. 3, Dec. 1966, pp. 75-78.

6. Kishi, F.H., Optimal and Suboptimal Designs of Proportional Navigation Systems, in Lavi, A. and Vogl, T.P. (ed.), *Recent Advances in Optimization Techniques (Proc. of the April 1965 Symposium),* John Wiley, 1965.

7. Bryson, A.E., Linear Feedback Solutions for Minimum Effort Interception, Rendezvous, and Soft Landing, *AIAA J.,* Vol. 3, No. 8, 1965, pp. 1542-1544.

8. Bryson, A.E., Application of Optimal Control Theory in Aerospace Engineering, *J. Spacecraft,* Vol. 4, No. 5, 1967, pp. 545-553.

9. Kreindler, E., Optimality of Proportional Navigation, *AIAA J.,* Vol. 11, No. 6, 1973, pp. 878-880.

10. Sridhar, B., Gupta, N.K., Missile Guidance Laws Based on Singular Perturbation Methodology, *J. of Guidance, Control and Dynamics,* Vol. 3, No. 2, 1980, pp. 158-165.

11. Hardtla, J.W., Milligan, K.H., Cramer, E.J., Design and Implementation of a Missile Guidance Law Derived from Modern Control Theory, *AIAA-87-2447, Proc. Guidance, Navigation and Control Conference,* Monterey, CA, 1987.

12. Cheng, V.H.L, Gupta, N.K., Advanced Midcourse Guidance for Air-to-Air Missiles, *J. of Guidance, Control and Dynamics,* Vol. 9, No. 2, 1986, pp. 135-132.

13. Menon, P.K.A., Briggs, M.M., A Midcourse Guidance Law for Air-to-Air Missiles, *AIAA-87-2509, Proc. Guidance, Navigation and Control Conference,* Monterey, CA, 1987.

14. Cheng, V.H.L., Menon, P.K.A., Gupta, N.K., Briggs, M.M., Reduced-Order Pulse-Motor Ignition Control Logic, *J. of Guidance, Control and Dynamics,* Vol. 10, No. 4, 1987, pp. 343-350.

15. Katzir, S., Cliff, E.M., Kelley, H.J., Best-Range Study for a Boost-Sustain Missile, *Proceedings of the ACC,* IEEE, 1988, pp. 145-149.

16. Hibbs, A.R., Optimum Burning Program for Horizontal Flight, *J. of American Rocket Society,* Vol. 22, No. 4, 1952.

17. Bryson, A.E., Ross, S.E., Optimum Rocket Trajectories with Aerodynamic Drag, *J. of Jet Propulsion,* July 1958, pp. 465-468.

18. Leitmann, G., The Calculus of variation and Optimal Control, Plenum Press, 1981.

19. Wasow, W., Asymptotic Expansion for Ordinary Differential Equations, John Wiley and sons, New York, 1965.

20. Kelley, H.J., Edelbaum, T.N., Energy Climbs, Energy Turns and Asymptotic Expansion, *J. of Aircraft,* Vol. 7, No. 1, 1970, pp. 93-95.

21. Kelley, H.J., Singular Perturbation for a Mayer Variational Problem, *AIAA J.,* Vol. 8, 1970, pp. 1177.

22. Kelley, H.J., Boundary-Layer Approximation to Powered-Flight Altitude Transients, *J. of Spacecraft and Rockets* Vol. 7, 1970, pp. 879.

23. Kelley, H.J., Flight Path Optimization with Multiple Time Scales, *J. of Aircraft,* Vol. 8, April 1971, pp. 238-240.

24. Kelley, H.J., Reduced-Order Modeling in Aircraft Mission Analysis, *AIAA J.,* Vol. 9, 1971, pp. 349-350.

25. Kelley, H.J., Lefton, L., Super Sonic Aircraft Energy Turns, presented at *5th IFAC Congress,* Paris, France, also *Automatica,* Vol. 8, 1972, pp. 575.

26. Kelley, H.J., Aircraft Maneuver Optimization by Reduced-Order Approximation, *Control and Dynamic Systems,* Vol. 10, edited by Leondes C.T., Academic Press, New York, 1973, pp. 131-178.

27. Breakwell, J.V., Optimal Flight-Path-Angle Transition in Minimum-Time Airplane Climbs, *J. of Aircraft*, Vol. 14, No. 8, 1977, pp. 782-786.

28. Breakwell, J.V., More about Flight-Path-Angle Transition in Optimal Airplane Climbs, *J. of Guidance, Control and Dynamics*, Vol. 1, No. 3, 1978, pp. 205-208.

29. Ardema, M.D., Solution of the Minimum-Time-To-Climb Problem by Matched Asymptotic Expansions, *AIAA J.*, Vol. 14, July 1976, pp. 843-850.

30. Ardema, M.D., Singular Perturbation in Flight Mechanics, NASA TMX-62, 1974 (revised 1977).

31. Ardema, M.D., Rajan, N., Separation of Time Scales in Aircraft Trajectory Optimization, *J. of Guidance, Control and Dynamics*, Vol. 8, No. 2, 1985, pp. 275-278.

32. Ardema, M.D., Tracking Equations For Three-Dimensional Aircraft Pursuit-Evasion, presented at the 1988 ACC, Atlanta, GA, June 1988.

33. Calise, A.J., Singular Perturbation Methods for Variational Problems in Aircraft Flight, *IEEE Transactions on Automatic Control*, Vol. AC-21, No. 3, June 1976, pp. 345-353.

34. Calise, A.J., Extended Energy Management Methods for Flight Performance Optimization, Aircraft Flight, *AIAA J.*, Vol. 15, No. 3, March 1977, pp. 314-321.

35. Calise, A.J., A New Boundary Layer Matching Procedure for Singularly Perturbed Systems, *IEEE Transactions on Automatic Control,* Vol. AC-23, No. 3, June 1978, pp. 434-438.

36. Calise, A.J., Singular Perturbation Analysis of Optimal Aerodynamic and Thrust Magnitude Control, *IEEE Transactions on Automatic Control,* Vol. AC-24, No. 5, Oct 1979, pp. 345-353.

37. Calise, A.J., Singular Perturbation Techniques for On-Line Optimal Flight Path Control, *J. of Guidance, Control and Dynamics,* Vol. 3, No. 4, 1981, pp. 398-405.

38. Shinar, J., On Applications of Singular Perturbation Techniques in Nonlinear Optimal Control, *Automatica,* Vol. 19, No. 4, 1983, pp. 203-211.

39. Shinar, J., Negrin, M., An Explicit Feedback Approximation for Medium Range Interception in the Vertical Plane, *Optimal Control Applications and Methods,* Vol. 4, No. 4, 1983, pp. 303-323.

40. Shinar, J., Zeroth-Order Feedback Strategies for Medium Range Interception in the Horizontal Plane, *J. of Guidance, Control and Dynamics,* Vol. 8, No. 1, 1985, pp. 9-15.

41. Visser, H.G., An Introduction to the Technique of Singular Perturbation Applied to the Performance Optimization Problems in Atmospheric Flight Mechanics, Report LR-374, Dept. of Acrospace Engineering, Delft University of Technology, Delft, The Netherlands, Dec. 1982.

42. Kelley, H.J., Comments on 'A New Boundary Layer Matching Procedure for Singularly Perturbed Systems', *IEEE Transactions on Automatic Control,* Vol. AC-23, No. 3, June 1978.

43. Weston, A.R., Cliff, E.M., Kelley, H.J., Altitude Transitions in Energy Climbs *Automatica,* Vol. 19, No. 2, 1983, pp. 199-202.

44. Kaiser F., Der Steigflug mit Stragflugzeugen - Teil I, Bahngeschwindigkiet für Bensten Steigen, Versuchsbericht 262 - 02 -L44, Messerschmitt A.G., Augsburg, April 1944 (Translated as Ministry of Supply RTP/TIB translation GDC/15/148T).

45. Lush, K.J., A Review of the Problem of Choosing a Climb Technique with Proposals for a New Climb Technique for High Performance Aircraft, Aeronautical Research Council Report Memo, No. 2557, 1951.

46. Rutowski, E.S., Energy Approach to the General Aircraft Performance Problem, *J. of the Aeronautical Science,* Vol. 21, March 1954, pp. 187-195.

47. Kelley, H.J., Guidance Theory and Extremal Fields, *IRE Transactions on Automatic Control,* Vol. 7, No. 5, 1962, pp 75-82.

48. Breakwell, J.V., Speyer, J.L., Bryson, A.E., Optimization and Control of Nonlinear System using Second Variation, *SIAM J. of Control,* Vol. 1., No. 2, Jan.-Feb. 1963, pp. 193-223.

49. Kelley, H.J., An Optimal Guidance Approximation Theory, *IEEE Transactions on Automatic Control,* Vol. 9, No. 4, 1964, pp. 370-380.

50. Powers, W.F., Techniques for Improved Convergence in Neighboring Optimum Guidance, *AIAA Journal,* Vol. 8, No. 12, Dec. 1970, pp. 2235-2241.

51. Kelley, H.J., Well, K., An Approach to Intercept On-Board Calculations, Optimization Incorporated/DFVLR Memorandum, Sep. 1980; an updated version appears in *Proceedings of the ACC,* IEEE, 1983, pp. 799-800.

52. Weston, A.R., Cliff, E.M., Kelley, H.J., On Board Near-Optimal Climb-Dash Energy Management *J. of Guidance, Control and Dynamics,* Vol. 8, No. 3, 1985, pp. 320-324.

53. Visser, H.G., Kelley, H.J., Cliff, E.M., Energy Management of Three Dimensional Minimum-Time Intercept *12th AIAA Atmospheric Flight Mechanics Conference* Snowmass, CO, 1985, also *J. of Guidance, Control and Dynamics,* Vol. 10, No. 6, 1987, pp. 574-580.

54. Bulirsch, R., Einfuehrung in die Flugbahnoptimierung ; Mehrzielmethode zur Numerischen Loesung von nichtlinearen Randwertproblemen und Aufgaben der Optimalen Steuerung, Lehrgang Flugbahnoptimierung Carl-Cranz-Gesellschaft e.v. ,October, 1971.

55. Kelley, H.J., Second Variation Test for Singular Extremals, *AIAA J.,* Vol. 2, 1964, pp. 1380-1382.

56. Kelley, H.J., A Transformation Approach to Singular Subarcs in Optimal Trajectory and Control Problems, *SIAM J. Control,* Vol. 2, 1964, pp. 234-240.

57. Kelley, H.J., Kopp, R.E., Moyer, H.G., Singular Extremals, in 'Topics in Optimization' (G. Leithmann, ed), Academic Press, New York, 1967, pp. 63-101.

58. Bell, D.J., Jacobson, D.H., Singular Optimal Control Problems, Academic Press, New York, 1975.

59. Gelfand, I.M., Fomin, S.V., Calculus of Variations, Prentice Hall, 1963.

60. Ewing, G.M., Calculus of Variations with Applications, Dover, 1985.

61. McDanell, J.P., Powers, W.F., Necessary Conditions for Joining Singular and Nonsingular Subarcs, *SIAM J. of Control,* Vol. 9, May 1971, pp. 161-173.

62. Bryson, A.E., Ho, Y.C., Applied Optimal Control, Ginn, Xerox, Walthan, Mass., 1969.

63. Lee, E.B., Markus, L., Foundations of Optimal Control Theory, Robert E. Krieger, Malbar, Florida, 1986.

64. Marec, J.P., Optimal Space Trajectories, Elsvier, New York, 1979.

65. Vinh, N.X., Optimal Trajectories in Atmospheric Flight, Elsvier, New York, 1981.

66. Kirk, D.E., Optimal Control Theory, Prentice Hall, 1970.

The vita has been removed from the scanned document